BEILSTEIN JOURNAL OF ORGANIC CHEMISTRY

Concept-driven strategies in target-oriented synthesis

Edited by David Yu-Kai Chen, Chao Li and Yefeng Tang

Imprint

Beilstein Journal of Organic Chemistry
www.bjoc.org
ISSN 1860-5397
Email: journals-support@beilstein-institut.de

The *Beilstein Journal of Organic Chemistry* is published by the Beilstein-Institut zur Förderung der Chemischen Wissenschaften.

Beilstein-Institut zur Förderung der Chemischen Wissenschaften
Trakehner Straße 7–9
60487 Frankfurt am Main
Germany
www.beilstein-institut.de

BEILSTEIN JOURNAL OF ORGANIC CHEMISTRY

Total synthesis of (±)-simonsol C using dearomatization as key reaction under acidic conditions

Xiao-Yang Bi, Xiao-Shuai Yang, Shan-Shan Chen, Jia-Jun Sui, Zhao-Nan Cai, Yong-Ming Chuan and Hong-Bo Qin*

Full Research Paper

Open Access

Address:
School of Chemistry and Environment, Yunnan Minzu University, Kunming 650000, China

Email:
Hong-Bo Qin* - qinhb@ymu.edu.cn

* Corresponding author

Keywords:
acidic dearomazation; benzofuran; (±)-simonsol C; total synthesis

Beilstein J. Org. Chem. **2025,** *21,* 601–606.
https://doi.org/10.3762/bjoc.21.47

Received: 18 January 2025
Accepted: 07 March 2025
Published: 17 March 2025

This article is part of the thematic issue "Concept-driven strategies in target-oriented synthesis".

Guest Editor: C. Li

Abstract

The total synthesis of (±)-simonsol C was accomplished using a dearomatization under acidic conditions as key step to construct an aryl-containing quaternary center. The 6/5/6 benzofuran unit was formed through reductive elimination with Zn/AcOH and a spontaneous oxy-Michael addition. This synthesis consists of 8 steps and achieves an overall yield of 13%, making it the shortest known route.

Introduction

Star anise, derived from *Illicium* species cultivated in southeastern China [1] possesses significant economic, culinary, and medicinal value [2]. Particularly noteworthy are its medicinal properties, including insecticidal, antibacterial, anti-inflammatory, analgesic, and neurotrophic activities [3]. In 2013, Wang's group isolated (±)-simonsol C from star anise, which features a unique 6/5/6 tricyclic benzofuran structure [4]. They found that it exhibits biological activity that promotes neuronal synapse growth and inhibits acetylcholinesterase.

(±)-Simonsol C (Figure 1) has received considerable attention due to the presence of an aryl- and allyl-containing quaternary carbon center, which is common in natural products such as galanthamine and morphine. To construct the quaternary carbon in simonsol C, two reports have utilized alkaline dearomatization strategies and another report used an intramolecular Heck reaction as the key reaction [5-7]. However, there have been no reports or studies utilizing acidic dearomatization, which is also effective, to synthesize an arylated quaternary carbon center.

In the first report on the total synthesis of simonsol C (Scheme 1), in 2016 Banwell's group employed an intramolecular Heck reaction as key step to furnish the aryl-containing quaternary center and simultaneously construct the benzofuran

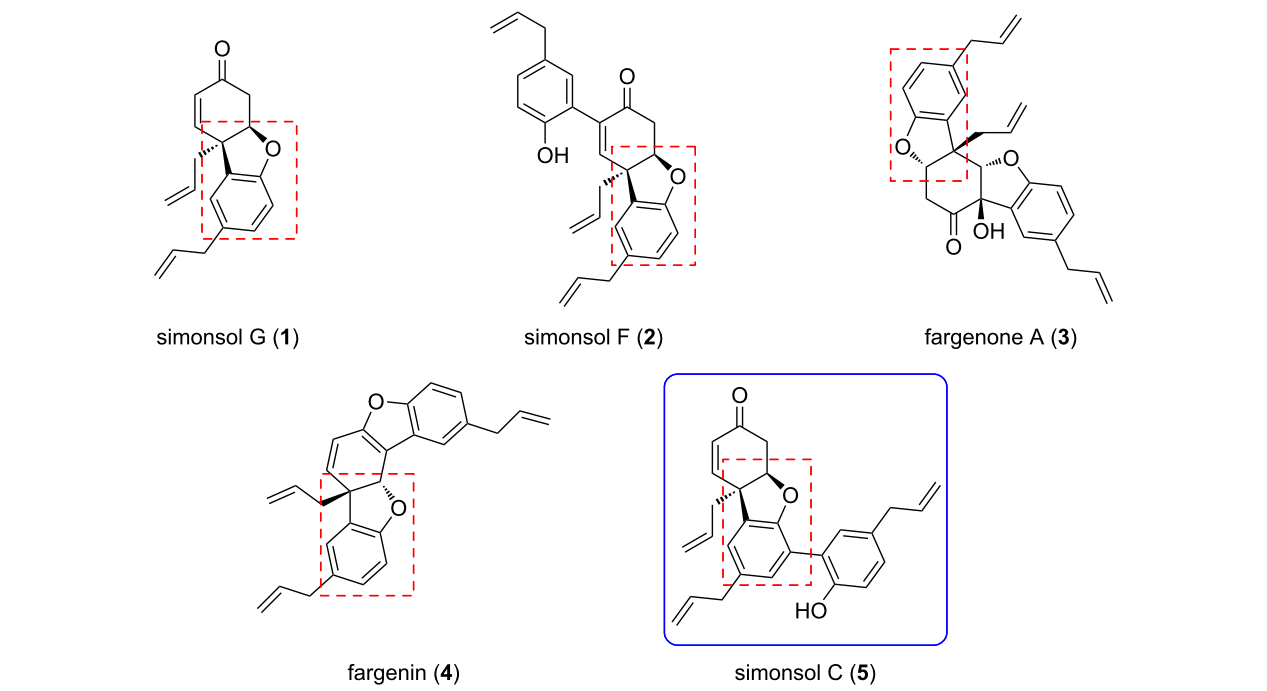

Figure 1: Representative sesquineolignan compounds.

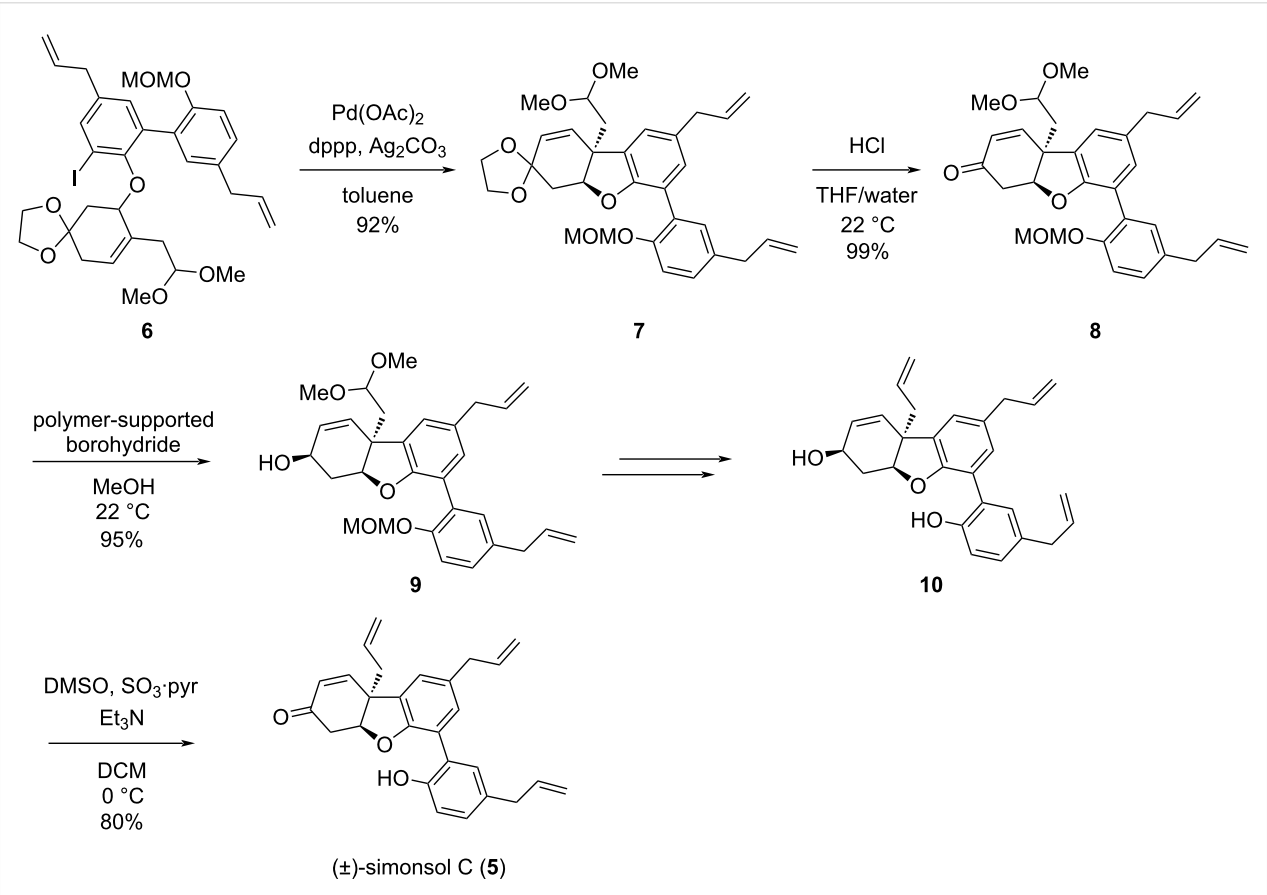

Scheme 1: The first total synthesis of (±)-simonsol C by Banwell's group.

skeleton [7]. This synthesis involved a total of 12 steps and achieved 12% overall yield.

In May 2024, the Qin group reported the second total synthesis of (±)-simonsol C (Scheme 2) [5]. An effective strategy to form the 6/5/6 benzofuran scaffold was developed which specifically involved a basic dearomatization and reductive elimination with Zn/AcOH to construct the aryl and allyl-containing quaternary center, and a simultaneous phenol-initiated oxy-Michael addition to afford the benzofuran unit. This synthesis took 9 steps and achieved an overall yield of 13%. Also in 2024, the Denton group reported another efficient way to access the 6/5/6 benzofuran scaffold of simonsol C, utilizing an alkaline dearomatization as the key reaction, followed by a functional-group-selective Wittig reaction and concurrent oxy-Michael addition [6]. A bromophenol acetal was used in the intramolecular alkylative dearomatization, which was first reported by Magnus et al. [8] and has been used in syntheses of natural products containing aryl quaternary carbon centers [9,10].

Unlike the intramolecular alkylation strategy of a phenol derivative, which can only be applied in basic dearomatization reactions, our approach using an α-iodophenol ether as precursor of the dearomatization offers considerable versatility. Not only can it be employed under basic dearomatization conditions, but it is also effective under Lewis acid conditions. Combined with a reductive elimination using Zn/AcOH, the benzofuran skeleton can be easily synthesized. This dual applicability of the new approach will be demonstrated next in the synthesis of simonsol C.

Results and Discussion

Based on extensive literature investigations, the retrosynthetic analysis strategy for our synthesis of (±)-simonsol C is as

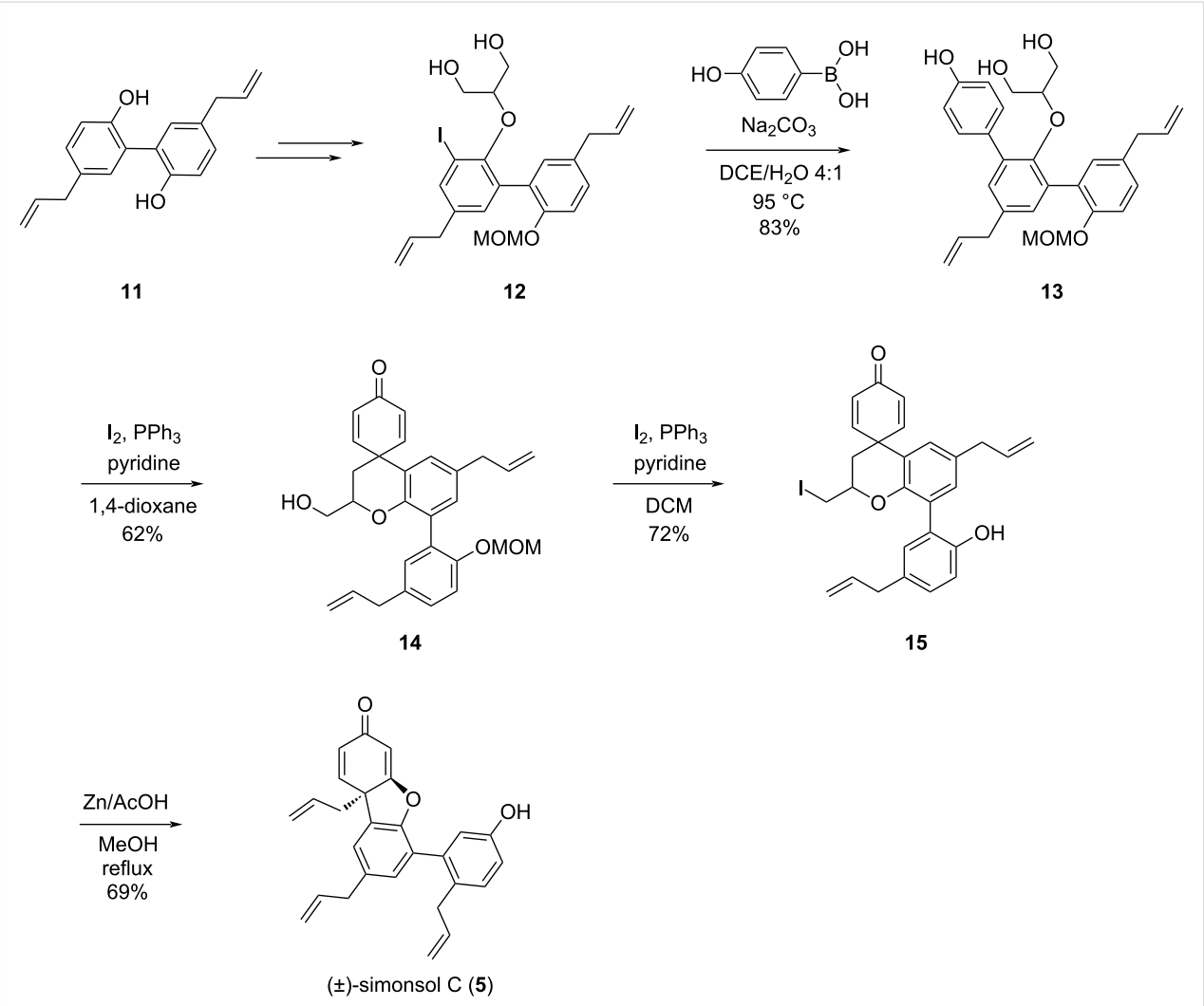

Scheme 2: The second total synthesis of (±)-simonsol C developed by the Qin group.

follows (Figure 2): The 6/5/6 benzofuran skeleton of (±)-simonsol C can be accessed via an oxy-Michael addition from dienone **15**. The 6/6/6 tricyclic structure in **15** can be constructed through dearomatization of compound **16**, which in turn can be readily synthesized through consecutive alkylation steps starting from magnolol (**11**). Additionally, using magnolol as the starting material brings two allyl groups into the product, thus avoiding the challenges associated with allyl formation reactions.

The chosen synthetic route towards (±)-simonsol C is shown in Scheme 3. Starting with magnolol (**11**), one of the phenol groups was selectively protected by controlling the equivalents of MOMCl and DIPEA, affording compound **17** with an 89% yield [11].

For the following alkylation step with *tert*-butyl bromoacetate, three bases were tested: potassium carbonate, cesium carbonate, and sodium hydride. Considering the targeted alkylation of a phenolic hydroxy group and the pK_a requirements of this reaction, weaker bases like potassium carbonate and cesium carbonate should theoretically suffice. However, the reaction outcomes with these two bases did not meet the desired expectations, as some starting material remained after 5 hours of reaction. Extending the reaction time did not lead to full consumption of the starting material. Subsequently, when the base was

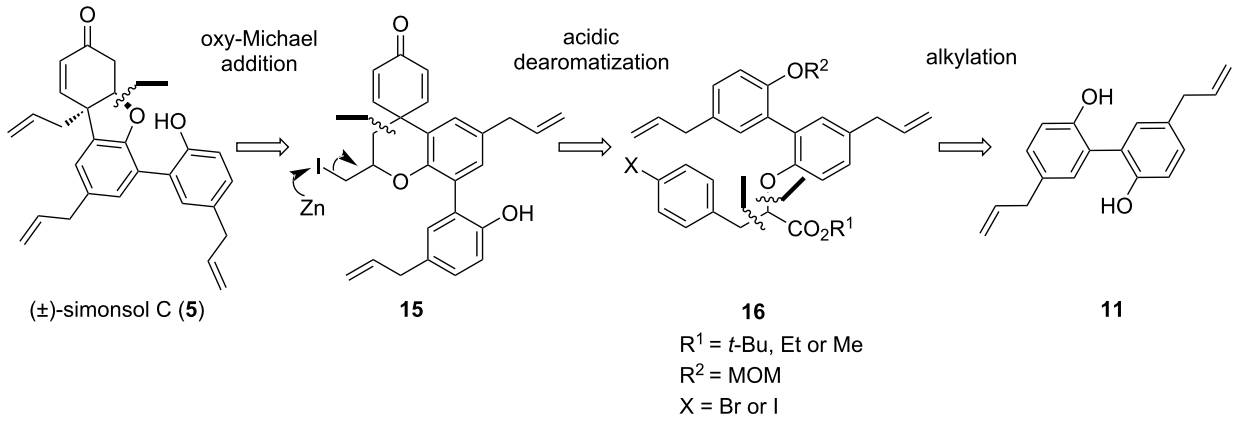

Figure 2: Retrosynthetic analysis of (±)-simonsol C.

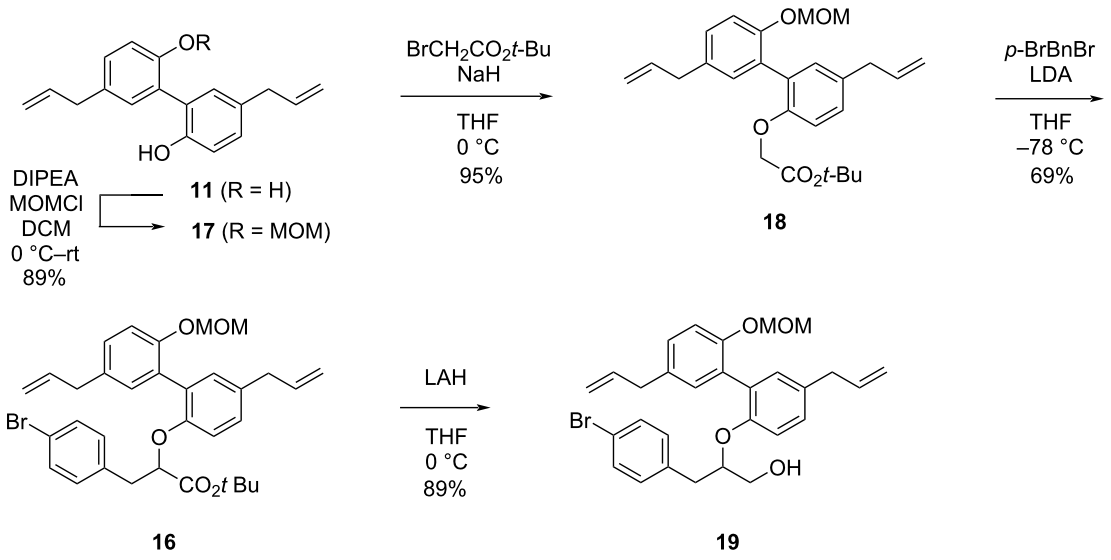

Scheme 3: Rapid access of the basic skeleton of (±)- simonsol C.

changed to the stronger base sodium hydride [12], the reaction proceeded much better. Within 2 hours, the starting material was completely converted, yielding compound **18** with 95% isolated yield.

Proton abstraction of the hydrogen in the α-position to the carbonyl group in **18** was achieved by using LDA, followed by the addition of 4-bromobenzyl bromide for alkylation, giving compound **16** with 69% isolated yield. Compound **16** was then reduced to alcohol **19** with 2 equiv LAH at 0 °C. The reaction was completed within 10 minutes and the desired alcohol **19** was isolated in 89% yield.

The copper-catalyzed replacement of the bromine substituent in **19** with a hydroxy group was achieved in the presence of a catalytic amount of oxalamide ligand **I** [13]. This transformation is critical for enabling further functionalization and the reaction conditions were optimized to achieve product **20** with 85% yield, minimizing potential side reactions. The subsequent dearomatization step is crucial for the construction of the cyclohexadienone unit. Oxidation of compound **20** with PIDA in trifluoroethanol, the original phenol was converted into a quinone moiety, successfully forming the aryl-containing quaternary center. However, in this step, the reaction was too rapid to control. After optimizing the reaction time and temperature, the reaction was carried out at −30 °C for 15 minutes and product **14** was isolated in a yield as high as 58% [14]. Iodination of compound **14** was performed next and the desired iodide was isolated and, to our delight, the cleavage of the MOM group occurred concomitantly, affording compound **15** in 75% yield. This reaction is likely triggered by the in situ-generated acid. As in our previously reported synthesis, a Zn/AcOH reductive elimination was utilized to liberate the allyl group and to simultaneously construct the 6/5/6 tricyclic skeleton via an oxy-Michael addition affording (±)-simonsol C in 70% yield (Scheme 4). The spectral data were in agreement with the reported ones [4,15,16] and the *cis* relation between the protons at C5 and C7 in simonsol C was confirmed by ^{1}H-^{1}H ROESY spectroscopy.

Conclusion

The total synthesis of (±)-simonsol C was accomplished using a dearomatization reaction under acidic conditions as key step to construct the aryl-containing quaternary center. The 6/5/6

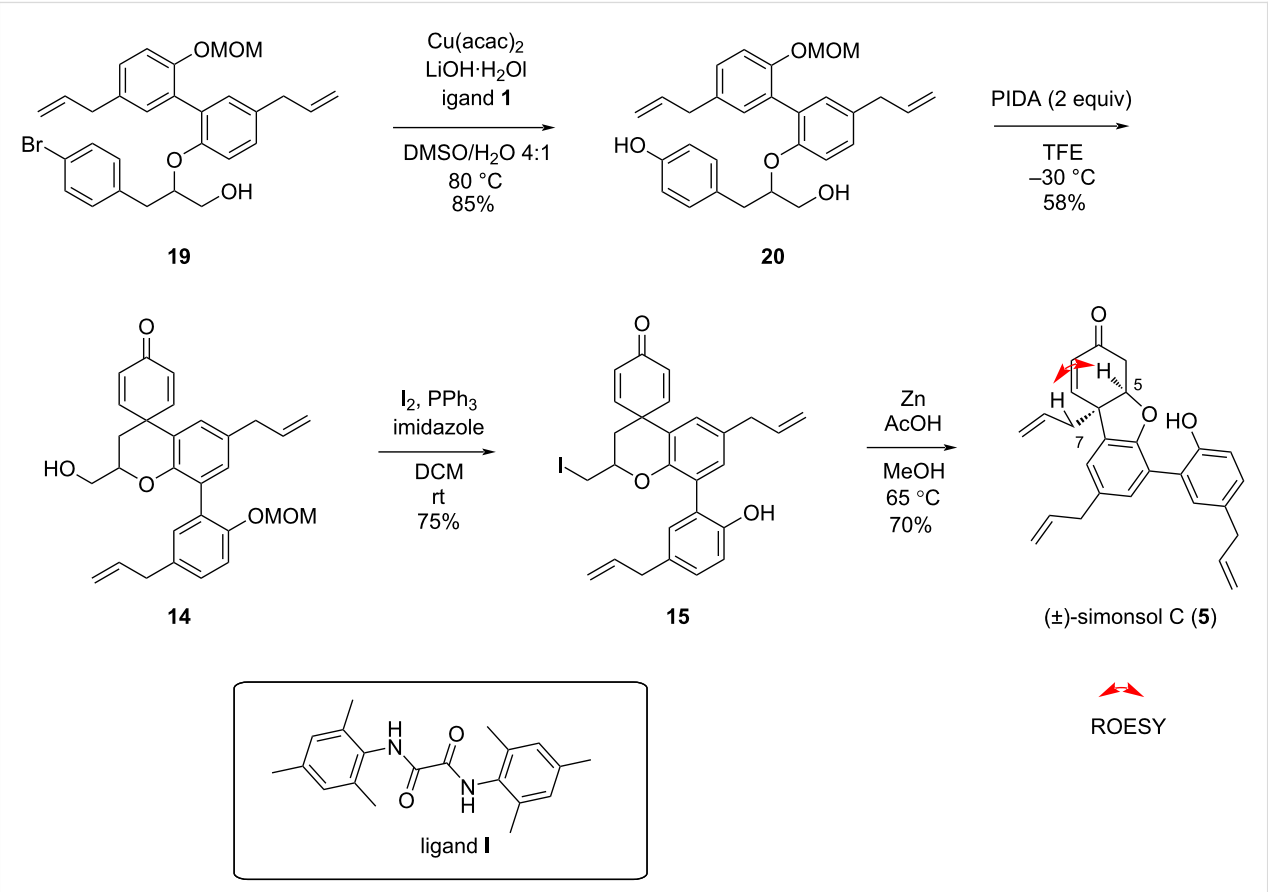

Scheme 4: Synthetic details to (±)-simonsol C.

benzofuran unit was formed through reductive elimination with Zn/AcOH and spontaneous oxy-Michael addition. This route largely enhances the synthetic efficiency and shortens the number of synthetic steps. The whole synthesis route involves 8 steps and affords the final product in a total yield of 13%, which could be the shortest synthesis route to date.

The structural motif of an all-carbon quaternary center containing an aryl group is common in many natural products, such as galanthamine and morphine. Our current strategy provides an alternative approach for the synthesis of aryl-containing quaternary carbon centers, which could be valuable for the synthesis of related natural products and their derivatives.

Supporting Information

Supporting Information File 1

Experimental procedures and characterization data of new compounds.
[https://www.beilstein-journals.org/bjoc/content/supplementary/1860-5397-21-47-S1.pdf]

Funding

This work was financially supported by start-up package of Yunnan Minzu University.

ORCID® iDs

Yong-Ming Chuan - https://orcid.org/0000-0003-3394-8618
Hong-Bo Qin - https://orcid.org/0000-0003-2603-9520

Data Availability Statement

All data that supports the findings of this study is available in the published article and/or the supporting information of this article.

Preprint

A non-peer-reviewed version of this article has been previously published as a preprint: https://doi.org/10.3762/bxiv.2025.3.v1

References

1. Zhang, X.; Meng, X.; Wu, J.; Huang, L.; Chen, S. *Chin. Med. (London, U. K.)* **2018,** *13,* 31. doi:10.1186/s13020-018-0186-9
2. Zou, Q.; Huang, Y.; Zhang, W.; Lu, C.; Yuan, J. *Molecules* **2023,** *28,* 7378. doi:10.3390/molecules28217378
3. Assiry, A. A.; Karobari, M. I.; Bhavikatti, S. K.; Marya, A. *BioMed Res. Int.* **2021,** 5510174. doi:10.1155/2021/5510174
4. Dong, C.; Liu, L.; Li, X.; Guan, Z.; Luo, H.; Wang, Y. *Planta Med.* **2013,** *79,* 338–347. doi:10.1055/s-0032-1328287
5. Sui, J.-J.; Wang, K.; Luo, S.-J.; Guo, K.; Yuan, M.-W.; Qin, H.-B. *J. Org. Chem.* **2024,** *89,* 7821–7827. doi:10.1021/acs.joc.4c00518
6. Arnold, R. E.; Saska, J.; Mesquita-Ribeiro, R.; Dajas-Bailador, F.; Taylor, L.; Lewis, W.; Argent, S.; Shao, H.; Houk, K. N.; Denton, R. M. *Chem. Sci.* **2024,** *15,* 11783–11793. doi:10.1039/d4sc03232b
7. Nugent, J.; Banwell, M. G.; Schwartz, B. D. *Org. Lett.* **2016,** *18,* 3798–3801. doi:10.1021/acs.orglett.6b01799
8. Magnus, P.; Sane, N.; Fauber, B. P.; Lynch, V. *J. Am. Chem. Soc.* **2009,** *131,* 16045–16047. doi:10.1021/ja9085534
9. Magnus, P.; Seipp, C. *Org. Lett.* **2013,** *15,* 4870–4871. doi:10.1021/ol402302k
10. Li, Q.; Zhang, H. *Chem. – Eur. J.* **2015,** *21,* 16379–16382. doi:10.1002/chem.201503594
11. Luo, G.; Li, X.; Zhang, G.; Wu, C.; Tang, Z.; Liu, L.; You, Q.; Xiang, H. *Eur. J. Med. Chem.* **2017,** *140,* 252–273. doi:10.1016/j.ejmech.2017.09.015
12. Nam, S.; Ware, D. C.; Brothers, P. J. *Org. Biomol. Chem.* **2018,** *16,* 6460–6469. doi:10.1039/c8ob00957k
13. Zhou, W.; Fan, M.; Yin, J.; Jiang, Y.; Ma, D. *J. Am. Chem. Soc.* **2015,** *137,* 11942–11945. doi:10.1021/jacs.5b08411
14. Roche, S. P.; Porco, J. A., Jr. *Angew. Chem., Int. Ed.* **2011,** *50,* 4068–4093. doi:10.1002/anie.201006017
15. Hu, J.; Bian, M.; Ding, H. *Tetrahedron Lett.* **2016,** *57,* 5519–5539. doi:10.1016/j.tetlet.2016.11.007
16. Küenburg, B.; Czollner, L.; Fröhlich, J.; Jordis, U. *Org. Process Res. Dev.* **1999,** *3,* 425–431. doi:10.1021/op990019q

License and Terms

BEILSTEIN JOURNAL OF ORGANIC CHEMISTRY

Recent advances in controllable/divergent synthesis

Jilei Cao[1], Leiyang Bai[*1] and Xuefeng Jiang[*1,2,3]

Review

Open Access

Address:
[1]Hainan Institute of East China Normal University, State Key Laboratory of Petroleum Molecular & Process Engineering, Shanghai Key Laboratory of Green Chemistry and Chemical Process, School of Chemistry and Molecular Engineering, East China Normal University, 3663 North Zhongshan Road, Shanghai 200062, PR China, [2]School of Chemistry and Chemical Engineering, Henan Normal University, Xinxiang, Henan 453007, PR China and [3]State Key Laboratory of Organometallic Chemistry, Shanghai Institute of Organic Chemistry, Chinese Academy of Sciences, 345 Lingling Road, Shanghai 200032, PR China

Email:
Leiyang Bai[*] - lybai@chem.ecnu.edu.cn; Xuefeng Jiang[*] - xfjiang@chem.ecnu.edu.cn

* Corresponding author

Keywords:
controllable; divergent; diverse products; switchable synthesis

Beilstein J. Org. Chem. **2025,** *21,* 890–914.
https://doi.org/10.3762/bjoc.21.73

Received: 10 February 2025
Accepted: 22 April 2025
Published: 07 May 2025

This article is part of the thematic issue "Concept-driven strategies in target-oriented synthesis".

Guest Editor: C. Li

Abstract

The development of streamlined methodologies for the expeditious assembly of structurally diverse organic architectures represents a paramount objective in contemporary synthetic chemistry, with far-reaching implications across pharmaceutical development, advanced materials innovation, and fundamental molecular science research. In recent years, controllable/divergent synthetic strategies for organic functional molecules using common starting materials have garnered significant attention due to their high efficiency. This review categorizes recent literatures focusing on key regulatory factors for product divergent formation, in which controlling chemical selectivity primarily relies on ligands, metal catalysts, solvents, time, temperature, acids/bases, and subtle modifications of substrates. To gain a deeper understanding of the mechanisms underlying reaction activity and selectivity differentiation, the review provides a systematic analysis of the mechanisms of critical steps through specific case studies. It is hoped that the controllable/divergent synthesis concept will spark the interest of practitioners and aficionados to delve deeper into the discipline and pursue novel advancements in the realm of chemical synthesis.

Introduction

In the era of synthetic organic chemistry, divergence can produce stereodivergence (including diastereodivergence and enantiodivergence) [1-4] and regiodivergence [5,6]. In both cases, starting from the same substrate, different stereoisomers (diastereomers and enantiomers) or regioisomers can be obtained under different reaction conditions. Over the past two decades, researchers have found that by changing reaction conditions and modifying the substrate, two structurally distinct

products that are neither stereoisomers nor regioisomers can be obtained from the same starting material (using the same reagents, if necessary), and significant progress has been made in recent years. Controllable/divergent synthetic strategies have increasingly attracted attention [5,7-14], for example, in 2024, Rana [15] and co-workers reported advances in solvent-controlled stereodivergent catalysis. Surprisingly, to our knowledge, there is currently no comprehensive review of studies on controllable/divergent synthesis. This review systematically examines, how these multidimensional control elements (including ligands, metal catalysts, solvents, time, temperature, acids/bases, and subtle modifications of substrates) synergize to achieve predictable product diversification. In addition, mechanistic insights are discussed providing illustrative examples across reaction classes, and emerging strategies for programming synthetic outcomes. The integration of these approaches promises to accelerate drug discovery and materials development through sustainable, atom-economic synthesis of complex molecular libraries.

Review

Ligand control

The precise regulation of product selectivity represents a fundamental challenge in transition-metal-catalyzed organic transformations, with significant implications for complex molecule synthesis. In this context, ligand-modulated divergent catalysis has emerged as a paradigm-shifting strategy, enabling programmable access to structurally distinct molecular architectures from identical substrate precursors through precise manipulation of metal coordination [16-18]. This sophisticated approach capitalizes on the stereoelectronic tunability of ancillary ligands to dictate reaction pathways, thereby offering unprecedented control over chemo-, regio-, and stereoselectivity parameters in catalytic manifolds. In 2015, the Jiang group developed a palladium-catalyzed regioselective three-component C1 insertion reaction (Scheme 1) [19]. In this reaction, an *o*-iodoaniline **1**, phenylacetylene, and carbon monoxide were used as starting materials, and two natural product frameworks of phenanthridone and acridone alkaloids could be selectively obtained by controlling ligands. The reaction of *o*-iodoaniline with in situ-generated arynes under CO atmosphere under ligand-free conditions selectively afforded phenanthridinones. Intriguingly, switching to the electron-rich bidentate ligand bis(diphenylphosphino)methane (dppm) redirected the pathway to yield acridones. Time-dependent NMR studies revealed that the selectivity hinges on the aryne release kinetics from its precursor. Employing CsF, tetrabutylammonium iodide (TBAI), and water significantly accelerated aryne generation, thereby increasing its local concentration. This favored aryne coordination to the palladium center, followed by CO insertion and reductive elimination to furnish phenanthridinones. In contrast, when dppm was introduced, oxidative addition of the C–I bond to palladium formed the four-membered aryl–palladium complex **Int-5**. Steric hindrance from the bulky dppm ligand, combined with slower aryne release (using KF as the fluoride source), attenuated aryne coordination. Under these electron-deficient conditions, CO preferentially occupied the palladium coordination site. Sequential insertion of CO and aryne, followed by reductive elimination, culminated in acridone formation. This ligand-dependent mechanistic dichotomy underscores the critical interplay between aryne availability, steric modulation, and electronic effects in steering catalytic selectivity.

In 2016, the Jiang group achieved regioselective control in the gold-catalyzed intramolecular hydroarylation of alkynes by modulating the electronic and steric effects of ligands (Scheme 2) [20]. Mechanistically, the electron-deficient phosphite ligand **L1** and the weakly coordinating OTf^- anion synergistically enhanced the electrophilicity of the gold center, enabling coordination with the amide group to form a three-coordinate Au(I)–π-alkyne intermediate **Int-12**. The umbrella-shaped steric shielding provided by the ligand-stabilized intermediate **Int-9**, followed by Friedel–Crafts-type addition and protonation to complete *ortho*-position cyclization. In contrast, *para*-position cyclization was exclusively achieved through π–π interactions between the electron-rich X-phos ligand and the substrate, compensating for the electron-deficient nature of the aromatic system and ensuring high regioselectivity.

In 2018, the Jiang group developed a regiodivergent synthetic method for indolo[3,2-*c*]coumarins **10** and benzofuro[3,2-*c*]quinolinones **9** via controllable palladium(II)-catalyzed carbonylative cyclization (Scheme 3) [21]. When ligand **L3** coordinates with the palladium center, the enhanced electrophilicity of palladium facilitates preferential coordination with the amino group and activates the alkyne to form the intermediate **Int-14** instead of **Int-14'**. Subsequent nucleophilic cyclization generates intermediate **Int-15**. Following CO insertion, complex **Int-16** is formed, and reductive elimination yields the benzofuro[3,2-*c*]quinolinone product **9** along with a Pd(0) species, which is reoxidized to Pd(II) by BQ (benzoquinone). When the ligand is switched to the sterically bulky and electron-rich dppm, the chemoselectivity is reversed: the palladium center now preferentially coordinates with the hydroxy group to form complex **Int-17** and the amino group undergoes nucleophilic attack to generate **Int-18**. After CO insertion complex **Int-19** is produced and reductive elimination ultimately affords the indolo[3,2-*c*]coumarin product **10**.

In 2023, the Garg group achieved the first example of utilizing in situ-generated π-allylpalladium complexes to capture strained

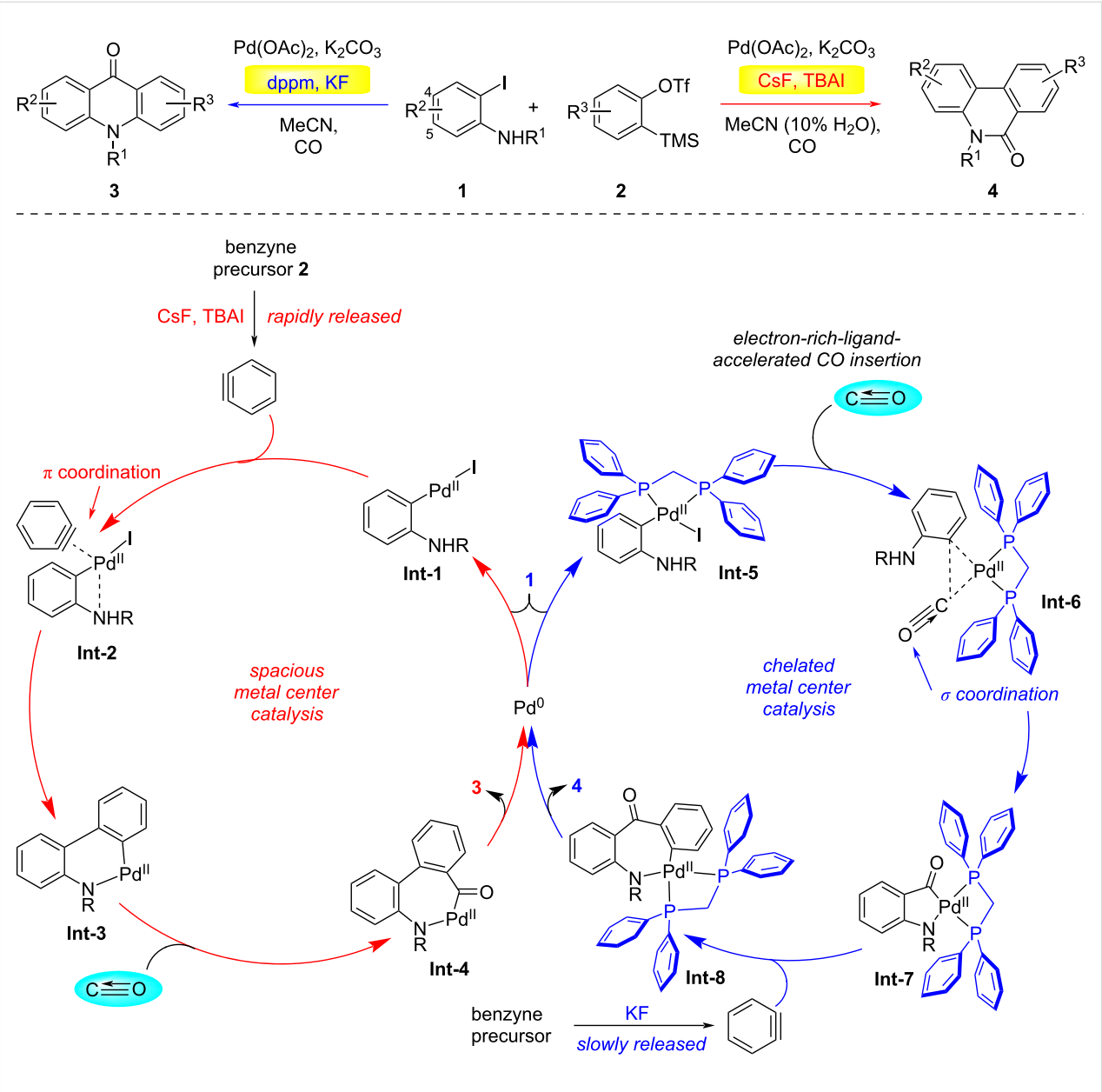

Scheme 1: Ligand-controlled regiodivergent C1 insertion into arynes [19].

cyclic allene intermediates (Scheme 4) [22]. By modulating the ligands in the reaction system, two distinct polycyclic scaffolds, **13** or **14**, could be synthesized with high selectivity. Mechanistically, the Pd(0) catalyst coordinates to substrate **11**, followed by oxidative addition and release of carbon dioxide to form the zwitterionic π-allylpalladium intermediate **Int-21**. Under the reaction conditions, silyl triflate **12** undergoes a fluoride-mediated 1,2-elimination to generate the cyclic allene intermediate **Int-22**. Through a ligand-controlled regioselective migratory insertion process, reaction of **Int-21** and **Int-22** leads to the formation of π-allylpalladium intermediates **Int-23** or **Int-24**, depending on the ligand employed. Finally, cyclization of **Int-23** or **Int-24** yields the tricyclic product **13** or the tetracyclic product **14**, respectively.

In 2024, the Song group achieved a ligand-controlled regiodivergent and enantioselective ring expansion of benzosilacyclobutenes with internal naphthylalkynes by strategically modulating the ligand steric profiles (Scheme 5) [23]. Employing cavity-engineered phosphoramidite ligands, the reaction pathway bifurcated based on the steric demands of Si–C-bond activation. The methyl-substituted ligand (*S*)-8*H*-binaphthyl phosphoramidite **L4**, featuring a spacious cavity, favored sterically encumbered Si–C(sp^3)-bond activation, selectively delivering

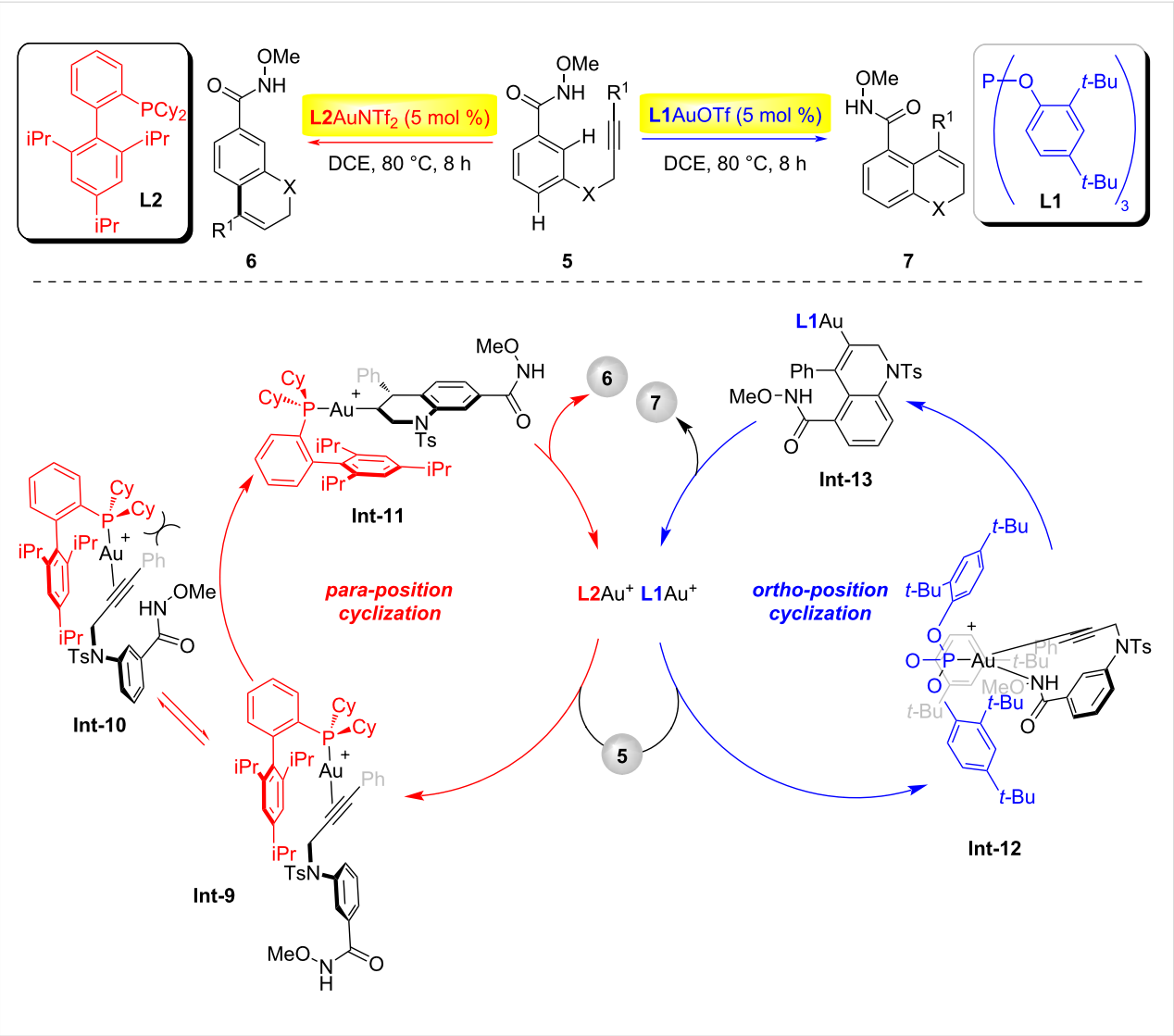

Scheme 2: Ligand effect in homogenous gold catalysis enabling regiodivergent π-bond-activated cyclization [20].

axially chiral (*S*)-1-silacyclohexenyl arenes **17** with high enantiocontrol. Conversely, the bulky *tert*-butyl-decorated (*R*)-spirophosphoramidite **L5** imposed a confined cavity, steering selectivity toward Si–C(sp^2)-bond activation and predominantly afforded the regioisomeric (*S*)-2-silacyclohexenylarenes **18**.

In 2025, Gong and co-workers reported a visible-light-mediated hydrogen atom transfer (HAT)/chiral copper dual catalytic system that achieved regiodivergent and enantioselective C(sp^3)–C(sp^3) and C(sp^3)–N oxidative cross-couplings between *N*-arylglycine ester/amide derivatives and abundant hydrocarbon C(sp^3)–H feedstocks (Scheme 6) [24]. This methodology also represents a highly challenging direct C(sp^3)–H asymmetric amination. Mechanistic insights: When using a bulky, electron-rich chiral bisphosphine ligand **L6**, the glycine ester substrate coordinates with the copper catalyst to form a key intermediate complex **Int-26**. The sterically hindered and electron-rich environment around the copper center disfavors a direct interaction with nucleophilic alkyl radicals. Instead, the reaction proceeds via an outer-sphere mechanism, where the alkyl radical reacts with the copper-activated C=N unsaturated bond, enabling stereocontrolled C(sp^3)–C(sp^3) coupling. In contrast, with the anionic cyano-substituted bisoxazoline ligand **L7**, the glycine ester and copper catalyst form a distinct intermediate complex **Int-28**. The ligand's reduced steric bulk and altered electronic properties facilitate direct interaction with alkyl radicals, forming a high-valent Cu(III) intermediate **Int-29**. This intermediate undergoes reductive elimination via an inner-sphere mechanism to generate the C(sp^3)–N-coupled chiral product **22**. Notably, benzoic acid acts as a critical additive, likely by stabilizing key intermediates and modulating the steric/electronic environment for enhanced enantiocontrol.

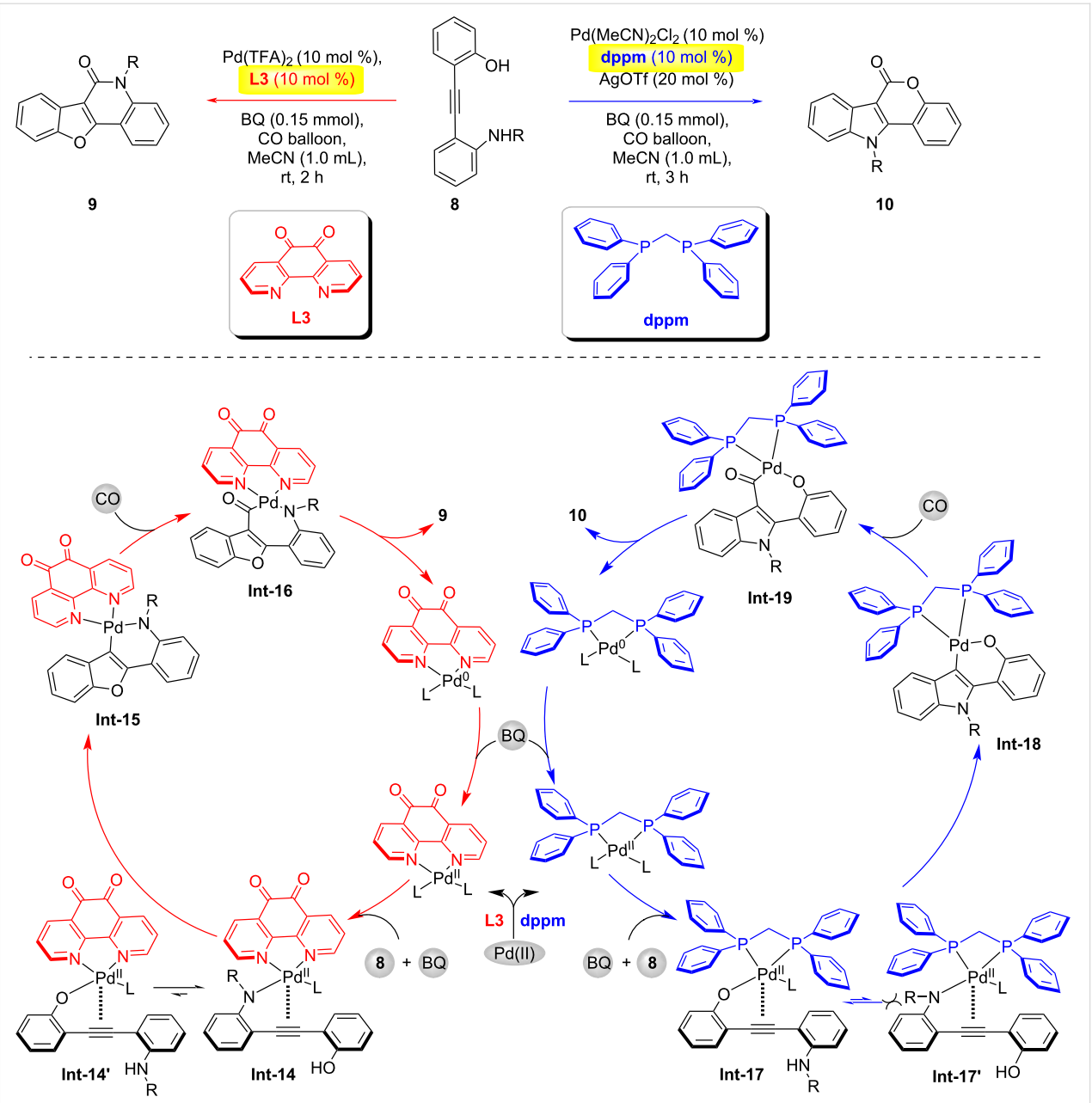

Scheme 3: Ligand-controlled palladium(II)-catalyzed regiodivergent carbonylation of alkynes [21].

Metal control

Over the past decade, the relentless pursuit of precision in natural products and pharmaceutical synthesis has driven remarkable advances in catalytic methodologies, particularly in the realm of catalyst-controlled chemoselective transformations [11,25-29]. In 2023, the Shu group developed a catalyst-controlled regioselective and enantioselective hydroamination reaction of electron-deficient alkenes (Scheme 7) [30]. By efficiently regulating the regioselectivity and enantioselectivity of alkene **23** hydrometallation through catalytic systems, they overcame the influence of steric and electronic effects during the hydrometallation process, simultaneously achieving the synthesis of chiral α-quaternary carbon amino acid derivatives **26** and α-chiral β-amino acid derivatives **27**. Using a copper catalyst, the chiral α-quaternary carbon amino acid derivatives **26** were obtained with exclusive regioselectivity and excellent enantioselectivity. Employing a nickel catalyst, α-chiral β-amino acid derivatives **27** were synthesized with single regioselectivity and outstanding enantioselectivity.

In the same year, Rong and co-workers reported a highly efficient catalyst-controlled regio- and enantioselective hydroalkyl-

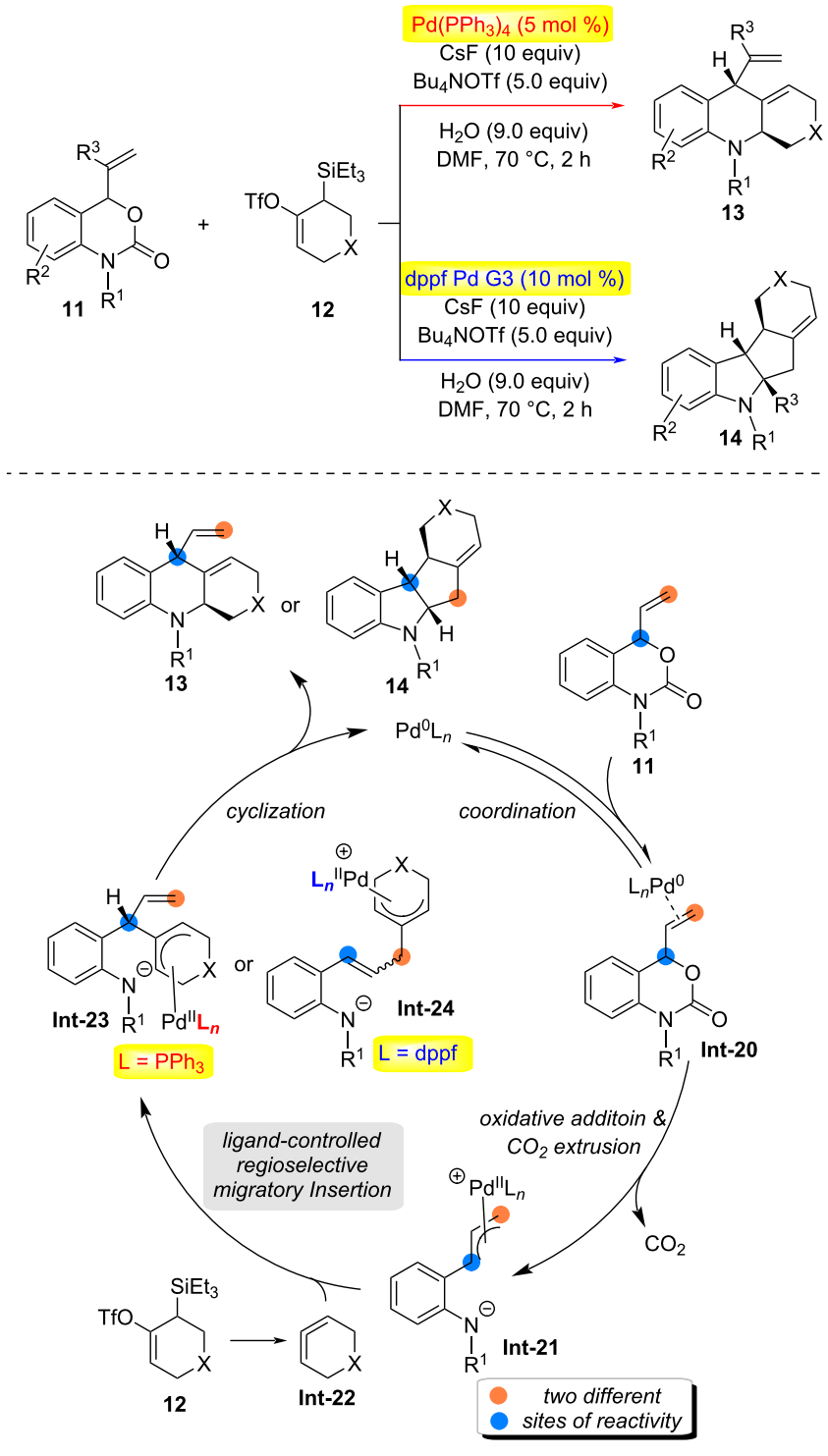

Scheme 4: Catalyst-controlled annulations of strained cyclic allenes with π-allyl palladium complexes and proposed mechanism [22].

ation reaction, enabling the divergent synthesis of chiral C2- and C3-alkylated pyrrolidines through desymmetrization of readily available 3-pyrrolines (Scheme 8) [31]. The cobalt catalytic system ($CoBr_2$ with modified bisoxazoline ligands) achieved asymmetric $C(sp^3)$–$C(sp^3)$ coupling via distal stereocontrol, efficiently producing C3-alkylated pyrrolidines, while the nickel catalytic system afforded C2-alkylated pyrrolidines through a tandem alkene isomerization/hydroalkylation process.

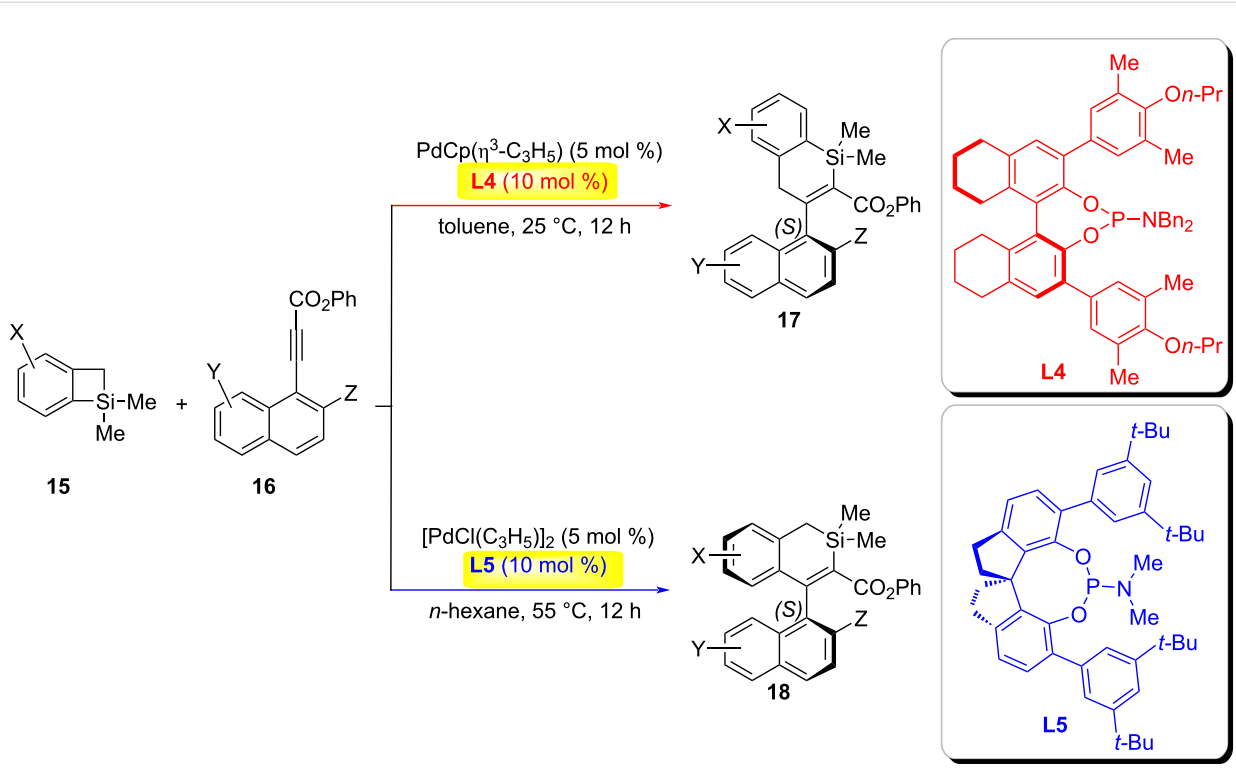

Scheme 5: Ring expansion of benzosilacyclobutenes with alkynes [23].

This method utilized readily accessible catalysts, chiral BOX ligands **L9**, and reagents, delivering enantioenriched 2-/3-alkyl-substituted pyrrolidines with excellent regio- and enantioselectivity (up to 97% enantiomeric excess). Radical-clock experiments and deuterium-labeled silane studies revealed that cobalt catalysis proceeded via irreversible Co–H migratory insertion to achieve C3 selectivity, whereas nickel catalysis involved alkene isomerization to generate a (2,3-dihydropyrrolyl) intermediate **Int-35**, followed by C2-selective coupling.

In 2024, the Zheng group reported a catalyst-controlled cyclization reaction of bicyclo[1.1.0]butanes (BCBs) **32** with α-alkenylazides **33**, achieving divergent synthesis of 2- and 3-azabicyclo[3.1.1]heptenes (aza-BCHepes) **35** or **36** (Scheme 9) [32]. This study developed a practical method for constructing novel 2- and 3-aza[3.1.1]heptene architectures from readily available α-alkenylazides and BCBs through catalyst-controlled (3 + 3) and (3 + 2) cyclization strategies. Two distinct pathways were established: (1) The titanium-catalyzed ring opening of bicyclobutane (BCB) **32** generates a γ-carbonyl radical intermediate **Int-42**, which undergoes trapping by vinylazide **33**. Subsequent dinitrogen extrusion produces an iminyl radical species **Int-44**. This reactive intermediate then engages with a Ti(IV)-enolate complex through radical recombination, ultimately delivering 2-aza-bicyclo[3.1.1]heptene (BCHepe) while regenerating the Ti(III) catalyst to complete the catalytic cycle. (2) Scandium-catalyzed pathway: Activation of the donor–acceptor BCB via $Sc(OTf)_3$ coordination to its carbonyl group facilitates nucleophilic attack by vinylazide **33**, forming an iminodiazonium intermediate **Int-40** accompanied by a δ-carbanion. Transannular cyclization of this species affords 2-azidobicyclo[3.1.1]hexane (2-azidoBCHs). Subsequent thermal activation induces selective migration of the less sterically hindered secondary carbon center with concomitant dinitrogen elimination, yielding 3-aza-BCHepe as the final product.

Solvent control

The solvent microenvironment emerged as a critical determinant in governing stereochemical outcomes, exerting profound influence through multifaceted solute–solvent interactions [5]. Solvent polarity, hydrogen-bonding propensity, and dielectric characteristics collectively orchestrate stereodivergent pathways through dynamic coordination effects and differential stabilization of transition states. Notably, these solvent-mediated electronic and steric modulations frequently dictate reaction stereoselectivity, with even subtle solvent permutations potentially inducing complete stereochemical inversion in sensitive systems [33-38]. In 2023, He and Sessler disclosed a versatile one-pot synthesis of structurally diverse macrocycles through the dynamic self-assembly of α,α'-linked oligopyrrolic

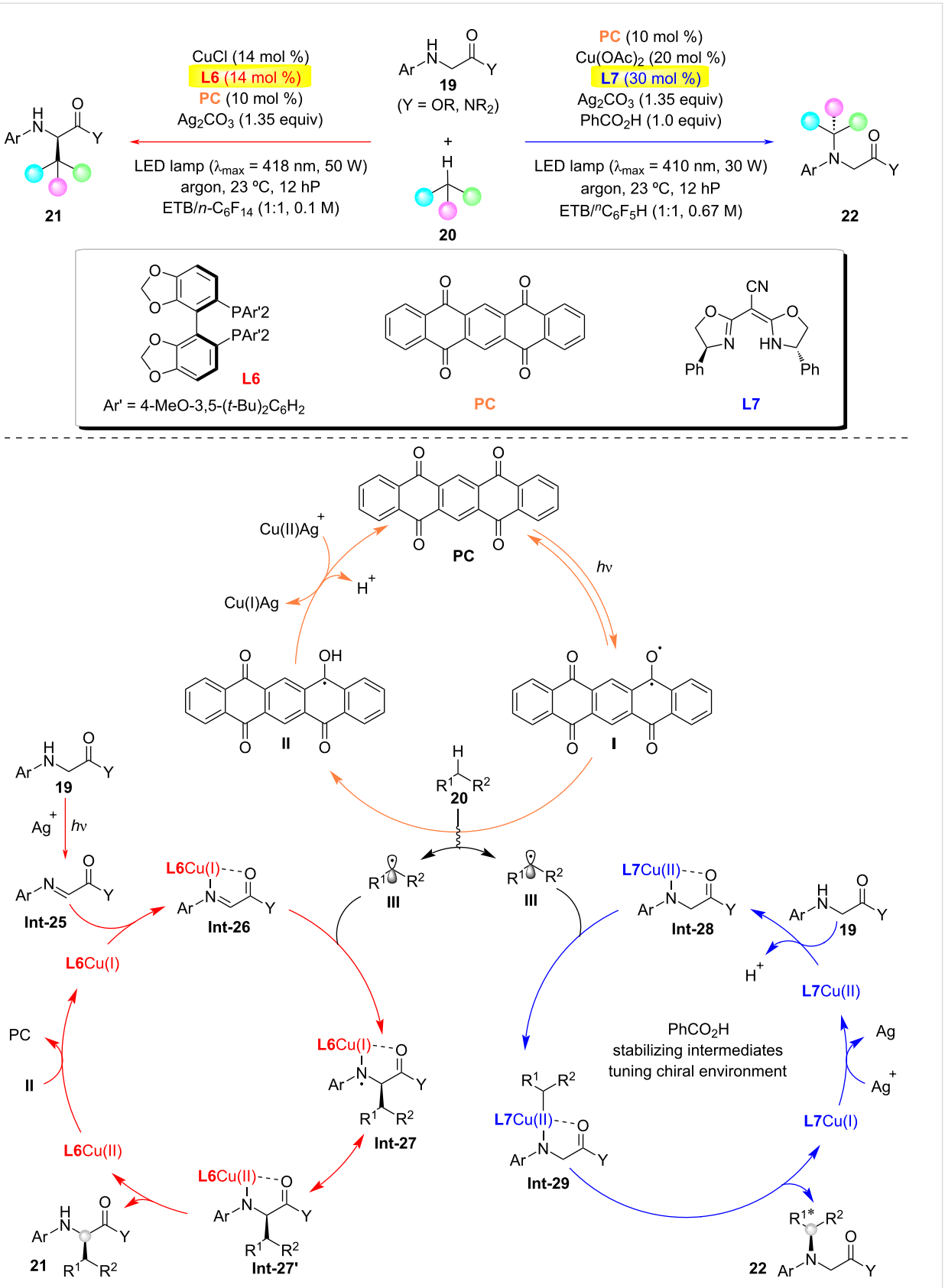

Scheme 6: Photoinduced regiodivergent and enantioselective cross-coupling [24].

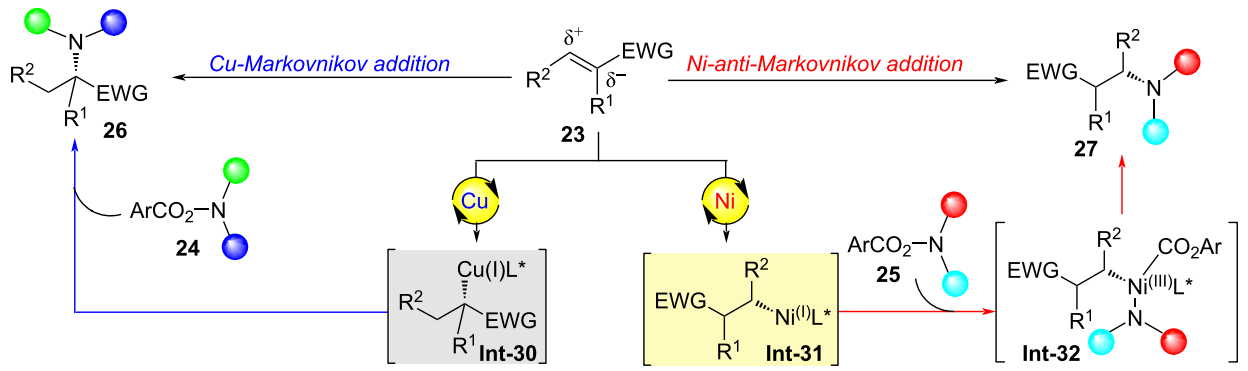

Scheme 7: Catalyst-controlled regiodivergent and enantioselective formal hydroamination of *N*,*N*-disubstituted acrylamides [30].

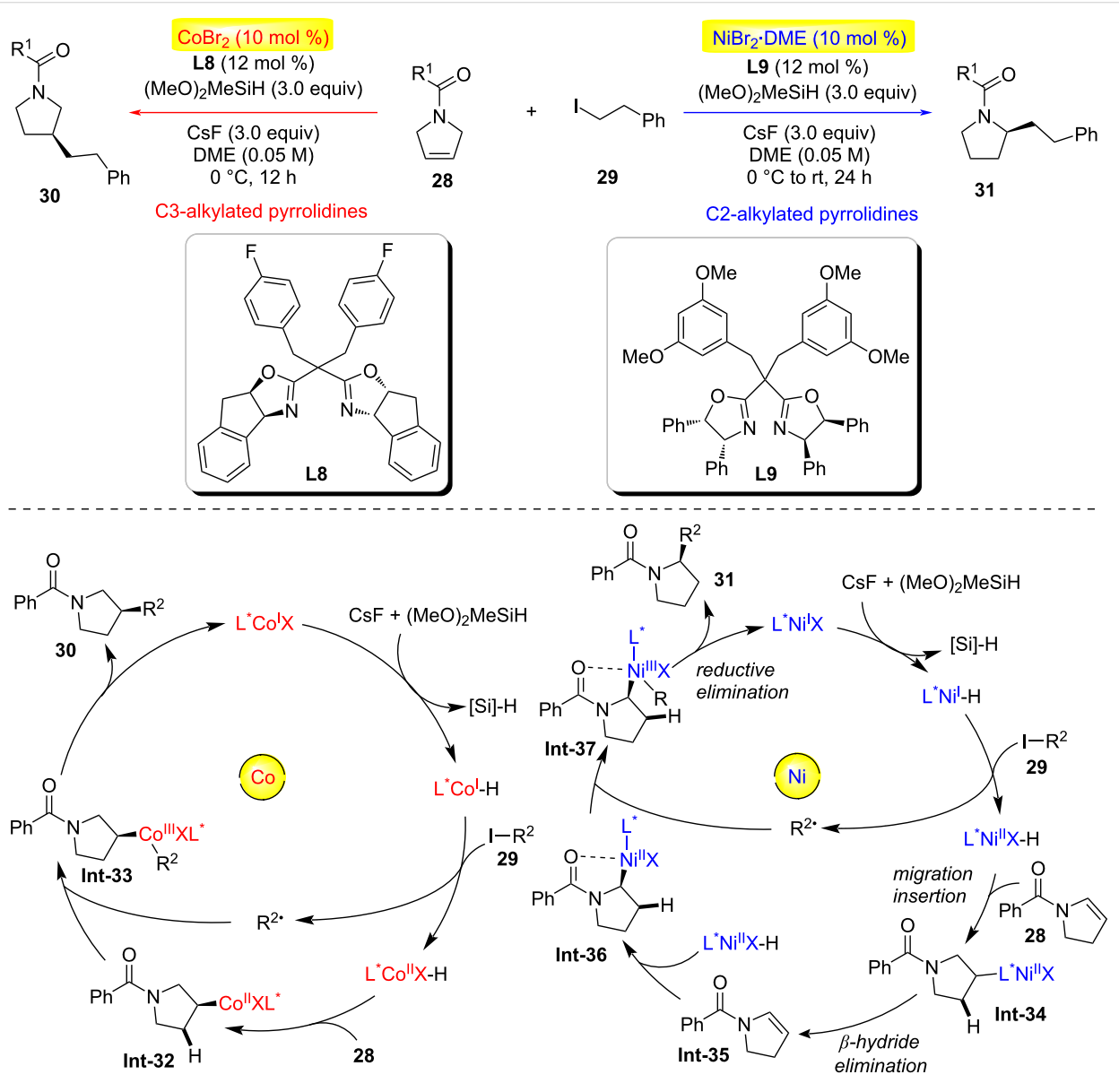

Scheme 8: Catalyst-tuned regio- and enantioselective C(sp^3)–C(sp^3) coupling [31].

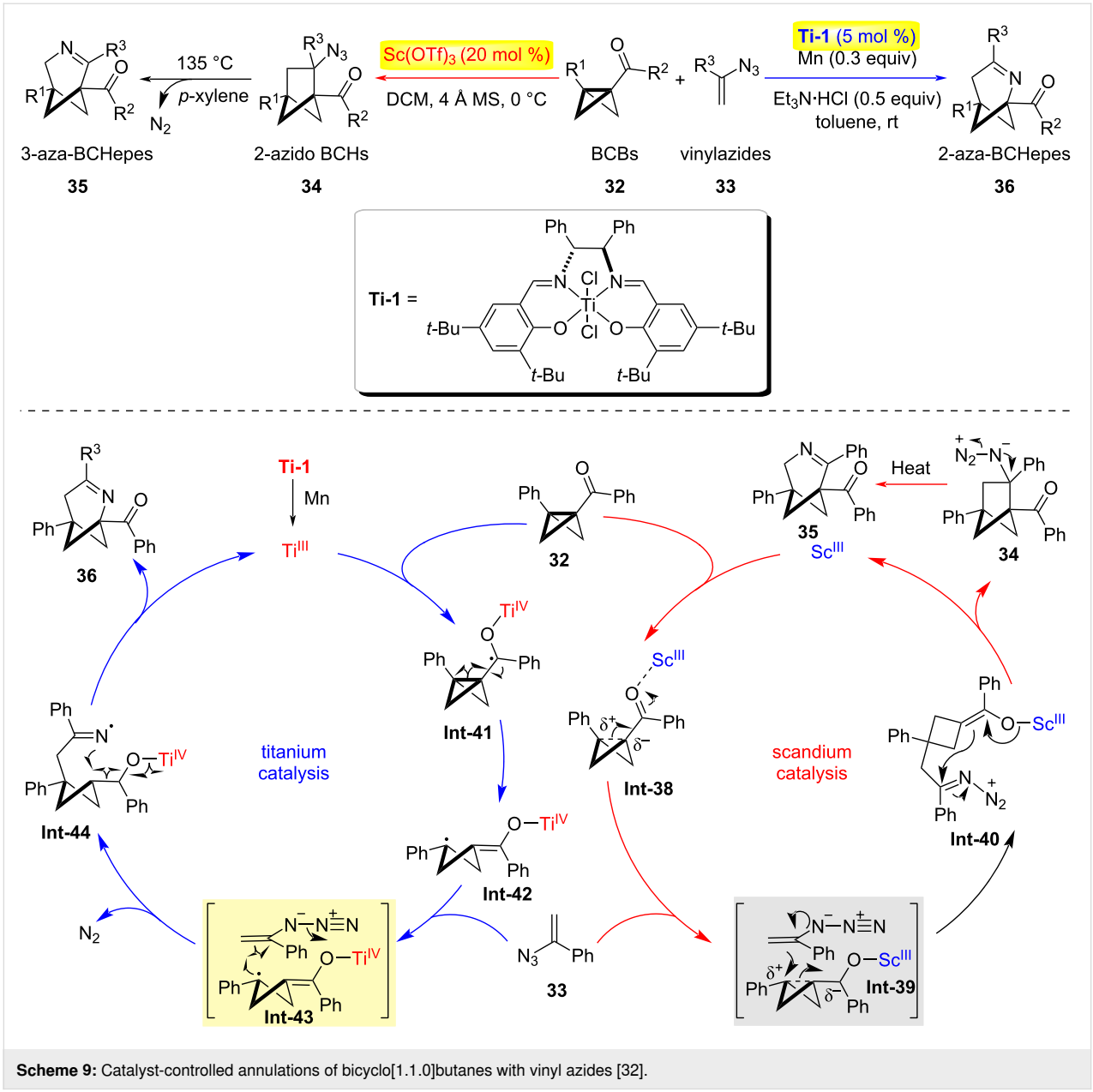

Scheme 9: Catalyst-controlled annulations of bicyclo[1.1.0]butanes with vinyl azides [32].

dialdehydes and alkyldiamines (Scheme 10) [39]. Their investigation revealed distinct solvent-mediated selectivity in product formation. Condensation of the pyridine-bridged oligopyrrolic dialdehyde **37** with simple alkyldiamines proceeded with solvent-independent regioselectivity, exclusively furnished [2 + 2] macrocyclic adducts. Strikingly, when **37** was combined with 2,2'-oxybis(ethylamine) (**38**), the reaction pathway exhibited pronounced solvent dependency. Reactions in methanol, ethanol, or chloroform selectively generated the [1 + 1] macrocycle **39** as the sole product. In contrast, polar aprotic solvents such as dimethyl sulfoxide (DMSO), *N*,*N*-dimethylformamide (DMF), or acetonitrile (MeCN) favored precipitation of the [2 + 2] macrocycle **40**. Notably, the macrocycle **40** underwent spontaneous structural reorganization in chloroform or dichloromethane (DCM), converting entirely into the thermodynamically stable [1 + 1] isomer **39**. This work demonstrates a solvent-driven approach for dynamically interconverting macrocycle sizes, governed by thermodynamic stability and solubility differences.

In the same year, Chauhan, Koenigs, and co-workers demonstrated solvent-controlled bifurcation in the light-driven reactivity of cyclic diazo imides **41** with thiols **42**, unveiling two mechanistically distinct pathways (Scheme 11) [40]. In dichloromethane (DCM), the reaction proceeds via a carbene intermediate, enabling cascade C(sp^2)–H functionalization/thio-

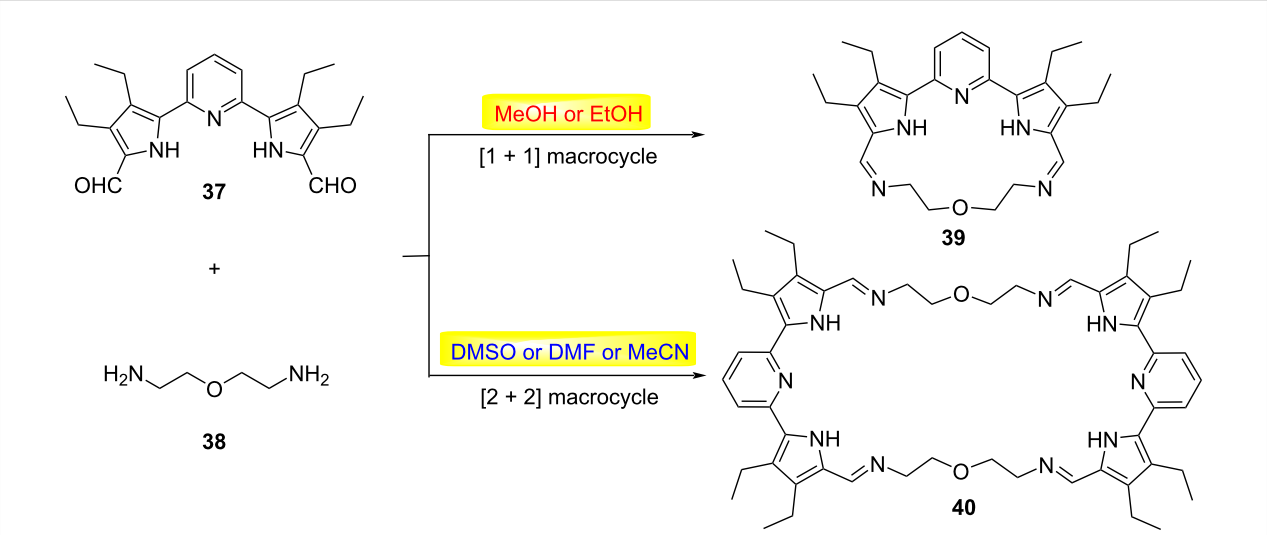

Scheme 10: Solvent-driven reversible macrocycle-to-macrocycle interconversion [39].

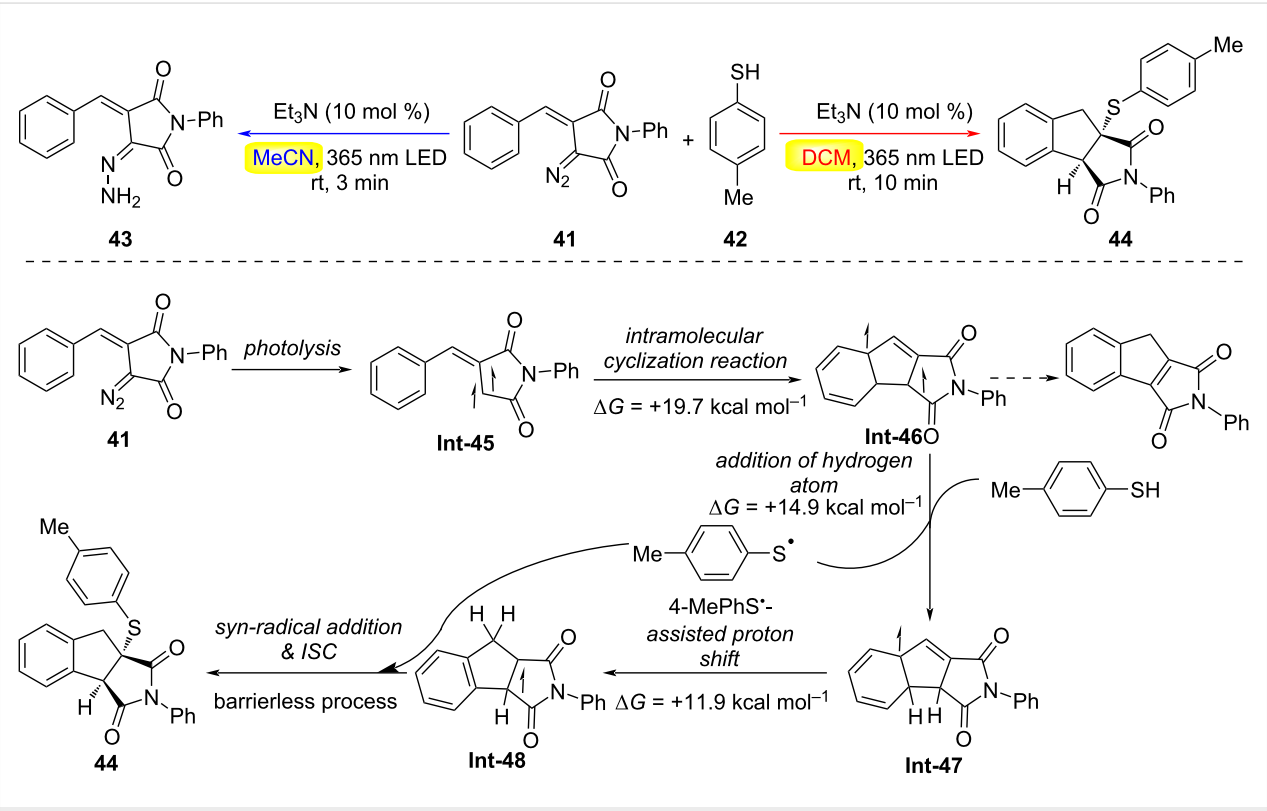

Scheme 11: Unexpected solvent-dependent reactivity of cyclic diazo imides and mechanism [40].

lation to deliver indane-fused pyrrolidines **43** in excellent yields (up to 92%). Strikingly, switching the solvent to acetonitrile completely suppresses carbene formation under identical conditions, redirecting the pathway toward an unconventional diazo reduction wherein aryl thiols act as stoichiometric reductants. Mechanistic insights, elucidated through control experiments and DFT calculations, revealed that photoexcitation of diazo imide **41** triggers nitrogen extrusion ($\Delta G^{\ddagger}$ = +10.0 kcal·mol^{-1}), generating the triplet carbene intermediate **Int-45**. In DCM, this species undergoes intramolecular cyclization into a proximal C(sp^2)–H bond ($\Delta G^{\ddagger}$ = +19.7 kcal·mol^{-1}) to form **Int-46**, which reacts with 4-MePhSH ($\Delta G^{\ddagger}$ = +14.9 kcal·mol^{-1}) to yield

radical intermediate **Int-47** and a thiyl radical (4-MePhS˙). Sequential thiol-assisted hydrogen shifts produce **Int-48**, followed by barrierless thiyl radical addition and intersystem crossing (ISC) to furnish the final product. In contrast, acetonitrile's polar aprotic environment destabilizes the carbene pathway, favoring direct reduction of the diazo moiety via electron transfer from the thiol. This solvent-gated selectivity underscores the critical role of reaction medium polarity in modulating reactive intermediates, offering a strategic lever to toggle between C–H functionalization and reductive manifolds in photochemical transformations.

In 2024, the Cheng group developed a palladium/chiral norbornene (NBE)-catalyzed cyclization reaction between aryl iodides **45** and phosphoramides **46** under varying solvent conditions of toluene (PhMe) and acetonitrile (MeCN), based on their studies of the Catellani reaction (Scheme 12) [41]. This method exhibited a broad substrate scope for both aryl iodides and phosphoramides, and enabled enantioselective access to both enantiomers of chiral P(V) molecules **47** or **48** using a single chiral NBE catalyst.

Time control

Time control of chemical reactivity offers an inherent strategy to program synthetic pathways through kinetic discrimination of transient intermediates. Diverging from additive-dependent or stimulus-responsive approaches, this paradigm capitalizes on the chronoselective evolution of reactive species to unlock sequence-controlled transformations. In 2020, the You group reported a reaction-time-dependent enantiodivergent synthesis method. Under the same chiral catalytic system, they achieved selective synthesis of either enantiomer of a target product by controlling the reaction duration (Scheme 13) [42]. When performing the asymmetric intermolecular allylic amination of 6-hydroxyisoquinoline (**49**) with *tert*-butyl(1-phenylallyl)carbonate ((*rac*)-**50**) using an Ir catalyst derived from $[Ir(cod)Cl]_2$ and the Carreira chiral phosphoramidite ligand (*S*)-**L10**, along with the addition of 3,5-dichlorobenzoic acid as an additive in MeOH at room temperature, the reaction proceeded smoothly for 10 hours to yield the aminated product **51**. Interestingly, when the reaction was quenched after 6 minutes in the absence of a Brønsted acid additive, the opposite enantiomer **52** was obtained. Mechanistically, an initial kinetic resolution (KR) of (*rac*)-**50** occurs via an Ir-catalyzed asymmetric allylic amination. Due to the higher reactivity of (*S*)-**50**, it reacts with 6-hydroxyisoquinoline within 6 minutes to generate **52**, while (*R*)-**50** remains largely unreacted during this period ($k_1^R << k_1^S$). However, as the reaction progresses, **52** undergoes further reaction with MeOH under the catalytic system to form **52'**. Meanwhile, the less reactive (*R*)-**50** gradually reacts with 6-hydroxyisoquinoline, leading to the accumulation of **51**. Since **51** is highly stable and resistant to reaction with MeOH ($k_2^R << k_2^S \approx k_1^R$), it can be obtained with high optical purity after an extended reaction time (10 hours)

In 2023, Yang and Liang jointly reported a tetrasilane (ODCS)-based method for time-controlled, palladium-catalyzed C–H activation in the divergent synthesis of silacyclic compounds

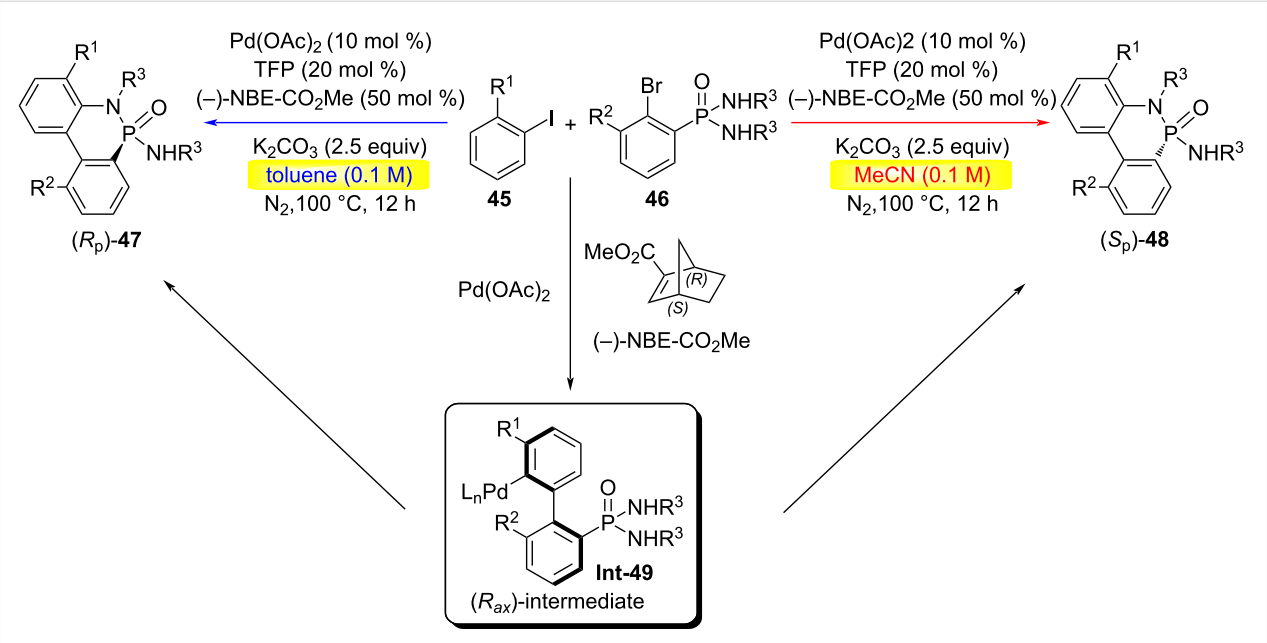

Scheme 12: Palladium-catalyzed annulation of prochiral *N*-arylphosphonamides with aromatic iodides [41].

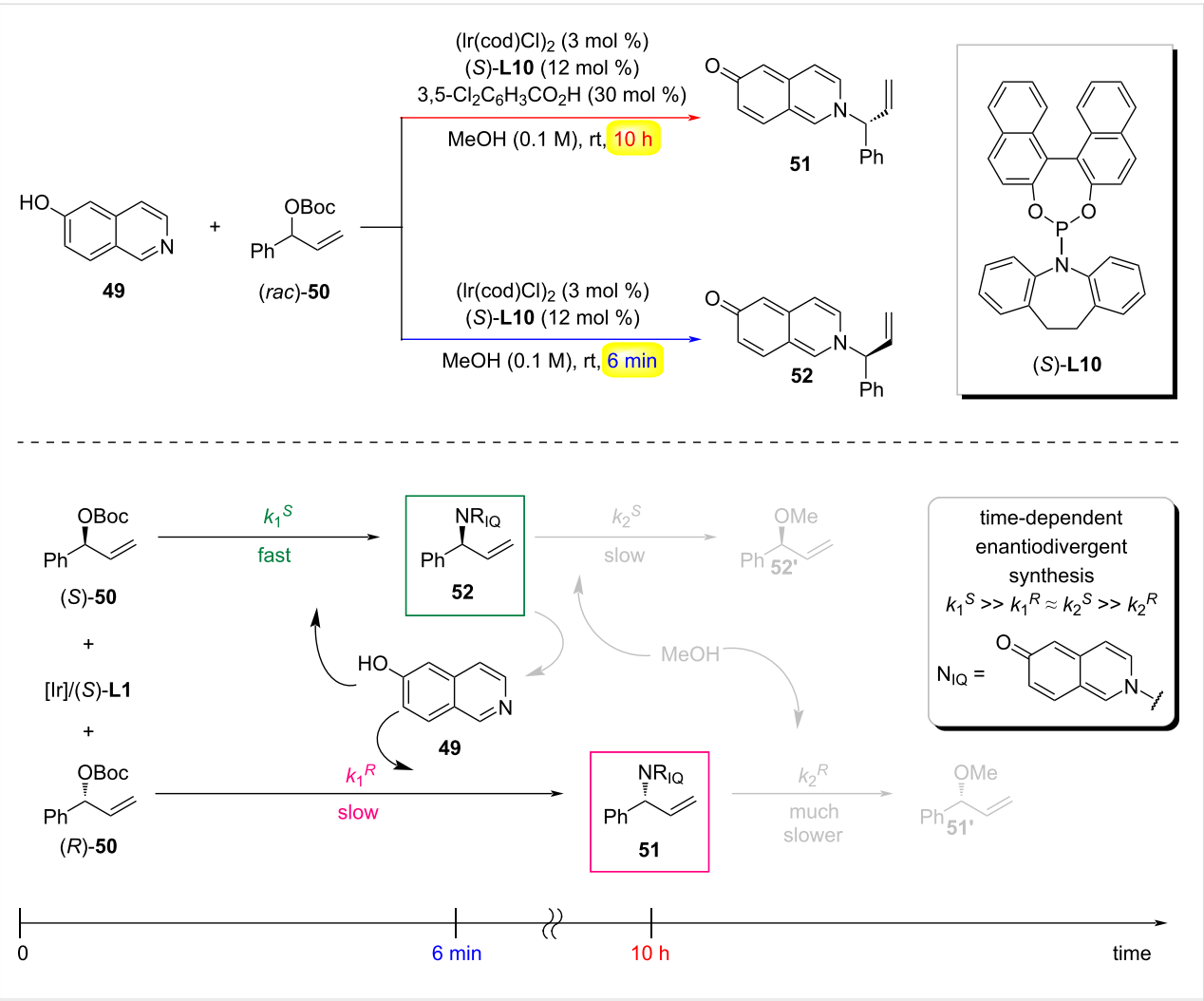

Scheme 13: Time-dependent enantiodivergent synthesis [42].

(Scheme 14) [43]. This reaction employs the ODCS reagent to capture a five-membered C,C-palladacycle species, using reaction time as a control switch to enable transformations of three distinct substrates – acrylamides, 2-halo-*N*-methylacryloylbenzamides, and 2-iodobiphenyls – thereby selectively synthesizing silacyclic compounds with varying ring sizes, including ten-membered, seven-membered, and five-membered rings. Mechanism (Scheme 15): Substrate **53** undergoes oxidative addition with Pd(0), followed by intramolecular carbopalladation to form the σ-alkylpalladium intermediate **Int-50**. The intermediate **Int-50** undergoes C–H activation to generate the spiro-palladacycle **Int-51**, which proceeds via two possible pathways: 1) Path a: oxidative addition/reductive elimination or 2) path b: transmetalation/reductive elimination giving rise to intermediates **Int-53** or **Int-53'**. Reductive elimination of **Int-53** or **Int-53'** regenerates Pd(0) and produces intermediate **55**. With the assistance of the base K_2CO_3, the ten-membered silacycle **55** undergoes rapid ring contraction via cleavage of two Si–O bonds and formation of one Si–O bond, leading to **56** and **Int-55**. Concurrently, **Int-55** dimerizes to form **54**, which is further transformed into cyclosiloxanes under K_2CO_3 and DMA conditions. Intermediate **56** undergoes additional ring contraction through cleavage of Si–O/Si–C bonds and formation of a Si–C bond, yielding **57** and **Int-56**, with **Int-56** polymerizing to generate cyclosiloxanes. An alternative pathway involving cleavage of another Si–O bond during the conversion from **55** to **56** and subsequently to **57** cannot be excluded.

Temperature control

Temperature, as a readily adjustable physical parameter in organic synthesis, offers a simple and versatile approach to control regioselectivity. It profoundly influences reaction kinetics, stability of intermediates, and reaction equilibria. Through precise temperature modulation, chemists can effectively steer the formation of regioisomers, often achieving desired selectivity with minimal alterations to other reaction

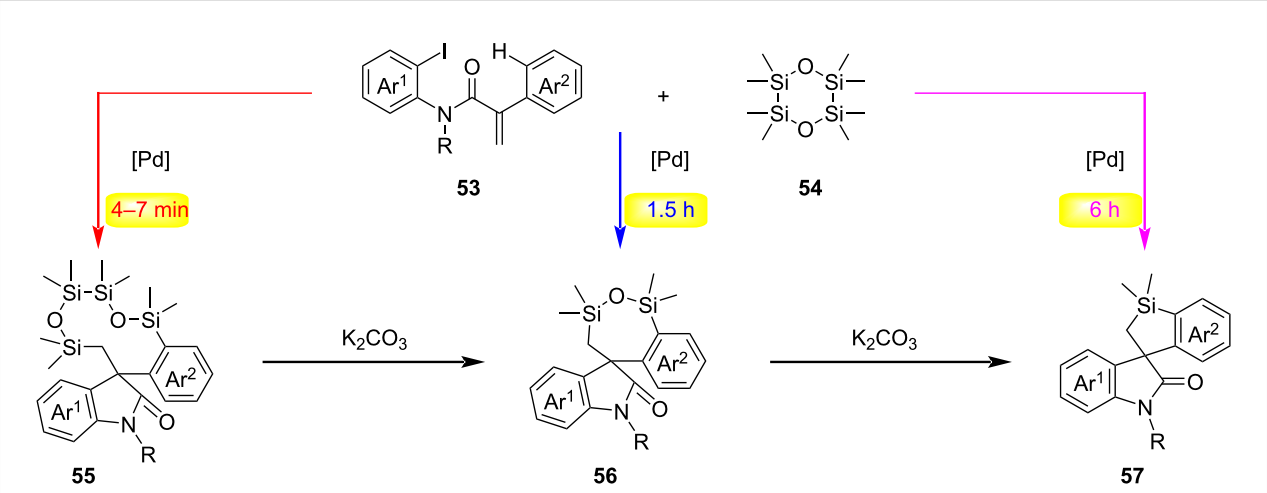

Scheme 14: Time-controlled palladium-catalyzed divergent synthesis of silacycles via C–H activation [43].

components. For instance, Rana and colleagues developed a temperature-dependent regiodivergent strategy to access functionalized maleimides and itaconimides [44]. This thermochemical strategy provides a robust platform for controlling reaction pathways while maintaining synthetic simplicity. In 2022, García-García and Fernández-Rodríguez reported on the practicality of metal-free BCl_3-catalyzed borylation cyclization reactions in synthesis (Scheme 16) [45]. Biphenyl-embedded 1,3,5-trienes-7-yne compounds **58** react with BCl_3 under catalyst-free and additive-free conditions to form novel polycyclic boronated structural units. By adjusting the temperature of the reaction medium, it is possible to precisely control the reaction pathway, thereby obtaining two different boronated frameworks from the same starting material: boronated phenanthrene derivatives **59** at 60 °C and phenanthrene-fused boronated cyclobutane **60** at 0 °C.

In the same year, Lu's research group reported a temperature-controlled site-selective olefin hydroalkylation reaction (Scheme 17) [46]. By adjusting only the reaction temperature, different skeletal structures of nitrogen α- and β-alkylated products could be obtained from the same olefin substrates **61**. At 10 °C, the catalytic system consisting of $NiBr_2$(diglyme), oxazoline ligand, $(EtO)_3SiH$, and $K_3PO_4(H_2O)$ achieved β-selective hydroalkylation. When the temperature was raised to 100 °C, the reaction selectively produced α-branched products. DFT calculations showed that at low temperatures, the six-membered nickel ring captures radicals and undergoes reductive elimination to form β-products (kinetic control); at high temperatures, the formation of a five-membered nickel ring leads to α-products (thermodynamic control). Therefore, the formation of the more stable nickel ring drives migration, while the thermodynamic and kinetic properties of different reductive elimination intermediates jointly determine the switchable site selectivity.

Acid–base control

The strategic modulation of acid–base interactions has emerged as a powerful paradigm in organic synthesis, enabling precise control over reaction pathways, selectivity, and catalytic efficiency. By exploiting dynamic acid–base equilibria or stimuli-responsive systems, chemists can manipulate substrate activation, stabilize reactive intermediates, and orchestrate complex multistep transformations under mild conditions [47]. In 2016, Lu's team designed a new class of acetylene carbonate reagents and successfully applied them to copper-catalyzed decarboxylative amination/hydroamination sequences (Scheme 18) [48]. By controlling acidic and basic reaction conditions, the authors achieved the controllable synthesis of two types of functionalized indoles. When treated with acid ($BF_3{\cdot}E_2O$), the intermediate 2-methylene-3-aminoindoline **69** undergoes an aza-Cope rearrangement to form 2-benzylindole **70**; when treated with a base (Cs_2CO_3), this intermediate undergoes a 1,3-proton migration process to convert back to 3-aminoindole **71**. The possible mechanism for the formation of the key intermediate **69** is outlined in Scheme 19: first, substrate **67**, under the action of a copper catalyst and diisopropylethylamine, undergoes a decarboxylation process to generate the allylidenecopper intermediate **Int-63** and its resonance form **Int-64**. Subsequently, these intermediates undergo a propargylation process (**Int-63**, **Int-64** to **Int-65**) followed by a proton elimination process to generate **Int-66** (**Int-5** to **Int-66**). Then, **Int-66** undergoes an intramolecular amination through copper-catalyzed activation to form **Int-68**, and finally, 2-methylene-3-aminoindoline **69** is generated via a proton transfer promoted by diisopropylethylamine.

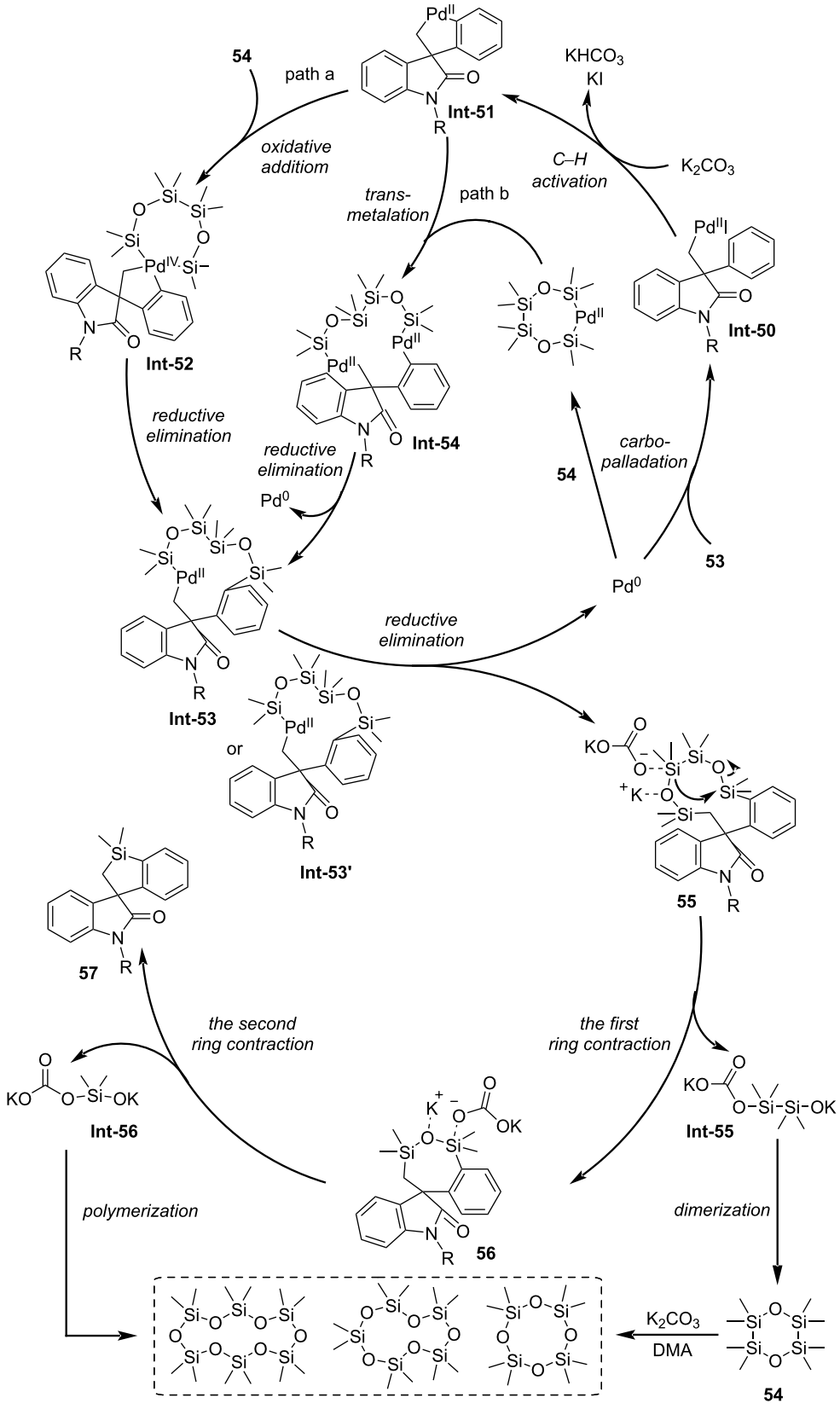

Scheme 15: Proposed mechanism for the time-controlled palladium-catalyzed divergent synthesis of silacycles [43].

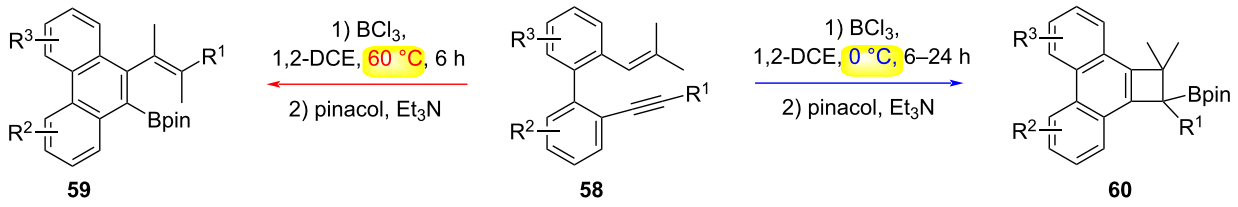

Scheme 16: Metal-free temperature-controlled regiodivergent borylative cyclizations of enynes [45].

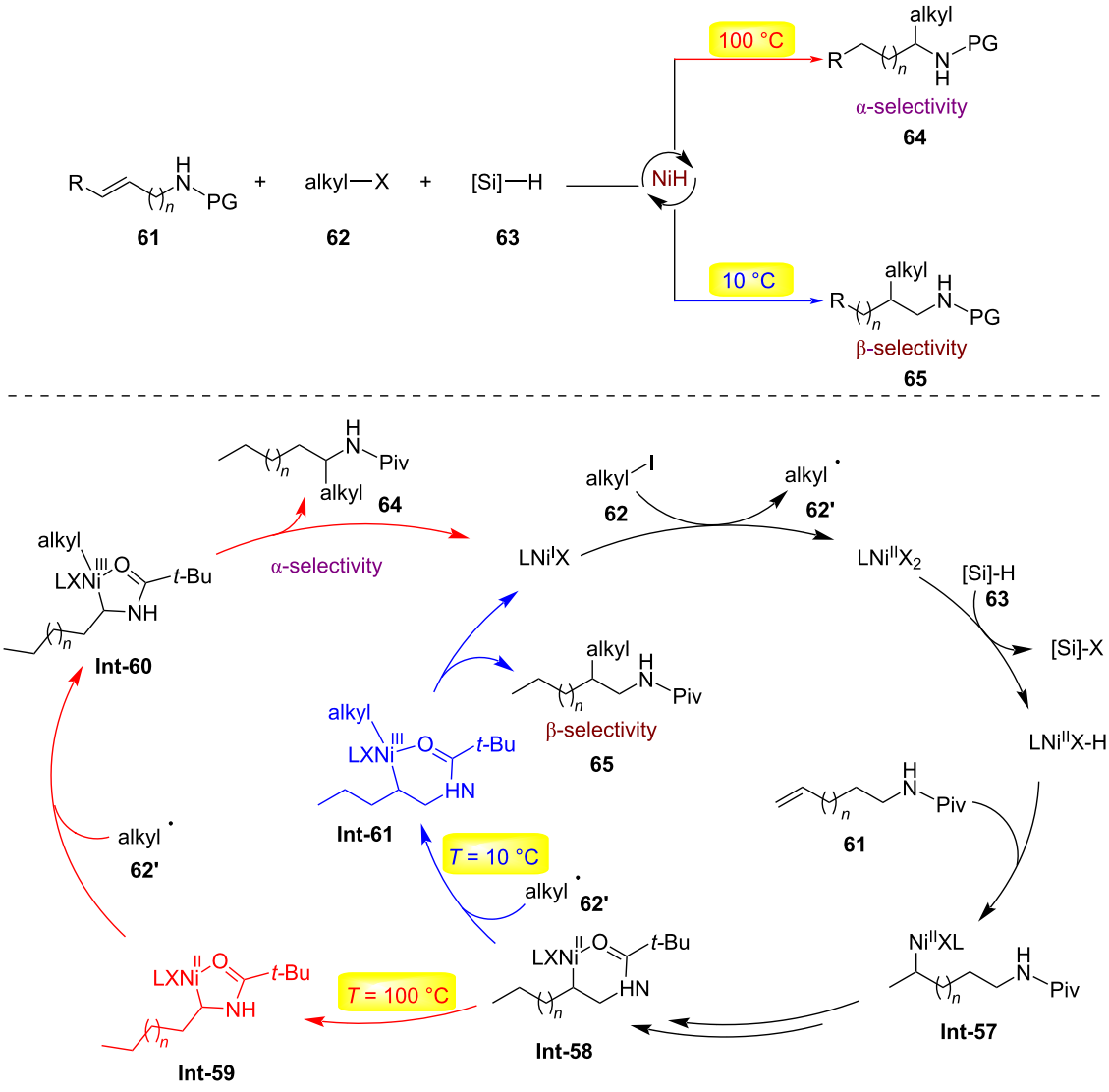

Scheme 17: Nickel-catalyzed switchable site-selective alkene hydroalkylation by temperature regulation [46].

In 2023, the Jiang research group achieved a chemically divergent photocatalytic asymmetric synthesis using a dual catalytic system consisting of a chiral phosphoric acid and dicyanopyrazine (DPZ) as the photosensitizer (Scheme 20) [49]. By regulating the chemical selectivity of a three-component radical cascade reaction involving α-brominated aryl ketones **72**, olefins **73**, and 1-methylquinoxalin-2(1*H*)-one (**74**) with an inorganic base, they were able to obtain two important types of products with high yield and enantioselectivity. Through mechanistic experiments and DFT calculations, the authors proposed

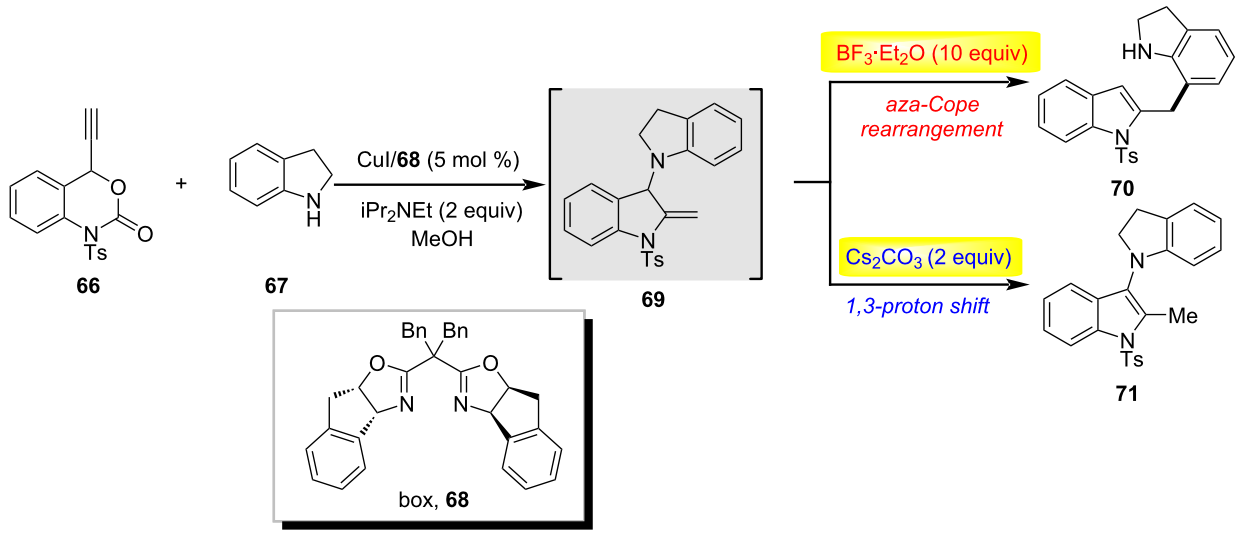

Scheme 18: Copper-catalyzed decarboxylative amination/hydroamination sequence [48].

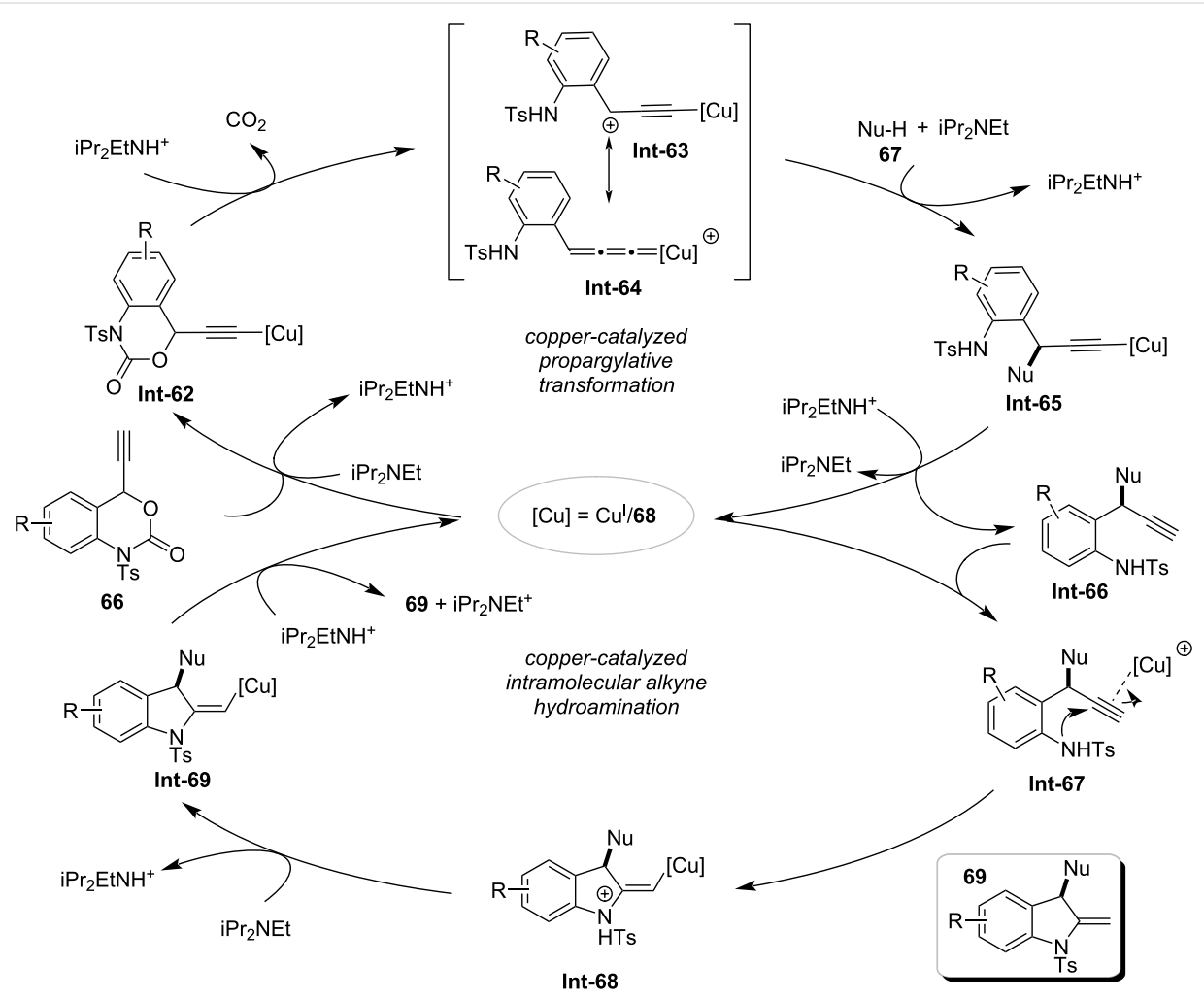

Scheme 19: Proposed mechanism of copper-catalyzed decarboxylative amination/hydroamination sequence [48].

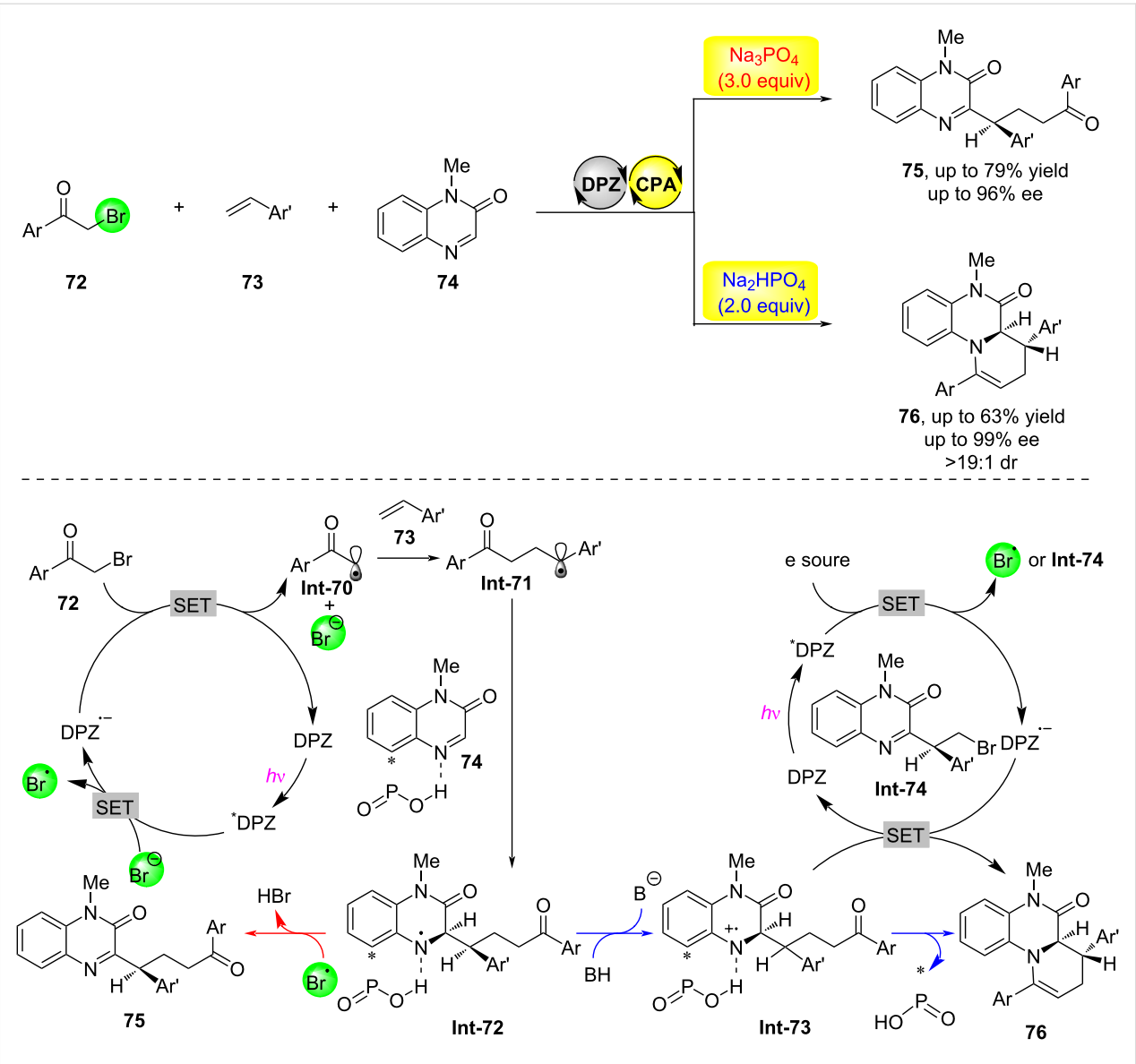

Scheme 20: Enantioselective chemodivergent three-component radical tandem reactions [49].

a possible mechanism for the reaction: first, DPZ is excited by light to form the excited state DPZ*, which then oxidizes bromide ions through single-electron transfer to generate corresponding radical anions. These radical anions undergo single-electron transfer with substrate **72** to form radical intermediate **Int-70**, completing the DPZ catalytic cycle. Intermediate **Int-70** adds to substrate **73** to form radical intermediate **Int-71**, which further adds to hydrogen-bond-activated substrate **74** to form hydrogen-bonded complex **Int-72**. When Na_3PO_4 is used as the inorganic base, bromine radicals abstract hydrogen to form product **75**; whereas when Na_2HPO_4 is used as the inorganic base, its weaker basicity leads to protonation of complex **Int-72** to form intermediate **Int-73**, which then preferentially undergoes single-electron transfer with the DPZ radical anion, followed by cyclization and dehydration to yield bicyclic product **76**.

Substrate control

Substrate control has emerged as a powerful strategy in organic synthesis, enabling precise manipulation of reaction pathways and stereochemical outcomes through the intrinsic structural and electronic features of the starting material. By exploiting preorganization, steric effects, or directing groups within the substrate, chemists can achieve high levels of regioselectivity, diastereoselectivity, and enantioselectivity without relying on external catalysts or additives. This approach has been successfully applied in the synthesis of complex natural products, pharmaceuticals, and functional materials, often streamlining multi-

step sequences and minimizing protecting-group strategies [50,51]. In 2016, Li and co-workers developed divergent coupling conditions for iminamides **77** with receptor-type diazo compounds **78** or **79** under ruthenium catalysis, generating indoles **81** and 3*H*-indoles **80**, respectively (Scheme 21) [52]. α-Diazo-β-ketoesters form indoles by cleaving the C(N_2)–C(acyl) bond, while diazomalonates form 3*H*-indoles through C–N-bond cleavage. Mechanistically, the cyclometalation of iminamides follows a concerted metalation–deprotonation (CMD) mechanism to generate ruthenium intermediate **Int-75**. Subsequently, diazo compound **78** or **79** coordinates with intermediate **Int-75**, followed by deazidation to form the ruthenium carbenoid species **Int-76**. The ruthenium–aryl bond in this intermediate migrates into the carbenoid unit, providing heptacyclic ruthenium ring intermediate **Int-77**. Intermediate **Int-78** is then formed via ruthenium migration insertion into the C=N bond from Ru–C(alkyl). For diazoketoester substrates, the final product **81** is released from **Int-78** through protonation, intramolecular nucleophilic addition, and subsequent release of one molecule of amide, reactivating the active ruthenium(II) catalyst. In contrast, for diazomalonates, intermediate **Int-78** releases ammonia with the help of Ru(II) or acetic acid, ultimately yielding 3*H*-indole **80**. This change in selectivity may be due to the reduced electrophilicity of the ester carbonyl.

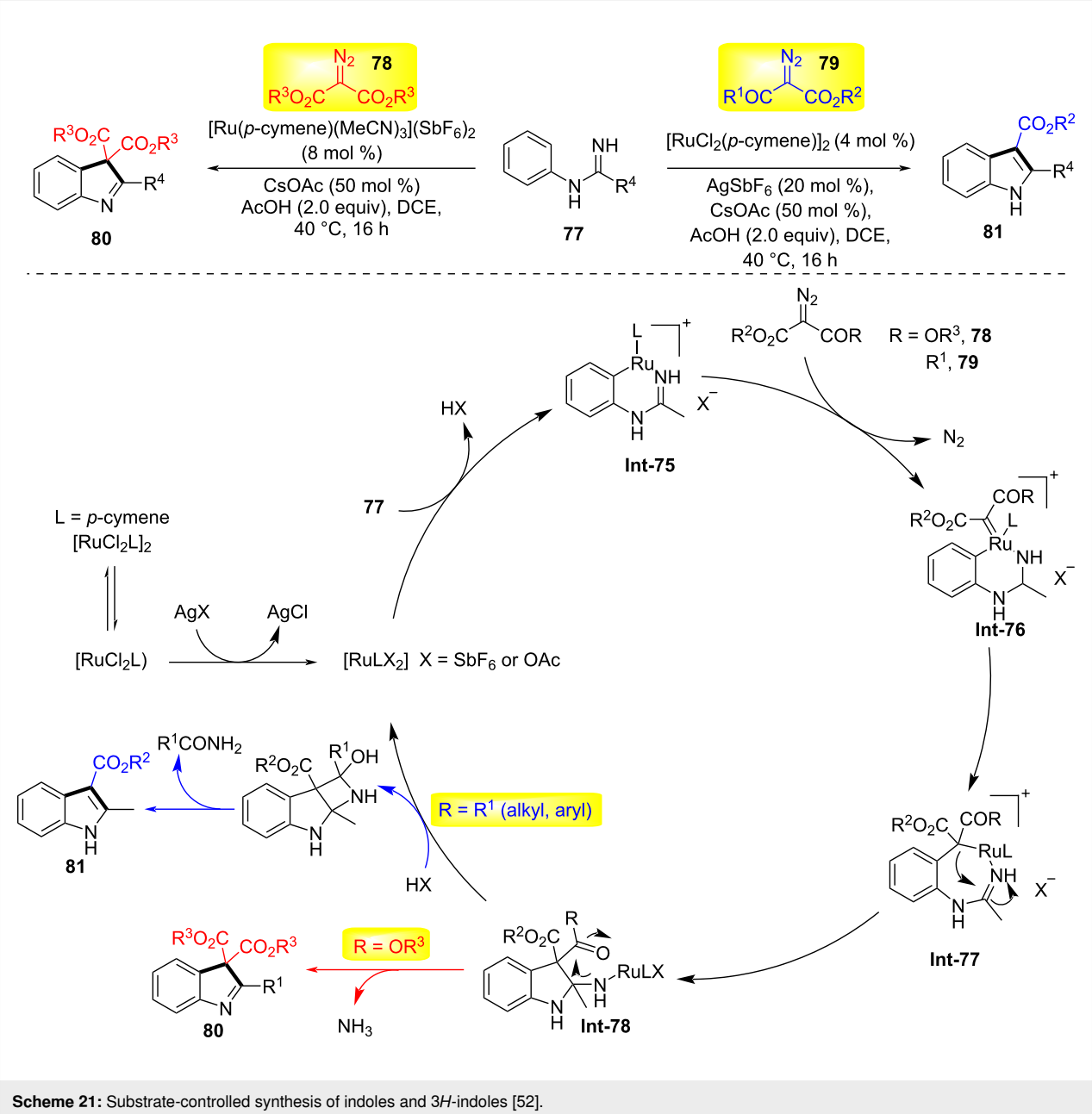

Scheme 21: Substrate-controlled synthesis of indoles and 3*H*-indoles [52].

In 2021, Dong and Xie reported the development of an azido Matteson reaction, which achieves carbene insertion into an N–B bond of aminoboranes **84** or **86** (Scheme 22) [53]. In this methodology, by controlling the carbene leaving group (alkyl chlorides/alkyl bromides) and the Lewis acid activator, a selective mono- or di-methylene insertion reaction can be carried out, generating α-/β-boryl-substituted tertiary organic amines **83** from simple secondary organic amines. Using *N*-alkyl-*N*-arylaminoboranes as the reactant, the reaction proceeds at −78 °C with CH_2Br_2 and *n*-BuLi, followed by a reaction with $ZnCl_2$ at room temperature. The product is then hydrolyzed with a NaOH solution of H_2O_2 to yield amino alcohols. The mechanism involves the formation of borate intermediate **Int-79** from substrate **83** under the action of CH_2BrLi. This is followed by an N-1,2-migration to form borate ester **86**, which then reacts with another molecule of CH_2BrLi to form the more stable borate **Int-80**. Subsequently, a C-1,2-migration leads to the formation of the double-insertion product **84**. If the amine portion is more electron-deficient or has more delocalized nitrogen electrons (such as indole substrates), **Int-79** is more stable at −78 °C, favoring the formation of the mono-insertion product **86**.

In 2022, Wu and colleagues reported a novel methodology for constructing α-ketoamides **90** or **92** and amides **91** through copper-catalyzed dicarbonylation and monocarbonylation reactions involving alkyl halides **88** (Scheme 23) [54]. Using alkyl bromides, CuBr as the catalyst, bpy as the ligand, $Co_2(CO)_8$ as the additive, Cs_2CO_3 as the base, and 1,4-dioxane as the solvent under 40 bar CO pressure at 80 °C, they successfully syn-

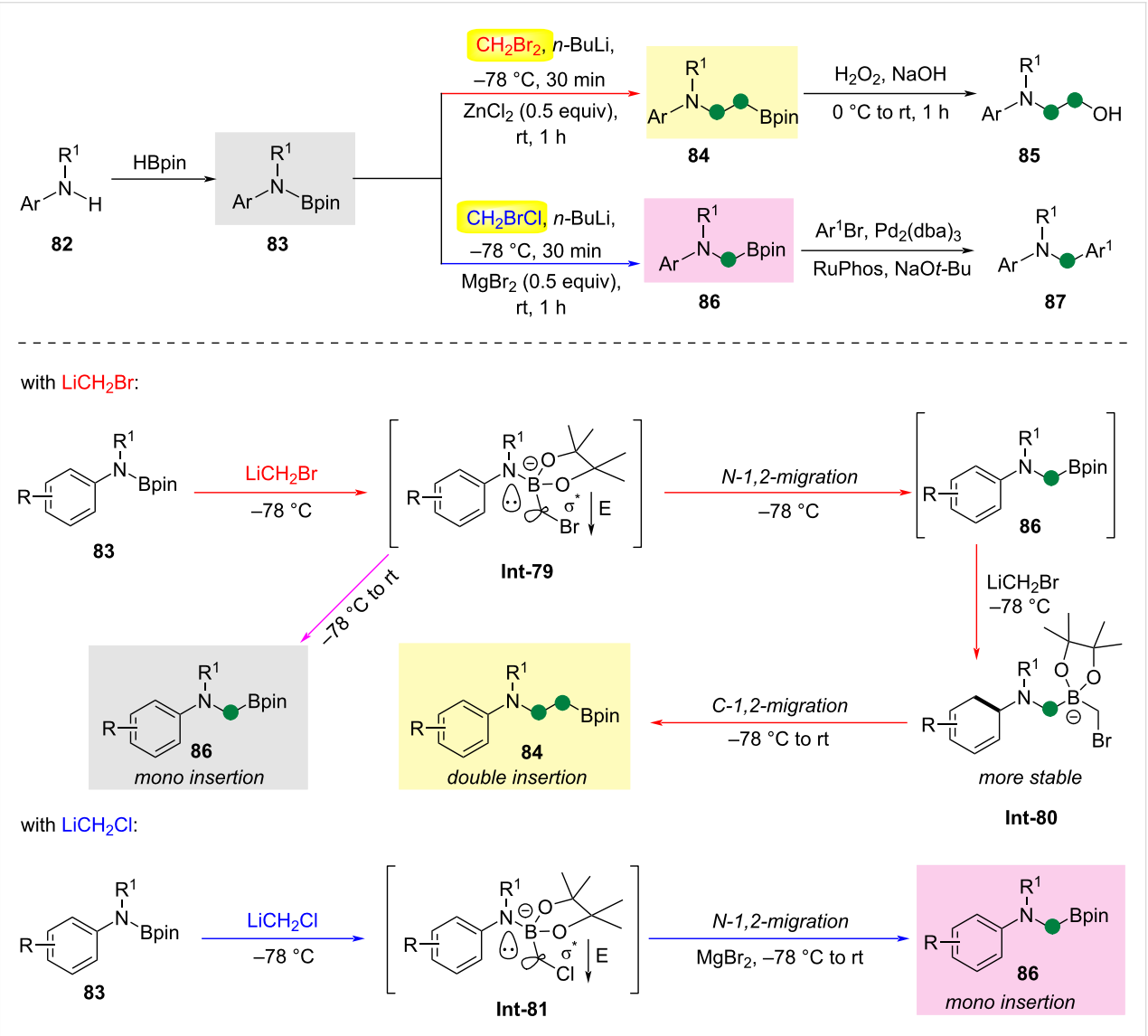

Scheme 22: Controlled mono- and double methylene insertions into nitrogen–boron bonds [53].

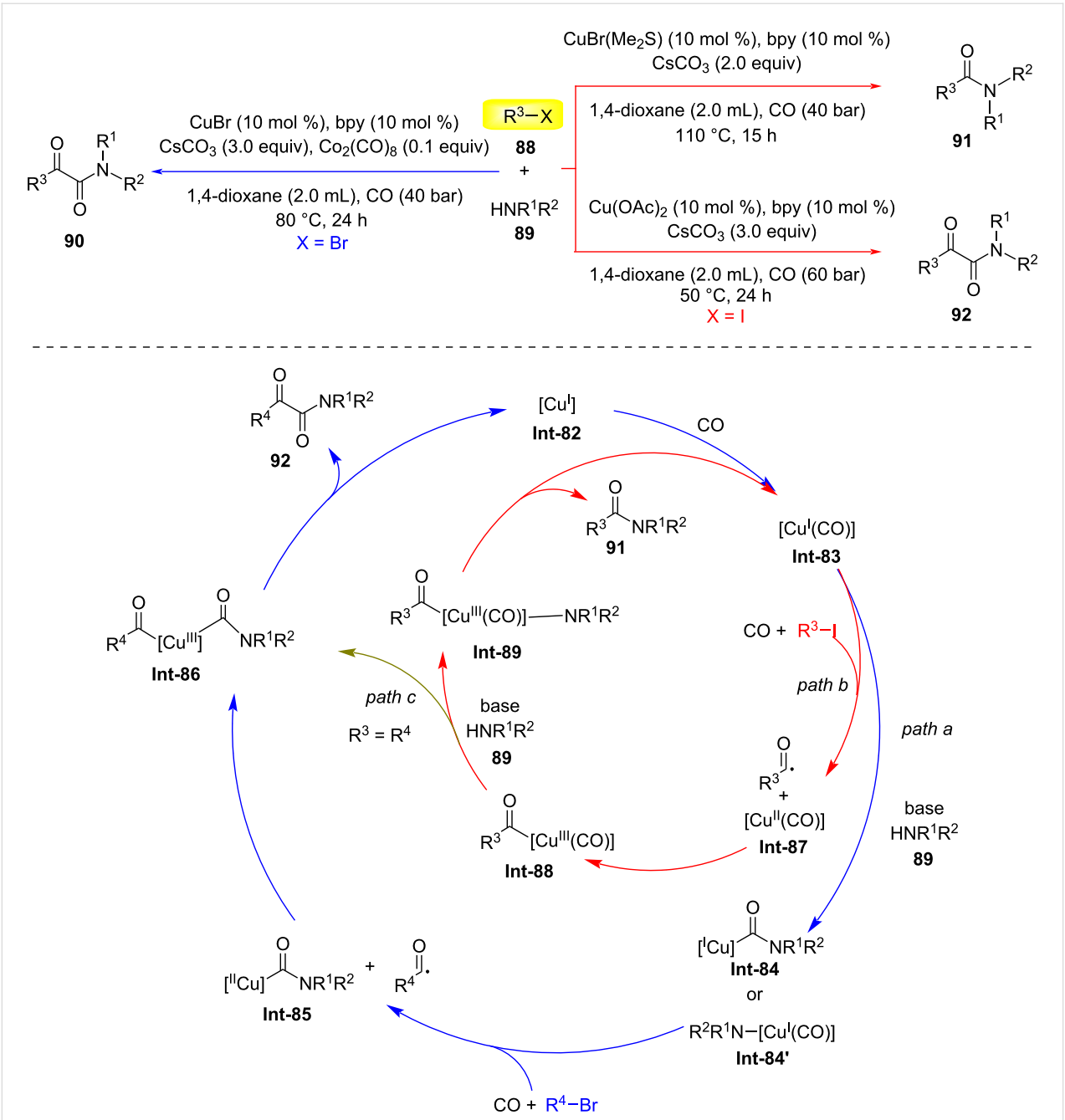

Scheme 23: Copper-catalyzed substrate-controlled carbonylative synthesis of α-keto amides and amides [54].

thesized α-ketoamides **90**. When alkyl iodides were used as substrates, both dicarbonylation and monocarbonylation processes occurred simultaneously with $Cu(OAc)_2$, favoring the dicarbonylation process. In contrast, using $CuBr(Me_2S)$ the monocarbonylation process was favored. Possible reaction mechanisms: First, CO coordinates with copper salts to form (carbonyl)copper species **Int-83**. Subsequently, in the presence of a base, the amine undergoes nucleophilic attack on the coordinated CO, generating (carbamoyl)copper complex **Int-84**. Then, alkyl bromide undergoes a single-electron-transfer (SET) process with **Int-84**, forming intermediate **Int-85** and an alkyl radical, which is captured by CO to yield an acyl radical. Alternatively, under the action of a base, the amine can undergo anionic ligand exchange with (carbonyl)copper species **Int-83**, generating an electron-rich amino copper(I) species **Int-84'**, which activates alkyl bromide through an SET process, followed by immediate insertion of CO to form complex **Int-85**. Nucleophilic activation of the acyl radical initiates through its

reaction with intermediate **Int-85**, generating the critical acyl(aminoacyl)copper species **Int-86**. Subsequent reductive elimination from this intermediate liberates the α-ketoamide product **92** while regenerating the catalytic species **Int-82**. Comparative kinetic analysis revealed a marked preference for alkyl iodide activation, as demonstrated by its substantially lower activation energy barrier compared to alkyl bromide analogs (path b). This energetic advantage facilitates preferential formation of intermediate **Int-87** via oxidative addition. Rapid coupling with the in situ-generated acyl radical produces copper-bound intermediate **Int-88**. Base-mediated anionic exchange then displaces the halide ligand with amine, yielding intermediate **Int-89**. Final reductive elimination from this species affords amide product **91** with concurrent regeneration of the catalyst **Int-83**. Notably, a competitive pathway emerges through alternative reactivity of **Int-88** (path c). The coordinated CO ligand undergoes nucleophilic attack by the amine, bypassing halide exchange to instead generate **Int-86**. This mechanistic crossover establishes a product dichotomy between α-ketoamide **92** and amide **91**, with the branching ratio governed by relative rates of base-mediated exchange versus CO activation at the copper center.

In 2022, the Jiang research team developed regulated SuFEx click chemistry between fluorosulfonyl imides and TMS-alkynes, enabling the rapid construction of S(VI)–C(sp^2) or S(VI)–C(sp) bonds efficiently (Scheme 24) [55]. This linkage utilizes the high bond dissociation energy (BDE =

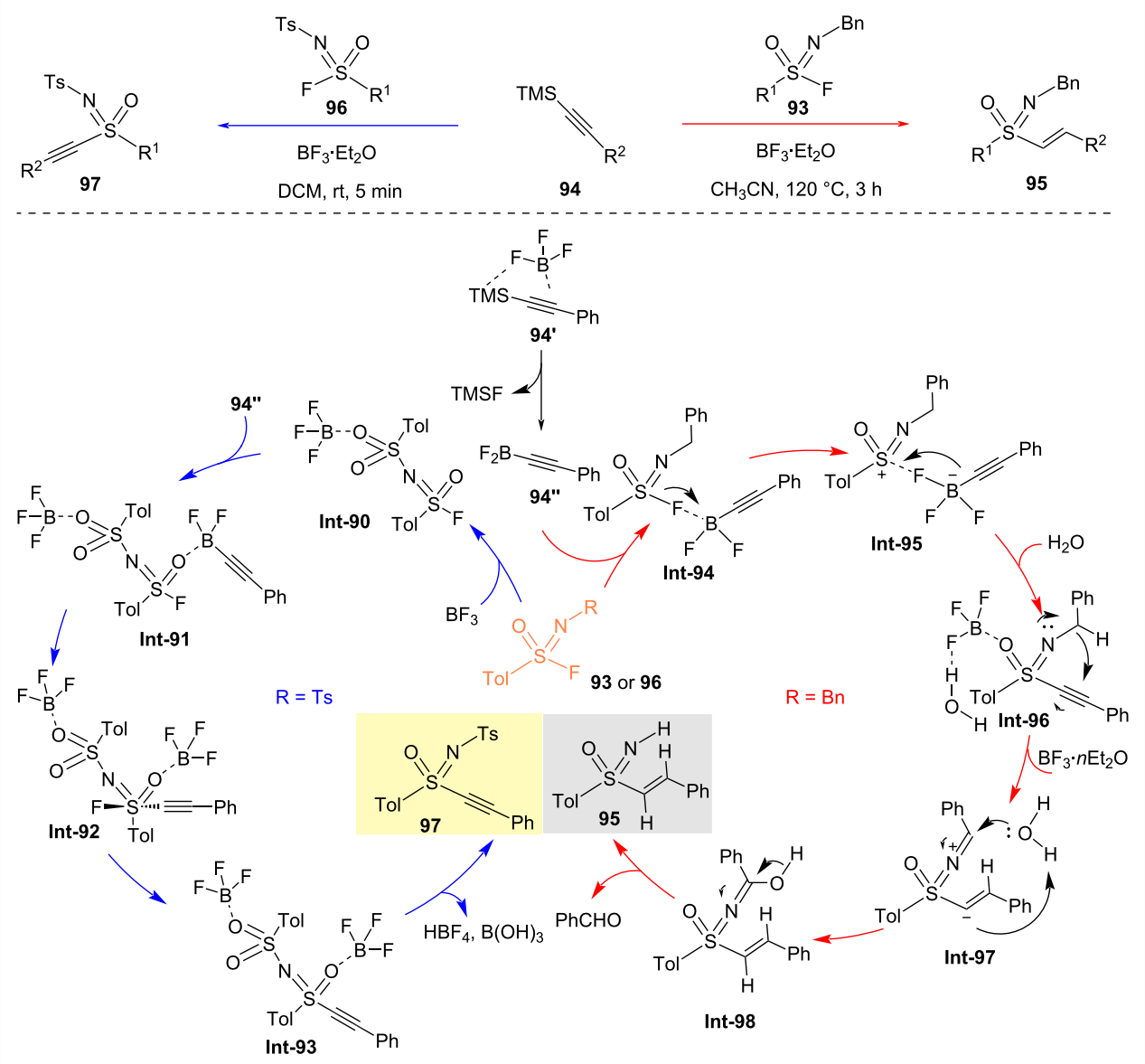

Scheme 24: Divergent sulfur(VI) fluoride exchange linkage of sulfonimidoyl fluorides and alkynes [55].

135 kcal/mol) of silicon–fluorine bonds, employing trifluoroborate as a fluorine transfer reagent to simultaneously cleave the S(VI)–F bond and activate the Si–C bond. DFT calculations indicate that the reaction proceeds via the formation of a difluoroborate phenylacetylene intermediate **94''** by in situ generation from boron trifluoride etherate and silicon-protected phenylacetylene **94**, which activates the S–F bond of the fluorosulfonyl imide to form sulfonyliminium cations **Int-95**. These then add to the activated phenylacetylene to construct the S–C bond, followed by intramolecular 1,5-hydrogen migration and aqueous workup to remove benzaldehyde, yielding the target sulfonylimine products.

Both original protoberberine and protonitidine alkaloids are characterized by an isoquinoline ring skeleton. An analysis of their molecular structures revealed that the two alkaloids share a basic structure, differing only in the junction of the B-ring. In 2021, Liu and Jiang designed new pyridyne precursors, which underwent cycloaddition reactions with substituted furans as diene component to produce the corresponding epoxy-cycloaddition adducts. The authors developed an Ir/Sc tandem catalytic reaction to convert these adducts into polysubstituted 3-haloisoquinolines **99** in one pot. After obtaining isoquinoline compounds **99** with different substituents and polysubstituted annular boronic acids **98**, a Suzuki coupling was employed to synthesize advanced isoquinoline intermediates **100**. Following this, a 6π electrocyclization reaction and nucleophilic reaction were developed to achieve C–C and C–N bond constructions, respectively, leading to the synthesis of differently substituted protonitidine alkaloids and protoberberine alkaloids (Scheme 25) [56].

Conclusion

Developing streamlined and versatile approaches for the rapid assembly of structurally diverse organic molecules represents a pivotal challenge in organic synthesis, pharmaceutical research, and advanced materials development. Recent advances in controllable/divergent synthesis methodologies, which enable

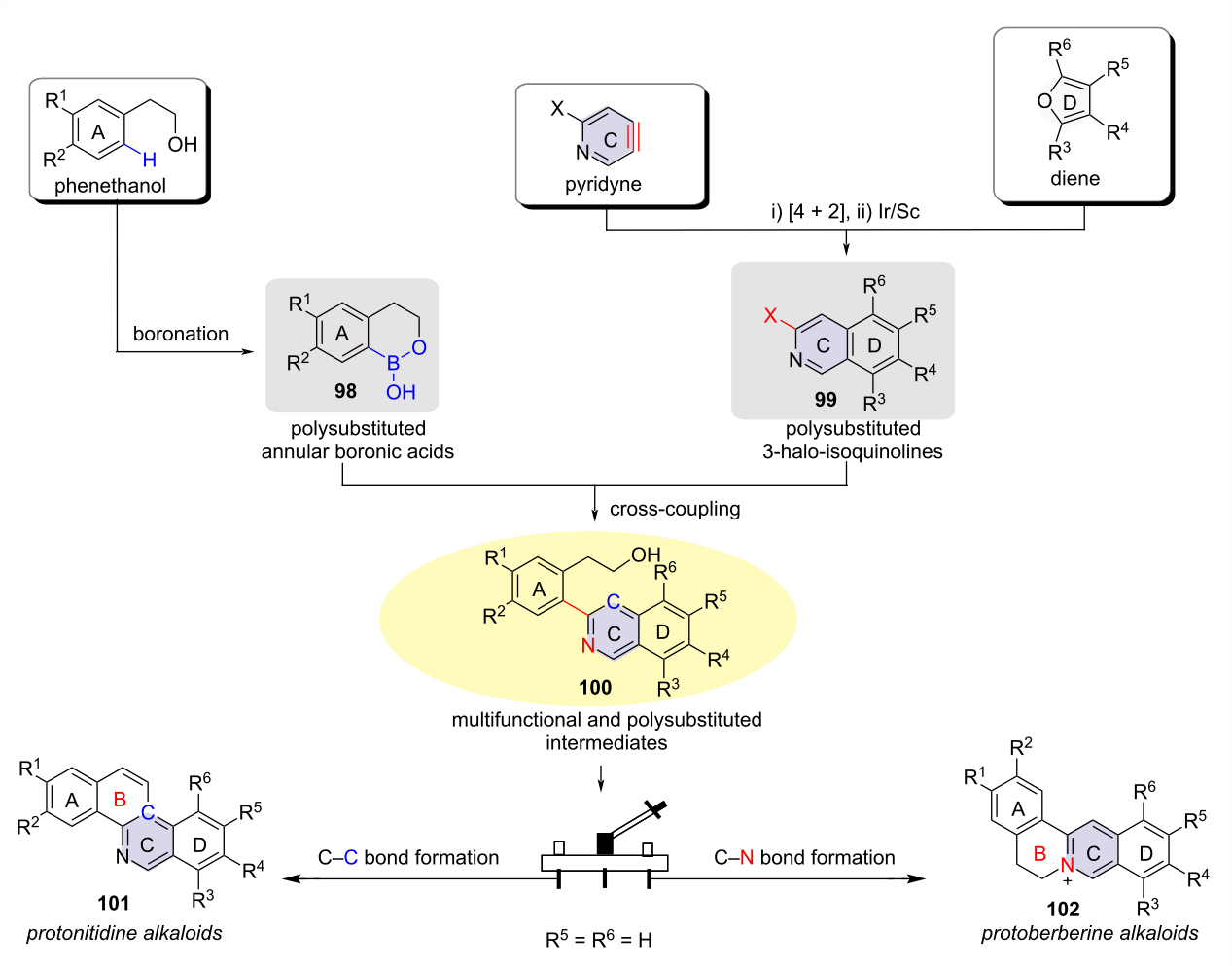

Scheme 25: Modular and divergent syntheses of protoberberine and protonitidine alkaloids [56].

the construction of variously functionalized architectures from common precursors, have emerged as particularly promising due to their inherent efficiency. Contemporary strategies for controlling reaction pathways and selectivity predominantly involve precise manipulation of catalytic systems (metal catalysts/ligands), reaction parameters (solvent, temperature, time), acid/base mediation, and strategic substrate engineering. This review systematically organizes recent breakthroughs according to critical control elements governing product divergence. Through mechanistic investigations of pivotal bond-forming steps and comparative analysis of representative case studies, we provide fundamental insights into the origin of selectivity variations and reaction pathway control. The discussion emphasizes structure–reactivity relationships and catalytic design principles that enable predictable access to distinct molecular architectures from shared synthetic intermediates. This review serves as a conceptualized platform for controllable/divergent synthesis, arousing more state-of-the-art tactics in chemical synthesis.

Funding

The authors are grateful for financial support provided by the NSFC (22125103, 22401095), Shanghai Rising-Star Program (24QB2704700), the STCSM (22JC1401000), and the China Postdoctoral Science Foundation (BX20230127).

Author Contributions

Jilei Cao: investigation. Leiyang Bai: investigation; writing – review & editing. Xuefeng Jiang: conceptualization; investigation; supervision; validation; writing – review & editing.

ORCID® iDs

Leiyang Bai - https://orcid.org/0000-0002-8159-4992
Xuefeng Jiang - https://orcid.org/0000-0002-1849-6572

Data Availability Statement

Data sharing is not applicable as no new data was generated or analyzed in this study.

References

1. Beletskaya, I. P.; Nájera, C.; Yus, M. *Chem. Rev.* **2018,** *118,* 5080–5200. doi:10.1021/acs.chemrev.7b00561
2. Nájera, C.; Foubelo, F.; Sansano, J. M.; Yus, M. *Org. Biomol. Chem.* **2020,** *18,* 1232–1278. doi:10.1039/c9ob02419k
3. Nájera, C.; Foubelo, F.; Sansano, J. M.; Yus, M. *Org. Biomol. Chem.* **2020,** *18,* 1279–1336. doi:10.1039/c9ob02597a
4. Katta, N.; Zhao, Q.-Q.; Mandal, T.; Reiser, O. *ACS Catal.* **2022,** *12,* 14398–14407. doi:10.1021/acscatal.2c04736
5. Nájera, C.; Beletskaya, I. P.; Yus, M. *Chem. Soc. Rev.* **2019,** *48,* 4515–4618. doi:10.1039/c8cs00872h
6. Beletskaya, I. P.; Nájera, C.; Yus, M. *Russ. Chem. Rev.* **2020,** *89,* 250–274. doi:10.1070/rcr4916
7. Mahatthananchai, J.; Dumas, A. M.; Bode, J. W. *Angew. Chem., Int. Ed.* **2012,** *51,* 10954–10990. doi:10.1002/anie.201201787
8. Lee, Y.-C.; Kumar, K.; Waldmann, H. *Angew. Chem., Int. Ed.* **2018,** *57,* 5212–5226. doi:10.1002/anie.201710247
9. Peng, J.-B.; Wu, X.-F. *Angew. Chem., Int. Ed.* **2018,** *57,* 1152–1160. doi:10.1002/anie.201709807
10. Cao, M.; Xie, H. *Chin. Chem. Lett.* **2021,** *32,* 319–327. doi:10.1016/j.cclet.2020.04.005
11. Chintawar, C. C.; Yadav, A. K.; Kumar, A.; Sancheti, S. P.; Patil, N. T. *Chem. Rev.* **2021,** *121,* 8478–8558. doi:10.1021/acs.chemrev.0c00903
12. Sakakibara, Y.; Murakami, K. *ACS Catal.* **2022,** *12,* 1857–1878. doi:10.1021/acscatal.1c05318
13. Pan, Q.; Ping, Y.; Kong, W. *Acc. Chem. Res.* **2023,** *56,* 515–535. doi:10.1021/acs.accounts.2c00771
14. Ke, Y.; Li, W.; Liu, W.; Kong, W. *Sci. China: Chem.* **2023,** *66,* 2951–2976. doi:10.1007/s11426-023-1533-y
15. Kumari, A.; Jain, A.; Rana, N. K. *Tetrahedron* **2024,** *150,* 133754. doi:10.1016/j.tet.2023.133754
16. Fuji, K.; Kawashima, K.; Mori, T.; Sekine, K.; Kuninobu, Y. *Org. Lett.* **2025,** *27,* 1614–1619. doi:10.1021/acs.orglett.4c04694
17. Long, Y.; Zhong, X.; Shi, M.; Wei, Y. *Chin. J. Chem.* **2025,** *43,* 1181–1189. doi:10.1002/cjoc.202401301
18. Zou, S.; Zhao, Z.; Yang, G.; Huang, H. *Nat. Commun.* **2024,** *15,* 10477. doi:10.1038/s41467-024-54328-5
19. Feng, M.; Tang, B.; Wang, N.; Xu, H.-X.; Jiang, X. *Angew. Chem., Int. Ed.* **2015,** *54,* 14960–14964. doi:10.1002/anie.201508340
20. Ding, D.; Mou, T.; Feng, M.; Jiang, X. *J. Am. Chem. Soc.* **2016,** *138,* 5218–5221. doi:10.1021/jacs.6b01707
21. Ding, D.; Zhu, G.; Jiang, X. *Angew. Chem., Int. Ed.* **2018,** *57,* 9028–9032. doi:10.1002/anie.201804788
22. Witkowski, D. C.; McVeigh, M. S.; Scherer, G. M.; Anthony, S. M.; Garg, N. K. *J. Am. Chem. Soc.* **2023,** *145,* 10491–10496. doi:10.1021/jacs.3c03102
23. Tang, X.; Tang, Y.; Peng, J.; Du, H.; Huang, L.; Gao, J.; Liu, S.; Wang, D.; Wang, W.; Gao, L.; Lan, Y.; Song, Z. *J. Am. Chem. Soc.* **2024,** *146,* 26639–26648. doi:10.1021/jacs.4c00252
24. Yang, F.; Chi, L.; Ye, Z.; Gong, L. *J. Am. Chem. Soc.* **2025,** *147,* 1767–1780. doi:10.1021/jacs.4c13321
25. Cheng, L.-J.; Mankad, N. P. *J. Am. Chem. Soc.* **2019,** *141,* 3710–3716. doi:10.1021/jacs.9b00068
26. Sun, Z.; Dai, M.; Ding, C.; Chen, S.; Chen, L.-A. *J. Am. Chem. Soc.* **2023,** *145,* 18115–18125. doi:10.1021/jacs.3c06253
27. Bai, L.; Ma, Y.; Jiang, X. *J. Am. Chem. Soc.* **2021,** *143,* 20609–20615. doi:10.1021/jacs.1c10498
28. Bai, L.; Li, J.; Jiang, X. *Chem* **2023,** *9,* 483–496. doi:10.1016/j.chempr.2022.10.021
29. Bai, L.; Jiang, X. *Chem Catal.* **2023,** *3,* 100752. doi:10.1016/j.checat.2023.100752
30. Wang, S.; Shi, L.; Chen, X.-Y.; Shu, W. *Angew. Chem., Int. Ed.* **2023,** *62,* e202303795. doi:10.1002/anie.202303795
31. Wang, X.; Xue, J.; Rong, Z.-Q. *J. Am. Chem. Soc.* **2023,** *145,* 15456–15464. doi:10.1021/jacs.3c03900
32. Lin, Z.; Ren, H.; Lin, X.; Yu, X.; Zheng, J. *J. Am. Chem. Soc.* **2024,** *146,* 18565–18575. doi:10.1021/jacs.4c04485
33. Zhu, H.; Zheng, H.; Zhang, J.; Feng, J.; Kong, L.; Zhang, F.; Xue, X.-S.; Zhu, G. *Chem. Sci.* **2021,** *12,* 11420–11426. doi:10.1039/d1sc03416b
34. Jain, A.; Kumari, A.; Shukla, K.; Selvakumar, S.; Rana, N. K. *ARKIVOC* **2023,** No. vi, 202211947. doi:10.24820/ark.5550190.p011.947

35. Zhou, Y.; Zhao, L.; Hu, M.; Duan, X.-H.; Liu, L. *Org. Lett.* **2023,** *25,* 5268–5272. doi:10.1021/acs.orglett.3c01787
36. Zhang, F.; Dutta, S.; Petti, A.; Rana, D.; Daniliuc, C. G.; Glorius, F. *Angew. Chem., Int. Ed.* **2025,** *64,* e202418239. doi:10.1002/anie.202418239
37. Huang, Z.; Zhang, C.; Zhou, P.; Wang, C.; Liang, T.; Zhao, S.; Zhang, Z. *J. Org. Chem.* **2025,** *90,* 1115–1125. doi:10.1021/acs.joc.4c02680
38. Kim, Y. L.; Yun, Y.; Choi, S.-M.; Kim, J. H. *Org. Chem. Front.* **2025,** *12,* 1452–1460. doi:10.1039/d4qo01980f
39. Wang, F.; Shi, X.; Zhang, Y.; Zhou, W.; Li, A.; Liu, Y.; Sessler, J. L.; He, Q. *J. Am. Chem. Soc.* **2023,** *145,* 10943–10947. doi:10.1021/jacs.3c01066
40. Hussain, Y.; Empel, C.; Koenigs, R. M.; Chauhan, P. *Angew. Chem., Int. Ed.* **2023,** *62,* e202309184. doi:10.1002/anie.202309184
41. Tian, Q.; Ge, J.; Liu, Y.; Wu, X.; Li, Z.; Cheng, G. *Angew. Chem., Int. Ed.* **2024,** *63,* e202409366. doi:10.1002/anie.202409366
42. Tu, H.-F.; Yang, P.; Lin, Z.-H.; Zheng, C.; You, S.-L. *Nat. Chem.* **2020,** *12,* 838–844. doi:10.1038/s41557-020-0489-1
43. Xu, Y.; Sun, M.; Xu, W.; Deng, G.; Liang, Y.; Yang, Y. *J. Am. Chem. Soc.* **2023,** *145,* 15303–15312. doi:10.1021/jacs.3c02875
44. Saha, S. K.; Bera, A.; Kumari, A.; Loitongbam, M.; Chakladar, D.; Rana, N. K. *Eur. J. Org. Chem.* **2025,** *28,* e202401448. doi:10.1002/ejoc.202401448
45. Milián, A.; Fernández-Rodríguez, M. A.; Merino, E.; Vaquero, J. J.; García-García, P. *Angew. Chem., Int. Ed.* **2022,** *61,* e202205651. doi:10.1002/anie.202205651
46. Wang, J.-W.; Liu, D.-G.; Chang, Z.; Li, Z.; Fu, Y.; Lu, X. *Angew. Chem., Int. Ed.* **2022,** *61,* e202205537. doi:10.1002/anie.202205537
47. Yu, S.; Zhou, X.; Tong, X. *ACS Catal.* **2025,** *15,* 72–80. doi:10.1021/acscatal.4c05561
48. Li, T.-R.; Cheng, B.-Y.; Wang, Y.-N.; Zhang, M.-M.; Lu, L.-Q.; Xiao, W.-J. *Angew. Chem., Int. Ed.* **2016,** *55,* 12422–12426. doi:10.1002/anie.201605900
49. Ma, C.; Shen, J.; Qu, C.; Shao, T.; Cao, S.; Yin, Y.; Zhao, X.; Jiang, Z. *J. Am. Chem. Soc.* **2023,** *145,* 20141–20148. doi:10.1021/jacs.3c08883
50. Chen, L.; Guo, L.-N.; Liu, S.; Liu, L.; Duan, X.-H. *Chem. Sci.* **2021,** *12,* 1791–1795. doi:10.1039/d0sc04399k
51. Tan, H.; Yu, S.; Yuan, X.; Chen, L.; Shan, C.; Shi, J.; Li, Y. *Nat. Commun.* **2024,** *15,* 3665. doi:10.1038/s41467-024-47952-8
52. Li, Y.; Qi, Z.; Wang, H.; Yang, X.; Li, X. *Angew. Chem., Int. Ed.* **2016,** *55,* 11877–11881. doi:10.1002/anie.201606316
53. Xie, Q.; Dong, G. *J. Am. Chem. Soc.* **2021,** *143,* 14422–14427. doi:10.1021/jacs.1c06186
54. Zhao, F.; Ai, H.-J.; Wu, X.-F. *Angew. Chem., Int. Ed.* **2022,** *61,* e202200062. doi:10.1002/anie.202200062
55. Zeng, D.; Ma, Y.; Deng, W.-P.; Wang, M.; Jiang, X. *Nat. Synth.* **2022,** *1,* 455–463. doi:10.1038/s44160-022-00060-1
56. Liu, K.; Jiang, X. *Org. Lett.* **2021,** *23,* 1327–1332. doi:10.1021/acs.orglett.0c04310

License and Terms

BEILSTEIN JOURNAL OF ORGANIC CHEMISTRY

Recent total synthesis of natural products leveraging a strategy of enamide cyclization

Chun-Yu Mi‡, Jia-Yuan Zhai‡ and Xiao-Ming Zhang*

Review

Open Access

Address:
State Key Laboratory of Natural Product Chemistry & College of Chemistry and Chemical Engineering, Lanzhou University, Lanzhou 730000, P. R. China

Email:
Xiao-Ming Zhang* - zhangxiaom@lzu.edu.cn

* Corresponding author ‡ Equal contributors

Keywords:
alkaloid; cyclization; enamide; natural product; total synthesis

Beilstein J. Org. Chem. **2025,** *21,* 999–1009.
https://doi.org/10.3762/bjoc.21.81

Received: 24 February 2025
Accepted: 08 May 2025
Published: 22 May 2025

This article is part of the thematic issue "Concept-driven strategies in target-oriented synthesis".

Guest Editor: Y. Tang

Abstract

Enamides are distinctive amphiphilic synthons that can be strategically incorporated into cyclization reactions. The iminium species generated from enamides via nucleophilic addition or substitution are capable of engaging in further electrophilic additions or isomerization processes. Exploiting the multiple reactivities of enamides facilitates the development of diverse cyclization modes that provide entries to various *N*-heterocycles, some of which serve as key structural motifs in natural alkaloids. This review highlights recent advancements in enamide-based cyclization reactions, including enamide–alkyne cycloisomerization, [3 + 2] annulation, and polycyclization, with a particular emphasis on their pivotal role as a strategy in the total synthesis of natural products.

Introduction

The use of enamines as surrogates for enols in nucleophilic reactions has been well-documented for decades since their first report by Stork in the 1950s [1-3]. Compared with enols, enamines benefit from the lone pair of electrons on the nitrogen atom, which enhances the nucleophilicity of the alkene, enabling it to react with a broad range of electrophiles. This activation mode of carbonyl compounds has been so well-established that it is featured in nearly every organic chemistry textbook. However, despite their versatility, enamines themselves are not easily handling compounds in experimental settings. Their sensitivity to hydrolysis complicates their isolation and identification, and following the nucleophilic addition or substitution, the resulting iminium ions often undergo direct hydrolysis, preventing further use in a cascade nucleophilic addition. As a result, enamines are not ideal partners in tandem reactions for the synthesis of nitrogen-containing products. As analogues to enamines, the enamides contain an *N*-acyl group in place of the original alkyl group. The electron-withdrawing effect of the amide group delocalizes the nitrogen lone pair, thereby reducing the electron density and nucleophilicity of the enamide double bond. These features significantly diminish the reactivity of enamides as nucleophiles, rendering them more stable than

enamines. This stability is reflected in their frequent occurrence in natural products [4]. As a result, research on the synthetic applications of enamides has historically lagged behind that of enamines [5,6]. Beyond their use in hydrogenation reactions [7,8], the exploration of enamides' nucleophilic reactivity has only gained momentum in recent years. Inspired by pioneering work from various research groups [9-15], the potential of enamides in nucleophilic reactions has become recognized. Among them, enamide cyclizations have attracted considerable attention due to their promise in the total synthesis of alkaloids [16]. Notably, these valuable compounds can be employed as efficient synthons in enamide–alkyne cycloisomerization, [*n* + *m*] cycloadditions, pericyclic reactions, and radical cyclizations. A comprehensive review of these advancements up until 2015 has already been documented [16]. In this review, recent breakthroughs of these enamide cyclizations will be surveyed from the viewpoint of natural product synthesis. Leveraging the enamide–alkyne cycloisomerization cyclizations, *Lycopodium* alkaloids (−)-dihydrolycopodine, (−)-lycopodine, (+)-lycoposerramine Q, (+)-fawcettidine, (+)-fawcettimine, and (−)-phlegmariurine have been synthesized in a concise and efficient manner, while employment of the [2 + 3] cycloadditions or a polycyclization enables the elegant total synthesis of *Cephalotaxus* alkaloids cephalotaxine, cephalezomine H, (−)-cephalotaxine, (−)-cephalotine B, (−)-fortuneicyclidin A, (−)-fortuneicyclidin B, and (−)-cephalocyclidin A.

Unlike enamines, tertiary enamides can participate in cyclization reactions initial as nucleophiles, and upon protonation, alkenylation, or alkylation, the resultant iminium intermediates can serve as electrophiles. Due to the presence of an amide, the resulting iminiums from the enamides can be stabilized to take part in the second nucleophilic addition, though direct isomerization of the iminiums to the enamides is also possible (Figure 1). Guided by these principles, tandem reactions or annulations can be designed to efficiently access *N*-heterocycles. As the enamides are also easily accessible via condensations, applications of these nitrogen-containing building blocks in the synthesis of *N*-heterocycles are synthetically straightforward. When applied properly, these methods offer promising strategies for the total synthesis of complex natural products.

Review

Aza-Prins cyclization – total synthesis of (–)-dihydrolycopodine and (–)-lycopodine

Cyclizations of enamides can proceed via several distinct pathways. If protonation of the enamide occurs first, the resulting iminium ion can be readily captured by a wide variety of nucleophiles, including alkenes and alkynes. These *aza*-Prins cyclizations have potential applications in the synthesis of natural alkaloids, as exemplified by She's total synthesis of (−)-dihydrolycopodine and (−)-lycopodine [17]. These *Lycopodium* alkaloids have long been valued in traditional Chinese medicine for their therapeutic effects on skin disorders and as analgesics [18]. Preliminary biological evaluations also suggest their antipyretic and anticholinesterase activities [19]. As a prominent member of the lycopodine-type alkaloids, lycopodine features a characteristic tetracyclic structure with a bridged cyclohexanone. To address the challenges associated with constructing the complex ring systems of this structure, She and co-workers devised an intramolecular *aza*-Prins cyclization strategy to form both the bridge ring and the *N*-hetero quaternary center in a single step. As depicted in Scheme 1, key enamide **1** was prepared from (*R*)-pulegone in 6 steps. In the

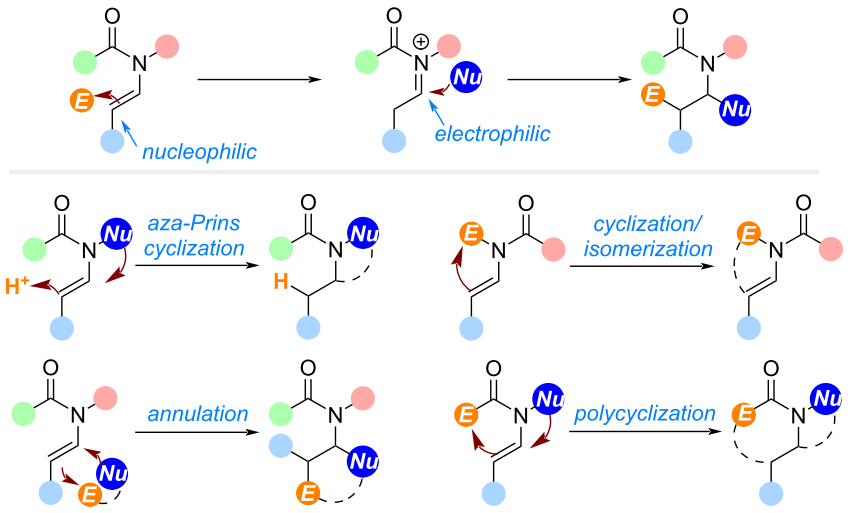

Figure 1: Reactivity of enamides and enamide cyclizations.

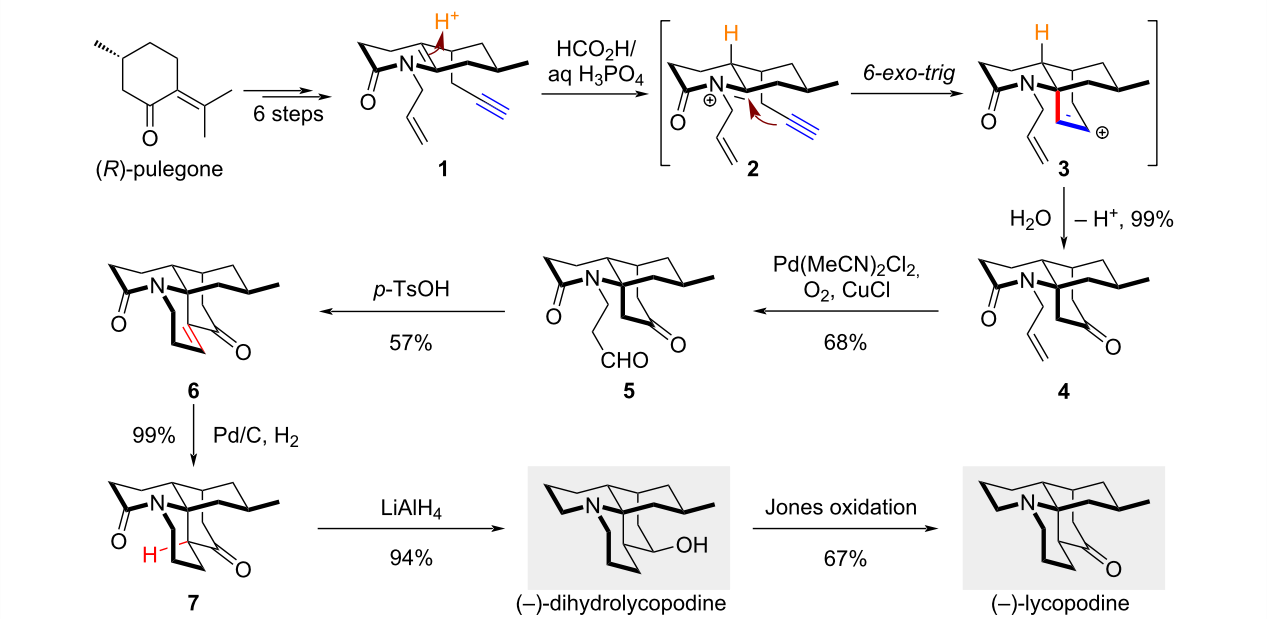

Scheme 1: Total synthesis of (–)-dihydrolycopodine and (–)-lycopodine.

presence of the weak acid H_3PO_4, protonation of **1** generates a stabilized iminium ion **2**, which then undergoes a *6-exo-trig* cyclization to deliver **4** after hydration of cation **3**. Notably, the terminal alkene remains intact during this process, and the initial protonation proceeds with full stereocontrol, rendering this transformation both highly chemo- and diastereoselective. From the cyclization result, it is presumed that the higher nucleophilicity of the alkyne functionality over the terminal alkene and the conformational strain of forming a bridge[3.2.1]bicycle might be responsible for a selective *6-exo-trig* cyclization.

From tricyclic compound **4**, *anti*-Markovnikov oxidation catalyzed by palladium led to the formation of aldehyde **5**. When treated with *p*-TsOH, the intramolecular aldol condensation of **5** provided the tetracyclic α,β-unsaturated enone **6** in 57% yield. Subsequent catalytic hydrogenation using Pd/C conditions delivered the hydrogen to the alkene from the less hindered face, producing ketone **7** with high diastereoselectivity. Final reduction of both the amide and ketone groups completed the total synthesis of (−)-dihydrolycopodine, which could then be further oxidized to (−)-lycopodine. The entire synthetic route hinges upon the development of a sterically congested *aza*-Prins cyclization, enabled by the presence of the enamide and its neighboring alkyne. Building on this strategy, the authors also accomplished the total synthesis of (−)-lycospidine A in only 10 steps [20], another *Lycopodium* alkaloid with a truncated tetracyclic skeleton and distinct oxidation levels, further highlighting the versatility and efficiency of the enamide *aza*-Prins approach.

Cyclization/isomerization – collective total synthesis of fawcettimine-type alkaloids

The bicyclic decahydroquinoline enamide motif can serve as a versatile precursor to access different types of tricyclic *N*-heterocycles. As demonstrated in the above work from She's group, the *aza*-Prins cyclization renders the α-position of enamide to be an active cyclization site, with the alkyne tether acting as the nucleophile. Since it is well-established that alkynes, when activated by transition metals such as gold or platinum, can also function as electrophiles, modulating the reactivity of the decahydroquinoline enamide motif to enable an enamide–alkyne cycloisomerization is also feasible. In this case, the initial nucleophilic cyclization of the enamide is followed by isomerization, shifting the cyclization site from the α- to the β-position of the enamide, resulting in the formation of a fused triangular ring system rather than a bridged tricycle. Building on this strategy, the same research group developed a divergent synthetic route that culminated in the concise and collective total synthesis of a series of fawcettimine-type *Lycopodium* alkaloids (Scheme 2) [21], which are well-known for their potent acetylcholinesterase (AChE) inhibitory activities [18].

In the presence of a catalytic amount of PPh_3AuCl and $AgSbF_6$, the enamide–alkyne cycloisomerization of bromo-substituted alkyne **8** proceeded via a *5-endo-dig* cyclization to afford tricyclic compound **10** through the formation of iminium intermediate **9**. The azepane ring was then constructed via an intramolecular reductive Heck reaction from vinyl bromide **10** with exclusive regioselectivity. Considering the strain of forming the

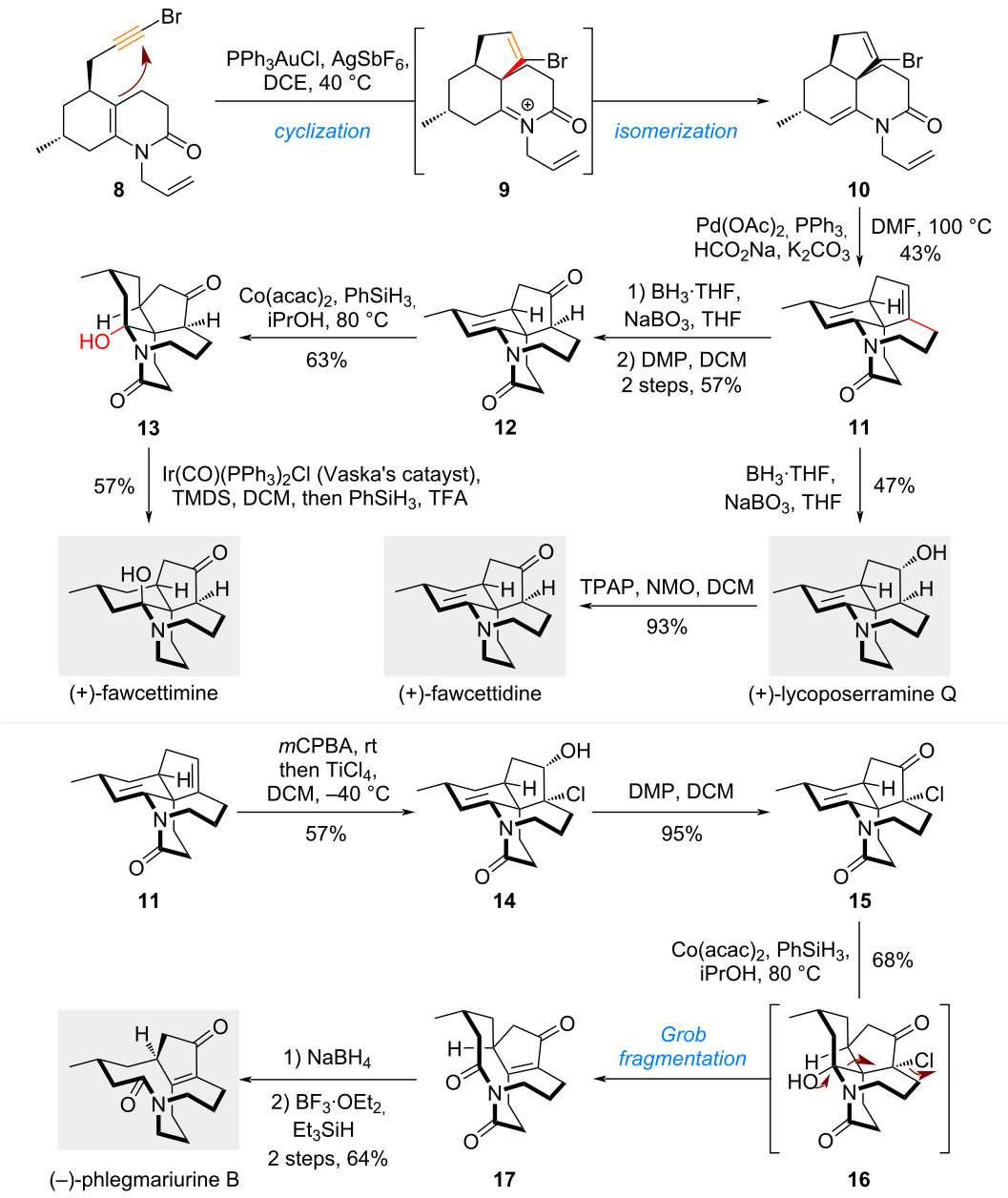

Scheme 2: Collective total synthesis of fawcettimine-type alkaloids.

7-membered ring, this highly efficient *7-endo-trig* (vs *6-exo-trig*) transannular Heck cyclization reaction was remarkable to be realized in a regioselective manner. From tetracyclic compound **11**, a one-pot facial and regioselective hydroboration/amide reduction followed by oxidation produced (+)-lycoposerramine Q, which was then converted to (+)-fawcettidine by Ley oxidation. Alternatively, hydroboration of **11** in mild conditions without the reduction of amide-generated ketone **12** after a subsequent Dess–Martin oxidation. Upon treatment of **12** with $Co(acac)_2$ and $PhSiH_3$ in iPrOH at 80 °C, the Mukaiyama hydration of enamide delivered hemiaminal **13**. Despite the incorrect configuration of the newly formed hydroxy group, it is considered inconsequential due to the reversibility of hemiaminal. Consequently, further reduction of the amide could complete the total synthesis of (+)-fawcettimine with in situ adjustment of the hemiaminal configuration.

The incorrect configuration observed in the Mukaiyama hydration also inspired the authors to develop a fragmentation process for the total synthesis of (−)-phlegmariurine B. A one-pot epoxidation/nucleophilic epoxide opening introduced both a hydroxy group and a chloride across the cyclopentene, produc-

ing **14** in 57% yield. After oxidation of alcohol **14** to ketone **15**, the Mukaiyama hydration then triggered a Grob fragmentation process of hemiaminal **16** and afforded the imide compound **17**. Final regioselective reduction of one of the two carbonyls on the imide completed the synthesis of (−)-phlegmariurine B.

Annulation

Total syntheses of cephalotaxine and cephalezomine H

The [2 + 3] annulation of enamides is a relatively underexplored reaction, particularly in the context of total synthesis. Its synthetic potential remains to be fully excavated, as it offers a modular approach for disassembling molecules into segments of comparable sizes. Recently, Fan's group reported the development of this annulation and applied it in the divergent total synthesis of *Cephalotaxus* alkaloids (Scheme 3) [22], including cephalotaxine whose ester, homoharringtonine, has been listed as an approved FDA drug for the treatment of chronic myeloid leukemia [23]. In their elegant study, an Au-catalyzed [2 + 3] annulation was utilized to transform enamine **18** and propargyl ester **19** into 1-azaspiro[4.4]nonane **20** with high diastereoselectivity. Notably, the combination of an *N*-heterocyclic carbene gold catalyst and a silver salt $AgSbF_6$ was found to be essential in guaranteeing the reactivity of the alkyne partner, probably due to the formation of a more acidic cationic gold complex. Following this annulation, reduction of the amide in **20**, catalytic hydrogenation of the alkene and the *N*-benzyl group, and subsequent nitrogen acylation yielded chloride **21** in a 42% total yield, setting the stage for the Witkop photocyclization. This transformation was carried out using a high-pressure mercury

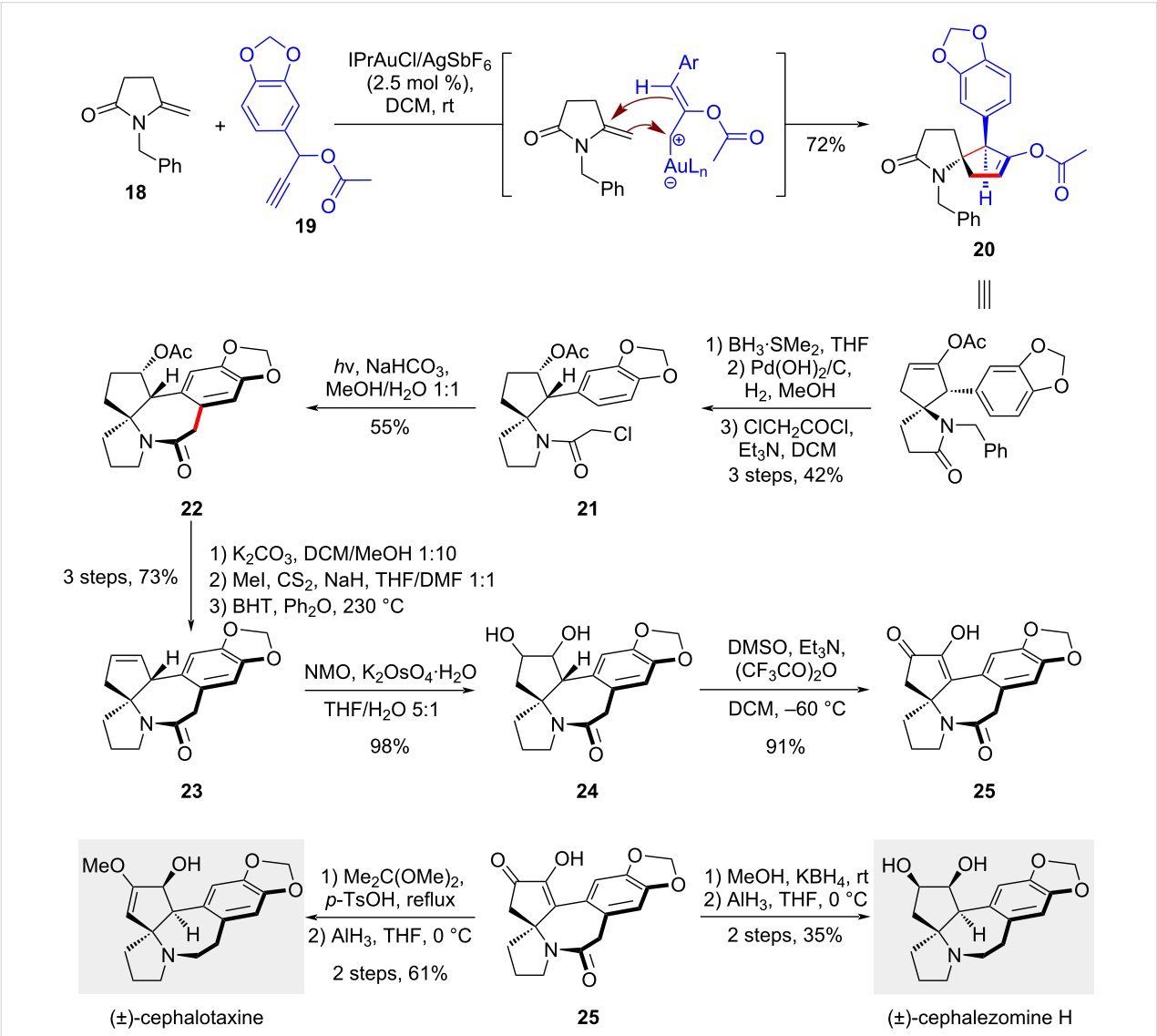

Scheme 3: Total syntheses of cephalotaxine and cephalezomine H.

vapor lamp to afford benzazepine **22**, completing the construction of the pentacyclic framework of the natural product. Subsequent functional group manipulations, including the Chugaev elimination of the hydroxy group on the cyclopentane ring, dihydroxylation, and oxidation of the diol to a diketone, produced intermediate **25** in its enol form. From this common intermediate, regioselective etherification at the less hindered position formed an enol ether. Final reduction of both the amide and the ketone using alane completed the total synthesis of cephalotaxine. Similarly, diastereoselective reduction of **25** with KBH_4 followed by alane reduction provided another alkaloid cephalezomine H.

Collective total syntheses of *Cephalotaxus* alkaloids

The cyclopentane ring in most *Cephalotaxus* alkaloids is characterized by the highest oxidation state within the pentacyclic framework. Installation of this cycle with suitable functional handles usually forms the key strategy of numerous total syntheses of these alkaloids [24-26]. Building upon earlier work, the same research group further advanced this approach by developing a Rh-catalyzed asymmetric [2 + 3] annulation of tertiary enamides with enoldiazoacetates, enabling highly efficient total syntheses of *Cephalotaxus* alkaloids (Scheme 4) [27]. In their recent study, the homopiperonyl alcohol **26** was transformed into tricyclic enamide **28** in five steps in a decagram scale. As no column chromatography was required during this process, the synthetic route is highly practical. The enantioselective annulation of tertiary enamide **28** with enoldiazoacetate **29** was then explored under the catalysis of a chiral dirhodium catalyst. While Doyle and co-workers had previously reported an elegant [2 + 3] cycloaddition of secondary enecarbamates [28], the extension of this reaction to enamides lacking an N–H group is a notable advancement. After extensive optimization, the chiral dirhodium catalyst **cat. 1** was found to be most capable in terms of both stereocontrol and efficiency. The use of 0.4% amount of **cat. 1** provided adduct **30** in 72% yield with 92% enantioselectivity, and the reaction could be scaled up to decagrams. Subsequent decarboxylation and recrystallization of the resulting ketone **31** yielded an enantiopure product (99% ee), which serves as a versatile intermediate for the divergent total synthesis of several *Cephalotaxus* alkaloids.

The α-hydroxylation of cyclopentanone, followed by amide reduction and methanol elimination in one-pot, produced (−)-cephalotaxine in 9 steps. Alternatively, Riley SeO_2 oxidation of **31**, benzylic bromination/hydrolyzation, facial selective ketone reduction, and epoxidation delivered compound **33** with the required oxidation level of the cyclopentane ring. In the final stages, Meinwald rearrangement/hemiketalization in a step-wise procedure, followed by amide reduction, completed the total synthesis of (−)-cephalotine B. Alternatively, after benzylic oxidation, the Meinwald rearrangement/aldol reaction gave rise to the bridge cyclic intermediate **35**, which can finally be converted into both (−)-fortuneicyclidin A and (−)-fortuneicyclidin B.

Polycyclization

Cyclization/Pictet–Spengler reaction

The hexahydropyrrolo[2,1-*a*]isoquinoline or tetrahydropyrrolo[2,1-*a*]isoquinolin-3(2*H*)-one framework is a pivotal core structure among various pyrrolo[2,1-*a*]isoquinoline alkaloids, exemplified by (+)-crispine, annosqualine, and erysotramidine, among others (Scheme 5) [29]. These bioactive alkaloids exhibit a broad spectrum of biological activities, including antitumor, antibacterial, antiviral, and antioxidizing properties. Previous synthetic strategies for these molecules typically rely on multi-step procedures to assemble the tricyclic core. However, the direct catalytic enantioselective formation of this scaffold from a linear precursor remains underexplored, despite the potential for such a tandem reaction to provide a more efficient route to these complex structures. In 2016, Wang and co-workers indigenously designed and developed a cyclization/Pictet–Spengler reaction cascade, leveraging the nucleophilicity of the tertiary enamides and the electrophilicity of the resulting acyliminium [30]. Unlike the monocyclization, which involves deprotonation of the acyliminium ion, the success of this polycyclization relies on the interception of the acyliminium ion by an aryl nucleophile, resulting in the formation of *N*-heterocyclic fused[6,6,5]tricycles. Optimization studies identified the tetraphenyl-substituted PyBox ligand **L1** as particularly effective in controlling the stereochemistry of the polycyclization, yielding high enantioselectivity for most substrates. As illustrated in Scheme 5, tertiary enamides with a tethered electron-rich arene could undergo cyclization to form products in high yields and excellent enantioselectivities. Notably, only a single diastereomer was produced in each case. The single-crystal X-ray crystallography revealed a *cis*-configuration for both the alkene and ketone substituents on the enamide, indicating that the intramolecular attack of the electron-rich arene on the acyliminium ion occurs from the *Si*-face. This stereochemical outcome is attributed to the steric discrepancy of the phenyl or *tert*-butyl group and the hydroxy group. The resulting tricyclic products could be further elaborated by elimination or amide reduction to yield hexahydropyrrolo[2,1-*a*]isoquinoline or tetrahydropyrrolo[2,1-*a*]isoquinolin-3(2*H*)-one frameworks, characteristic of alkaloids such as crispine analogs and erysotramidine.

Building on their previous work on cyclization/Pictet–Spengler reaction, the same group further designed cyclopentanone derived tertiary enamides as cyclization precursors (Scheme 6). The analogous polycyclization generated a tetracyclic *N*-hetero-

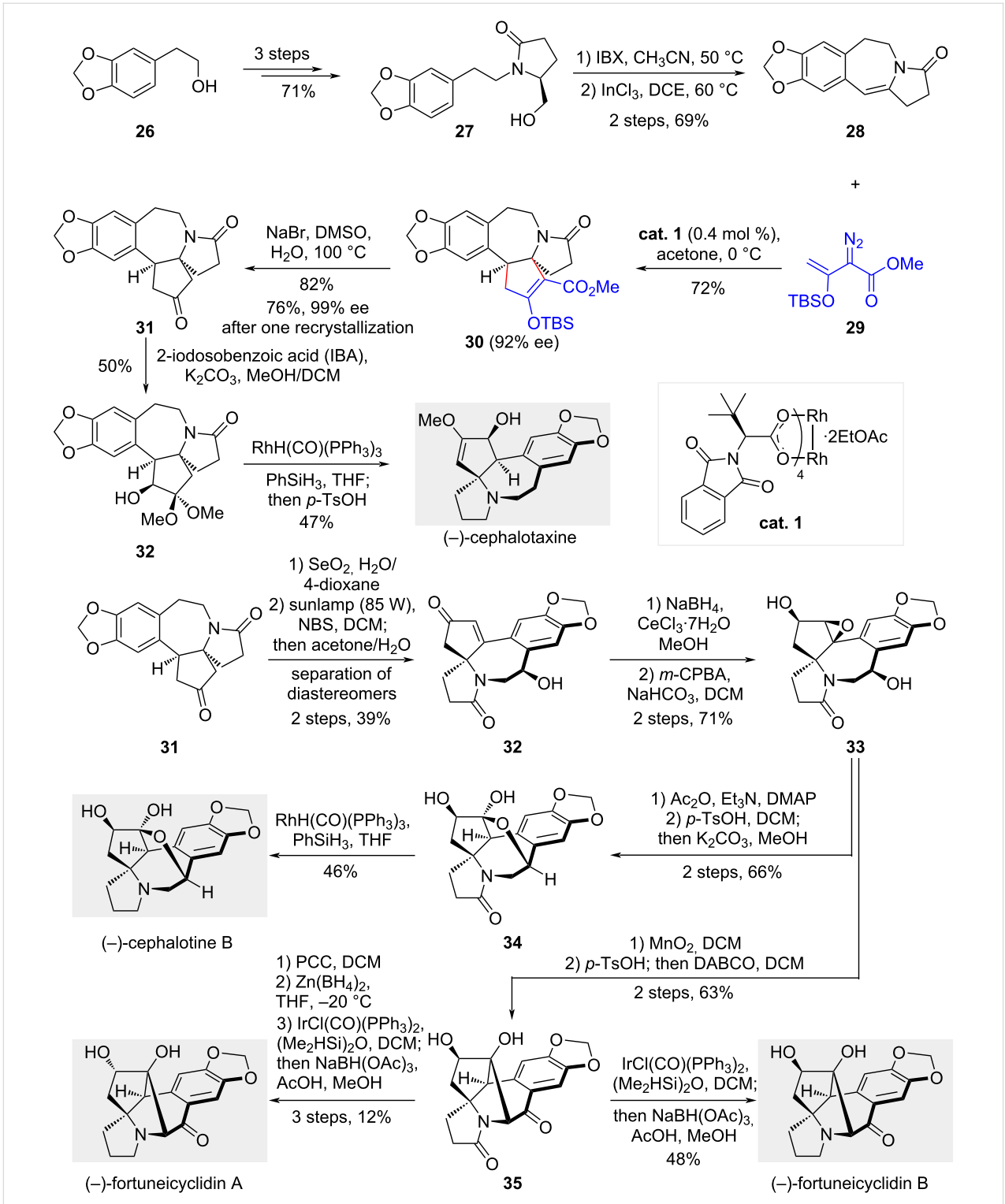

Scheme 4: Collective total syntheses of *Cephalotaxus* alkaloids.

cycle with three continuous stereogenic centers, one of them being an *aza*-quaternary carbon [31]. The resulting fused ring-system structurally resembles the nucleus of erysotramidine alkaloids, though it features a truncated cyclopentane rather than the characteristic cyclohexane or cyclohexene. In their optimization studies, the authors found the sequential catalysis of a chiral binol–Ti complex and $BF_3{\cdot}Et_2O$ to be the most efficient, providing products **39** in high yields with excellent

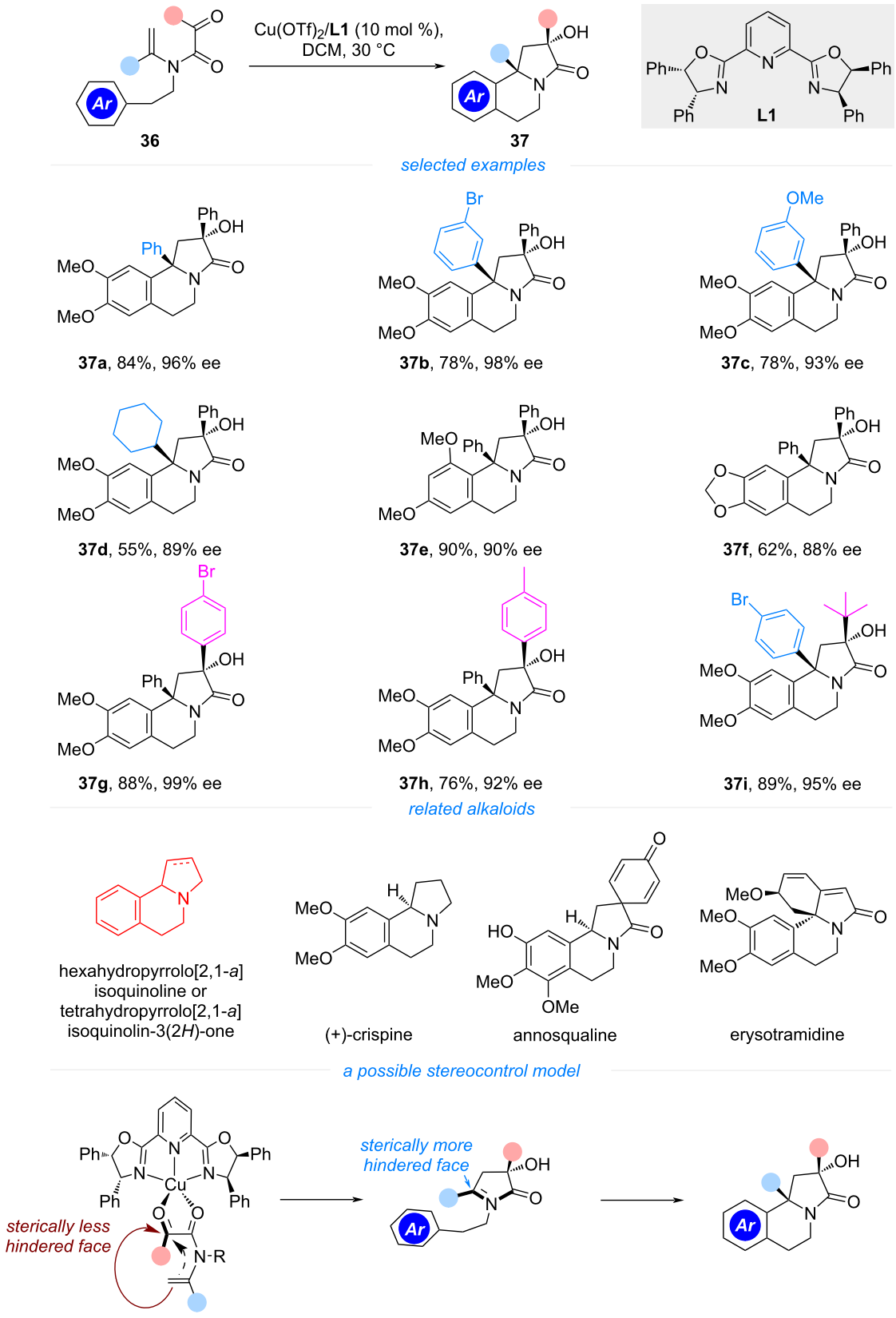

Scheme 5: Asymmetric tandem cyclization/Pictet–Spengler reaction of tertiary enamides.

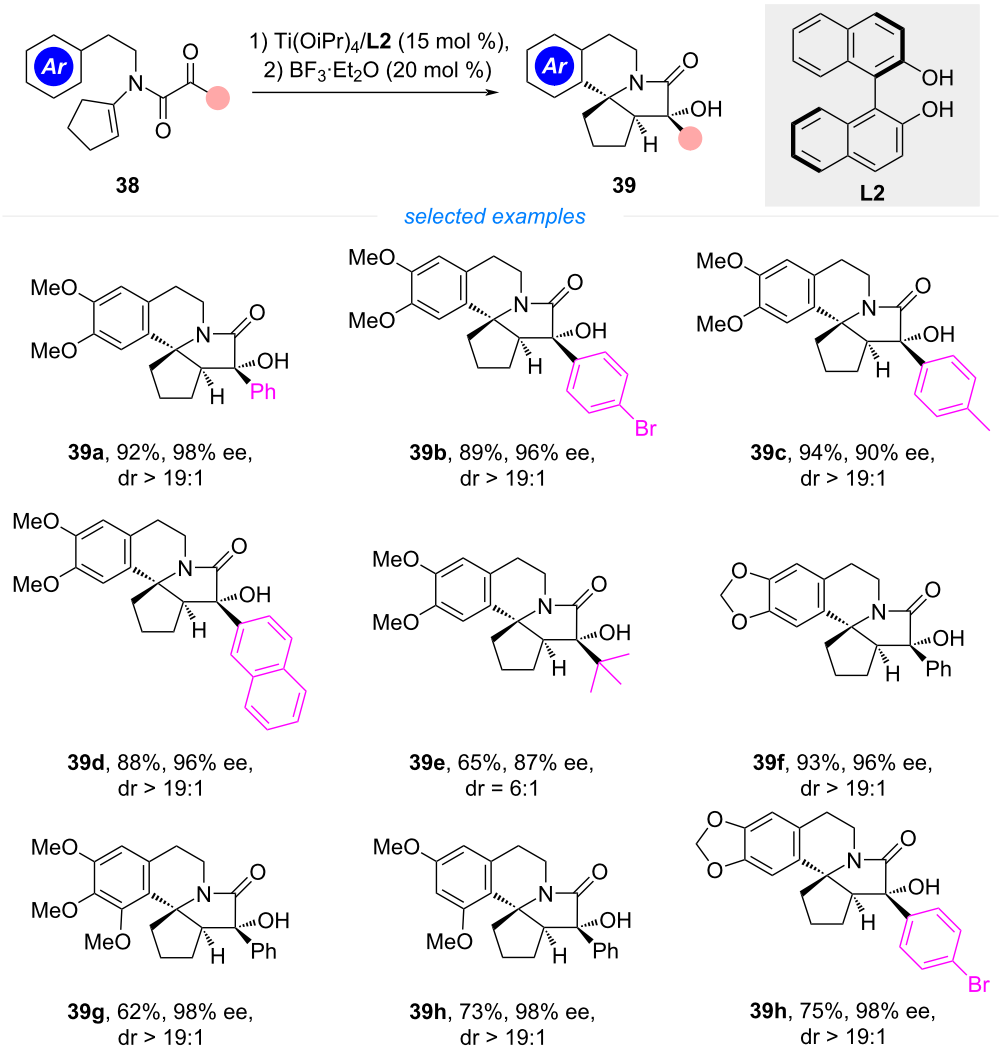

Scheme 6: Tandem cyclization/Pictet–Spengler reaction for the synthesis of chiral tetracyclic compounds.

diastereo- and enantioselectivities. The substituent on the enamide could be varied from aryl to *tert*-butyl groups, though the terminating aryl group still necessitates an electron-rich arene. As was found in their previous work, the steric hindrance of the phenyl or *tert*-butyl group was supposed to be responsible for the excellent diastereoselectivity observed in the second cyclization process. In their later studies, the authors also found cyclohexanone-derived tertiary enamides to be viable substrates for the polycyclization [32], affording erythrinane core skeletons in high yields. However, in these cases, the use of a chiral Cr(III)(salen)Cl complex in combination with $InCl_3$ was necessary to maintain a high level of stereocontrol.

Total synthesis of (−)-cephalocyclidin A

The bicyclic and tricyclic *N*-heterocycles without a fused arene are essential core structures in a wide array of alkaloids. A notable example is (−)-cephalocyclidin A, a cytotoxic pentacyclic cephalotaxus alkaloid [33,34]. Although the molecular structure contains a benzo-bridge ring system, disconnection of this bridge reveals a critical tricyclic *N*-heterocycle. To efficiently synthesize this tricycle, polycyclization of tertiary enamides is employed. Inspired by Wang's earlier work, Zhang and Tu's group developed a tandem cyclization/Mannich reaction to construct this architecture [35]. However, unlike the electron-rich arenes, the use of silyl enol ethers to terminate the second cyclization of the acyliminium intermediate would meet challenges associated with the instability of enolate derivatives. In their recent study, they successfully developed such a polycyclization taking advantage of a novel spiropyrroline-derived oxazole (SPDO) ligand (**L3**). As shown in Scheme 7, one-pot condensation of primary amine **40**, β-silyl substituted cyclopentanone **41**, and acyl chloride **42** produced enamide **43**. The polycyclization then took place under the catalysis of $Cu(OTf)_2$/

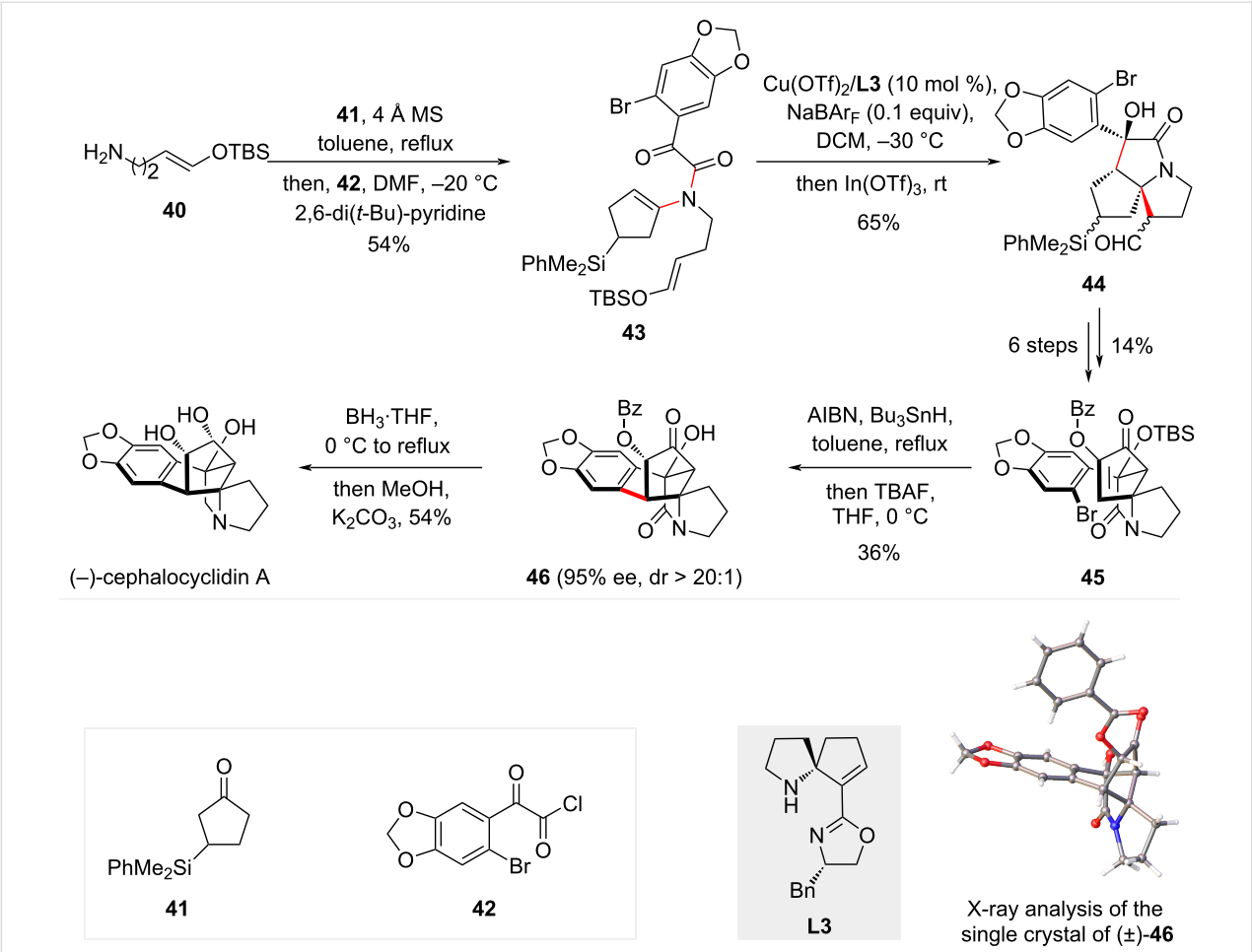

Scheme 7: Total synthesis of (–)-cephalocyclidin A.

L3 and $In(OTf)_3$, delivering tricyclic product **44** in high yield with excellent enantioselectivity. Despite formation of multiple diastereomers due to the presence of silyl and aldehyde groups on the tricycle, it is inconsequential as these groups are either removed or oxidized in subsequent steps. After adjustment of the oxidation levels, the cyclopentenone **45** obtained was subjected to an intramolecular Giese reaction, producing **46** with establishment of the bridge cycle [36,37]. The excellent diastereoselectivity in this radical cyclization was further rationalized by DFT calculations, which suggests an energy discrepancy of the hydrogen atom transfer process from different faces of the resulting α-hydroxyl radical. Final reduction of the ketone and amide followed by deprotection completed the total synthesis, giving rise to (−)-cephalocyclidin A in 10 steps from known compounds.

Conclusion

In summary, the perception of enamides as stable chemical entities with limited utilities in organic synthesis has evolved, and these compounds are now widely used in various cyclization reactions that play a pivotal role in the total synthesis of natural alkaloids. The nucleophilicity of enamides and the electrophilicity of the resulting acyliminium intermediates can be strategically manipulated in numerous ways to design cyclization and annulation reactions. Notably, these reactions – particularly tandem processes – are highly effective in constructing both fused and bridged ring systems, offering valuable new tools for chemical synthesis. Future advancements in the field could involve further applications of enamide cyclizations with other nucleophiles or in combination with other reaction patterns, potentially opening new avenues for the total synthesis of natural products.

Funding

We acknowledge NSFC (22371100, 22071147, and 92256303), the National Key R&D Program of China (2023YFA1506400, 2023YFA1506402, 2023YFA1506403), and The Science and Technology Major Program of Gansu Province of China (22ZD6FA006, 23ZDFA015, 24ZD13FA017) for financial supports.

ORCID® iDs

Xiao-Ming Zhang - https://orcid.org/0000-0002-9294-9672

Data Availability Statement

Data sharing is not applicable as no new data was generated or analyzed in this study.

References

1. Stork, G.; Terrell, R.; Szmuszkovicz, J. *J. Am. Chem. Soc.* **1954,** *76,* 2029–2030. doi:10.1021/ja01636a103
2. Stork, G.; Landesman, H. K. *J. Am. Chem. Soc.* **1956,** *78,* 5129–5130. doi:10.1021/ja01600a088
3. Stork, G.; Brizzolara, A.; Landesman, H.; Szmuszkovicz, J.; Terrell, R. *J. Am. Chem. Soc.* **1963,** *85,* 207–222. doi:10.1021/ja00885a021
4. Poulsen, T. B. *Acc. Chem. Res.* **2021,** *54,* 1830–1842. doi:10.1021/acs.accounts.0c00851
5. Carbery, D. R. *Org. Biomol. Chem.* **2008,** *6,* 3455–3460. doi:10.1039/b809319a
6. Beltran, F.; Miesch, L. *Synthesis* **2020,** *52,* 2497–2511. doi:10.1055/s-0040-1707403
7. Gopalaiah, K.; Kagan, H. B. *Chem. Rev.* **2011,** *111,* 4599–4657. doi:10.1021/cr100031f
8. Cabré, A.; Verdaguer, X.; Riera, A. *Chem. Rev.* **2022,** *122,* 269–339. doi:10.1021/acs.chemrev.1c00496
9. Matsubara, R.; Kobayashi, S. *Acc. Chem. Res.* **2008,** *41,* 292–301. doi:10.1021/ar700098d
10. Dake, G. R. *Synlett* **2012,** *23,* 814–824. doi:10.1055/s-0031-1290351
11. Gigant, N.; Chausset-Boissarie, L.; Gillaizeau, I. *Chem. – Eur. J.* **2014,** *20,* 7548–7564. doi:10.1002/chem.201402070
12. Wang, M.-X. *Chem. Commun.* **2015,** *51,* 6039–6049. doi:10.1039/c4cc10327k
13. Tong, S.; Wang, M.-X. *Synlett* **2021,** *32,* 1419–1427. doi:10.1055/a-1352-6358
14. Varlet, T.; Masson, G. *Chem. Commun.* **2021,** *57,* 4089–4105. doi:10.1039/d1cc00590a
15. Bouchet, D.; Varlet, T.; Masson, G. *Acc. Chem. Res.* **2022,** *55,* 3265–3283. doi:10.1021/acs.accounts.2c00540
16. Courant, T.; Dagousset, G.; Masson, G. *Synthesis* **2015,** *47,* 1799–1856. doi:10.1055/s-0034-1378706
17. Ma, D.; Zhong, Z.; Liu, Z.; Zhang, M.; Xu, S.; Xu, D.; Song, D.; Xie, X.; She, X. *Org. Lett.* **2016,** *18,* 4328–4331. doi:10.1021/acs.orglett.6b02072
18. Ma, X.; Gang, D. R. *Nat. Prod. Rep.* **2004,** *21,* 752–772. doi:10.1039/b409720n
19. Ortega, M. G.; Agnese, A. M.; Cabrera, J. L. *Phytomedicine* **2004,** *11,* 539–543. doi:10.1016/j.phymed.2003.07.006
20. Xu, S.; Zhang, J.; Ma, D.; Xu, D.; Xie, X.; She, X. *Org. Lett.* **2016,** *18,* 4682–4685. doi:10.1021/acs.orglett.6b02322
21. He, F.; Feng, S.; Zhao, Y.; Shi, H.; Duan, X.; Li, H.; Xie, X.; She, X. *Angew. Chem., Int. Ed.* **2022,** *61,* e202205439. doi:10.1002/anie.202205439
22. Ma, X.-Y.; An, X.-T.; Zhao, X.-H.; Du, J.-Y.; Deng, Y.-H.; Zhang, X.-Z.; Fan, C.-A. *Org. Lett.* **2017,** *19,* 2965–2968. doi:10.1021/acs.orglett.7b01202
23. Kantarjian, H. M.; O'Brien, S.; Cortes, J. *Clin. Lymphoma, Myeloma Leuk.* **2013,** *13,* 530–533. doi:10.1016/j.clml.2013.03.017
24. Weinreb, S. M.; Semmelhack, M. F. *Acc. Chem. Res.* **1975,** *8,* 158–164. doi:10.1021/ar50089a003
25. Chen, Y.; Li, W.-D. Z. *Chin. J. Org. Chem.* **2017,** *37,* 1885–1902. doi:10.6023/cjoc201705025
26. Jeon, H. *Asian J. Org. Chem.* **2021,** *10,* 3052–3067. doi:10.1002/ajoc.202100543
27. An, X.-T.; Ge, X.-M.; Liu, X.-Y.; Yang, Y.-H.; Zhao, X.-H.; Ma, X.-Y.; Peng, C.; Fan, Y.-J.; Qin, Y.; Fan, C.-A. *J. Am. Chem. Soc.* **2023,** *145,* 9233–9241. doi:10.1021/jacs.3c01572
28. Deng, Y.; Yglesias, M. V.; Arman, H.; Doyle, M. P. *Angew. Chem., Int. Ed.* **2016,** *55,* 10108–10112. doi:10.1002/anie.201605438
29. Yang, Y.-L.; Chang, F.-R.; Wu, Y.-C. *Helv. Chim. Acta* **2004,** *87,* 1392–1399. doi:10.1002/hlca.200490127
30. Xu, X.-M.; Zhao, L.; Zhu, J.; Wang, M.-X. *Angew. Chem., Int. Ed.* **2016,** *55,* 3799–3803. doi:10.1002/anie.201600119
31. Zhen, L.; Tong, S.; Zhu, J.; Wang, M.-X. *Chem. – Eur. J.* **2020,** *26,* 401–405. doi:10.1002/chem.201904596
32. Zhen, L.; Tong, S.; Zhu, J.; Wang, M.-X. *J. Org. Chem.* **2020,** *85,* 13211–13219. doi:10.1021/acs.joc.0c01992
33. Kobayashi, J.; Yoshinaga, M.; Yoshida, N.; Shiro, M.; Morita, H. *J. Org. Chem.* **2002,** *67,* 2283–2286. doi:10.1021/jo016327f
34. Kim, J. H.; Jeon, H.; Park, C.; Park, S.; Kim, S. *Angew. Chem., Int. Ed.* **2021,** *60,* 12060–12065. doi:10.1002/anie.202101766
35. Zhuang, Q.-B.; Tian, J.-R.; Lu, K.; Zhang, X.-M.; Zhang, F.-M.; Tu, Y.-Q.; Fan, R.; Li, Z.-H.; Zhang, Y.-D. *J. Am. Chem. Soc.* **2023,** *145,* 26550–26556. doi:10.1021/jacs.3c11178
36. Okada, K.; Ueda, H.; Tokuyama, H. *Org. Biomol. Chem.* **2022,** *20,* 5943–5947. doi:10.1039/d2ob00274d
37. Okada, K.; Ojima, K.-i.; Ueda, H.; Tokuyama, H. *J. Am. Chem. Soc.* **2023,** *145,* 16337–16343. doi:10.1021/jacs.3c05811

License and Terms